Interaction Forces between Biomembranes:
Surface Force Apparatus Studies of Supported Lipid Bilayers

By

JAMES KURNIAWAN
B.S. (University of Washington, Seattle) 2010
M.S. (University of California, Davis) 2012

DISSERTATION

Submitted in partial satisfaction of the requirements for the degree of
DOCTOR OF PHILOSOPHY
in
Chemical Engineering
in the
OFFICE OF GRADUATE STUDIES
of the
UNIVERSITY OF CALIFORNIA
DAVIS

Approved:

_____
Tonya L. Kuhl, Chair

_____
Marjorie Longo

_____
Stephanie R. Dungan

Committee in Charge
2016

ProQuest LLC.
789 East Eisenhower Parkway
P.O. Box 1346
Ann Arbor, MI 48106 – 1346

Table of Contents

James Kurniawan
December 2016
Chemical Engineering

Interaction Forces between Biomembranes: Surface Force Apparatus Studies of Supported Lipid Bilayers

Abstract

The complexity of cellular membranes, due in large part to the enormous variety of chemical species present and their active function, makes their study challenging. Due to the intricate nature of cellular membranes, fundamental biophysical studies have been carried out with model membrane platforms that capture the essential physical and chemical properties of biological membranes. Supported lipid bilayer (SLB) systems are one such platform and primarily studied in this work. Specifically, the surface force apparatus (SFA) was used to investigate membrane structure and the interaction forces between solid supported biomimetic membranes. The resulting SFA force-distance profiles were corroborated with various characterization techniques including atomic force microscopy (AFM), neutron reflectometry (NR), fluorescence microscopy (FM), zeta potential (ZP) and Langmuir monolayer experiments.

Systematic studies were done using various systems to reveal the contributions of van der Waals, electrostatic, hydration, and hydrophobic interactions between SLBs. Binary mixture of 1,2-dipalmitoyl-*sn*-glycero-3-phosphocholine (DPPC) and cholesterol was studied to reveal how cholesterol modifies the interactions between membranes. The interaction force-distance

profiles between DPPC-cholesterol membranes measured using SFA and AFM imaging of the membrane revealed the presence of nanoscopic defects leading to an enhanced hydrophobic attraction between the membranes in contact. The membranes were found to carry a distinct and non-negligible negative charge due to the presence of lipid contaminants resulting in a long range electrostatic repulsion. More complex membranes containing equimolar ternary mixtures of saturated lipids (DPPC), unsaturated lipids (1,2-dioleoyl-*sn*-glycero-3-phosphocholine (DOPC) or 1-palmitoyl-2-oleoyl-*sn*-glycero-3-phosphocholine (POPC)), and cholesterol were investigated and exhibited similar interaction behavior as the binary DPPC-cholesterol system. The pure component, ternary mixed membranes were then compared to a more biologically relevant lipid raft membranes composed of POPC, a complex mixture of brain sphingomyelin (BSM), and cholesterol. The heterogeneity of the sphingolipids used in the mixture led to a small variation in the long-range electrostatic repulsion and raft membrane adhesion. Nevertheless, these more complex raft membranes exhibited an adhesion magnitude and compressibility similar to the ternary mixed membranes containing pure components. In all of SLB studies, the quality of the resulting membrane is often overlooked and details such as membrane defects or holes can have a subtle to dramatic impact on the results and conclusions of an individual study. Thus, the deposition parameters required to construct SLBs with the fewest defects were delineated to generate general rules of thumb to guide preparation of novel SLB systems.

Finally, membrane interactions and the deprotonation behavior of oleic acid in a DPPC membrane at physiological pH were determined. The findings clearly demonstrate that oleic acid's degree of deprotonation can be tailored by the solution pH enabling the interaction between oleic acid containing membranes, which have not previously studied, to be controlled.

The SLB charge tunability combined with the ability to tailor the phase state and interactions of the membrane are important for targeted drug-delivery and biosensor applications where the selective binding of ligands or proteins to membranes is important.

Acknowledgement

I would like to express my utmost gratitude to my dissertation advisor, Professor Tonya L. Kuhl, for the guidance throughout my graduate education. This dissertation would not have been possible without her constant encouragement and valuable discussion. I wish to thank my committee members, Professor Marjorie Longo and Professor Stephanie R. Dungan for their advice and input for this dissertation. For the financial support, I wish to thank the National Science Foundation. I would like to express my gratitude to my co-authors, Keishi Suga for the contribution of the Langmuir monolayer experiment, João Ventrici and Naining Yin (Prof. Gang-yu Liu's group) for their contribution, specifically for all of the AFM scans on my dissertation. I would also like to thank my fellow graduate students Daniel Kienle and Amanda Dang, and all the undergraduate researchers who have been extremely helpful for my projects. Lastly, I wish to thank my family and friends for the wonderful personal support and encouragement.

Chapter I

Preparation and Characterization of Solid Supported Lipid Bilayers – Constructing an Ideal Biomimetic Membrane

James Kurniawan[†], João Ventrici[‡], Gang-yu Liu[‡] and Tonya L. Kuhl*[†#]
[†]Department of Chemical Engineering, [‡]Department of Chemistry, and [#]Department of Biomedical Engineering, University of California Davis, 95616, USA
Corresponding Authors: *E-mail: tlkuhl@ucdavis.edu

ABSTRACT

The structure, phase behavior and properties of cellular membranes are determined by their composition which includes phospholipids, sphingolipids, sterols, and proteins with various level of glycosylation. All of these molecules laterally interact and can segregate to form structures such as lipid rafts, which complex proteins and have emerged as the focus of many studies due to their potential importance in controlling the bioactivity of cells. Due to the intricate nature of cellular membranes, a plethora of *in vitro* studies have been carried out with model membrane platforms that capture specific properties such as fluidity and permeability, but vastly simplify the membrane composition in order to focus in detail on a single property or function. Supported lipid bilayer (SLB) systems are one such platform and this instructional review focuses specifically on the preparation and characterization of SLB systems. Preparation techniques for SLBs such as Langmuir deposition and vesicle fusion are described in detail. A number of characterization methods which take advantage of the flat orientation of SLBs are described and references which go into more depth are included. The instructional review is written so that non-experts may obtain a strong foundational understanding of how to create

and characterize a desired SLB system. Furthermore, this work goes beyond traditional instructional reviews to inform expert readers and includes new results that more fully characterize a wider range of SLB systems than has previously been described in the literature. The quality of the resulting SLB is often overlooked and details, such as membrane topological defects, can have a subtle to dramatic impact on the results and conclusions of an individual study. Here we quantify and compare the quality of the resulting SLBs fabricated from a variety of gel and fluid compositions using different preparation techniques to generate general rules of thumb to guide preparation of novel SLB systems. Finally, the deposition parameters required to construct SLBs with the fewest topological defects were delineated.

1. INTRODUCTION

The human body consists of billions of cells, the smallest building block of life. Cells themselves, their organelles, and other functional volumes are compartmentalized by membranes that encapsulate various essential biomolecules such as nucleic acid and proteins which regulate cellular function.[1] The membranes themselves contain hundreds of different constituent molecules, including lipids, sterols, and proteins. These moieties interact laterally to create lipid rafts where the majority of cellular signaling and transport is thought to take place.[2-4] One of the earliest studies to fundamentally determine the structure of a cell membrane was performed by Gortner and Grendel in 1925.[5] Using a Langmuir trough, they determined that the membrane of mammalian red blood cells was formed by two lipid monolayers. Langmuir troughs are still used extensively today to precisely measure the

properties of lipid monolayers as well as to deposit monolayers to form well-defined model membrane systems.

The complexity of cellular membranes, due in large part to the enormous variety of chemical species present and their active function, makes their study challenging. In addition, cellular membranes are constantly in flux and dynamically respond to their local environment. Together, these properties make it daunting to tease out the temporal and spatial variation and even more difficult to correlate structure-function relationships. To make headway, various biomimetic or model membrane platforms have been developed. Though vastly simplified, these model membranes can still mimic the essential physical and chemical properties of biological membranes such as membrane elasticity, fluidity, phase behavior, and can provide an appropriate environment for studying protein function.[6] Recently, biomimetic membranes which recapitulate the various phases that are thought to co-exist in biological membranes such as liquid-order (L_o), liquid-disordered (L_d), and gel phases are being actively studied. For example, membranes containing mixtures of saturated lipid with high melting point, unsaturated lipid with low melting point, and sterols can form a variety of coexisting phases and partitioning of different molecules into these phases has been of particular interest.

In an earlier review, Castellana and Cremer[7] described a number of lipid bilayer platforms that have been used as model membrane systems. These platforms allow studying a variety of processes. For example, free standing black lipid membranes are used to study transport across membrane, while phase behavior and membrane fluidity are frequently studied using giant unilamellar vesicles. Solid supported lipid bilayers (SLBs) are used to quantify membrane topography and adhesion. Some of the model membrane platforms

provide overlapping information, but the specific type of platform dictates the characterization techniques that can be used. Powerful surface sensitive techniques for probing adhesion and high-resolution scans of membrane topography can only be performed using solid supported membrane platforms. Free-standing membrane platforms such as unilamellar or multilammelar lipid vesicles enable studies free from the influence of the underlying inorganic support and are useful systems for micropipette mechanical measurements, small angle scattering, and various imaging microscopy, but are incompatible with most other high resolution, nanoscopic characterization techniques. As a result, solid supported biomimetic bilayers immobilized on clean smooth surfaces have emerged as a powerful platform to study biomimetic membranes, including lipid rafts and small-molecules such as polypeptides and membrane proteins on the nanoscale. However, studies of integral membrane proteins (IMPs) using SLB platforms are limited due to the potential interaction of the protein with the underlying support,[8-10] which can lead to the denaturation of the embedded proteins. SLBs can be modified with polymeric spacers and tethers to increase the separation between the membrane and support. Such platforms are typically referred to as polymer cushioned and are becoming more widely utilized.[11-16]

This instructional review focuses on solid-supported bilayer systems and is organized into three main sections. In the first, different methods to prepare SLBs are described in detail while the second part of the review covers commonly used characterization techniques of supported membrane systems. The last section of the paper discusses preparation techniques that can be used to create almost defectless SLBs with supporting data from various characterization techniques.

2. PREPARATION OF SOLID SUPPORTED BILAYERS

There are two main methods used to create solid supported bilayers: Langmuir trough deposition technique and vesicle fusion. These methods can be used separately or in conjunction to create symmetric and asymmetric membranes. Recently, solvent spreading and spin coating have emerged as additional, rapid means to fabricate solid supported membranes. Details for each deposition technique are provided below.

2.1. Langmuir-Blodgett (LB) Technique. The LB technique, which dates back to 1917, was pioneered by Irving Langmuir[17] for depositing fatty acid monolayers from the air-water interface onto solid substrates. Katherine Blodgett[18] then used the same technique to deposit multilayers of fatty acids with repeated dipping of the solid substrate through the air-water interface. The technique has subsequently been used to deposit monolayers of lipids and other surface active, water insoluble films onto substrates. The trough, usually made with a low surface energy material such as Teflon, is filled with water or any other subphase such as physiological buffer solution. Widely used substrates include mica,[19-20] quartz,[21-22] borosilicate glass (microscope slides),[21, 23] silicon wafers, and thin films of metal[24-25] or silicon dioxide (SiO_2).[26] The quality of the transfer is greatly enhanced by using ultra-clean, hydrophilic substrates with low surface roughness resulting in better packed, uniform SLBs. Most high resolution studies use mica or high quality oxidized silicon wafers because of their low root mean square roughness, 0.2 Å and 2-3 Å, respectively. To ensure substrate cleanliness, mica should be freshly cleaved right before use. We typically prepare our quartz and silicon wafer substrates through methodical cleaning steps: sonicated in acetone, transferred and sonicated in isopropanol and then rinsed in copious MilliQ water to remove contaminants. We then sonicate the substrate in Hellmanex (Hellma

Analytics) soap and again rinse with copious MilliQ water. The substrate is then dried using clean nitrogen gas. The cleaned and dried substrate is subsequently treated for at least 30 minutes with plasma-ozone and used immediately after the UV-ozone treatment. Hydrophilic substrates are immersed in the subphase before deposition of lipids on the air-water interface. For AFM measurements, mica is typically used because it can be easily cleaved to be atomically smooth over relatively large areas. The lipid spreading solution is prepared in a solvent, such as pure chloroform or a mixture of chloroform:methanol. The concentration of the spreading solution is typically between 0.1 to 1 mg/mL. The lipid must fully dissolve in the solvent, and lipid and solvent solubility in the trough subphase should be negligibly small. The choice of solvent and concentration is determined by the solubility of the lipids in the chosen solvent. For example, phosphatidylcholine (PC) lipids are fully dissolved in chloroform at room temperature, but phosphatidylethanolamine (PE) lipids require a mixture of 9:1 chloroform:methanol for complete dissolution.

The spreading solution is dispensed carefully onto the air-water interface, droplet by droplet, to create a thin layer of lipids whose hydrocarbon tails face away from the water subphase. An arbitrary solution concentration is chosen to achieve a recommendable volume of 50 to 100 µL, depending on the surface area of the LB trough and desired compression of the film. Once the solvent has evaporated, a barrier compresses the lipid monolayer to create a highly compressed two-dimensional film on the air-water interface at a pre-determined surface pressure. After reaching the target pressure and allowing the compressed film to equilibrate, the solid hydrophilic substrate is vertically drawn out of the water to deposit the inner monolayer. Throughout the deposition process, the surface pressure is usually kept constant by

compressing the remaining film as the transfer occurs. Once the substrate has cleared the water level, it is resubmerged to deposit the outer monolayer of the SLB. This process, known as LB/LB deposition, can deposit a bilayer featuring a single component lipid or mixtures of lipids with few topological defects. The composition of the bilayer leaflets may be identical or different for the inner and outer monolayer (symmetric versus asymmetric/hybrid bilayer). A diagram for bilayer deposition through LB/LB technique is shown in Figure 1.1A.

Some important parameters must be considered in order to achieve a high-quality solid supported membrane through the LB deposition technique. During deposition, the phase of the lipids greatly affects the resulting monolayer transfer onto the substrate. Lipid phase is dictated by lipid type, subphase temperature, and the film's surface pressure (as measured by a Wilhelmy plate). Optimum deposition pressures are usually assessed through surface pressure versus area per lipid molecule plots, Π-*A* isotherms of the lipid or mixture being deposited. In general, high changes in surface pressure per area, $\frac{d\Pi}{dA}$, correspond to better transfers to the substrate. The transfer ratio, $\mathrm{TR} = \frac{\Delta A_{trough}}{A_{substrate}}$, is used to quantify the quality of the transfer of material from the air-water interface, where a value of TR = 1 indicates that the area per molecule and surface pressure are maintained from the air-water interface to the substrate.[27-28] ΔA_{trough} is defined as the area of lipids removed from the air-water interface and $A_{substrate}$ is the area of the substrate coated during the deposition. Dipping speed must also be considered in order to achieve an efficient transfer of lipid from the air-water interface to the solid substrate. A relatively high transfer ratio cannot be obtained if the substrate moves too quickly

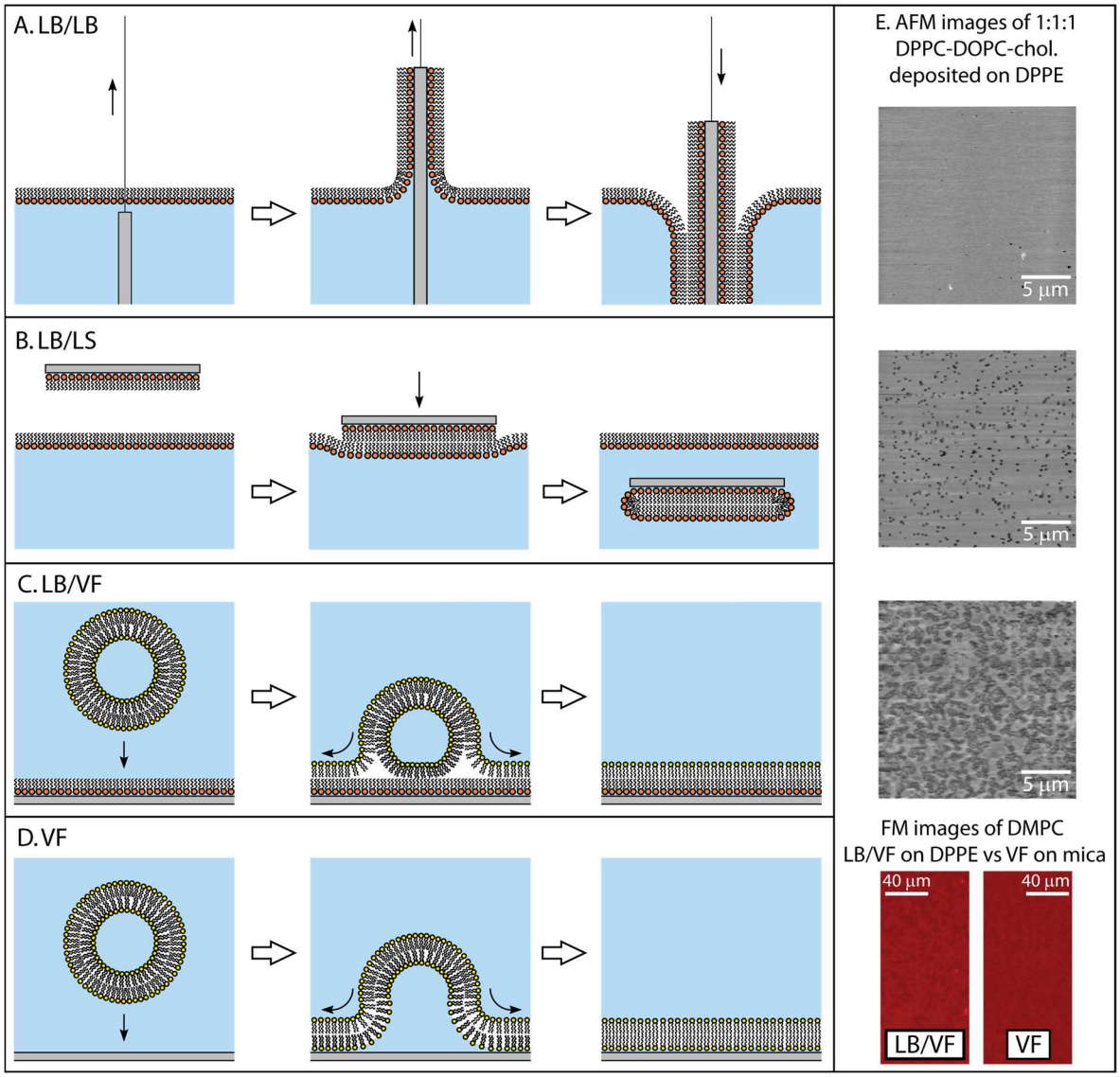

Figure 1.1. [A] Schematic of the process of LB deposition of solid supported bilayers. (Left) After immersing the substrate, lipid is deposited on the air-water interface and compressed to the desired surface pressure. (Center) The substrate is drawn out of the subphase through the interface to deposit the inner leaflet. (Right) After the inner monolayer deposition is done, the substrate is then lowered through the interface to deposit the outer leaflet layer. [B] Langmuir-Schaefer (LS) method to deposit the outer leaflet on an LB deposited inner monolayer leaflet. [C] Vesicle fusion on an LB deposited monolayer. [D] Vesicle fusion directly onto a clean hydrophilic substrate. [E] The first three images are 20 x 20 μm AFM topographical scans of 1:1:1 DPPC-DOPC-cholesterol deposited with various techniques onto a 1,2-dipalmitoyl-*sn*-glycero-3-phosphoethanolamine (DPPE) inner monolayer deposited using LB method at 45 mN/m and dipping speed of 1 mm/min: LB, LS, and VF from top to bottom [A,B,C] respectively. The LB and LS of the outer layer were done at pressure of 30 mN/m. Dark regions are topological defects on the supported membranes. The bottom images show the comparison of the SLB quality deposited as asymmetric versus symmetric bilayer on a glass substrate using vesicle fusion visualized using fluorescence microscopy.

through the lipid monolayer. In addition, a fast dipping speed sometimes causes delamination of the inner monolayer rather than deposition of the outer layer. Typically, a dipping speed between 1 to 4 mm/min is chosen in order to obtain a high transfer ratio (TR ~ 1.0). Details for parameters required to obtain an SLB with as few topological defects as possible are discussed in section 4, and Girard-Ergot and Blum provide an in-depth discussion of the LB technique.[29]

2.2. Langmuir-Schaefer (LS) Technique. Vincent Schaefer, in collaboration with Irving Langmuir, first deposited a monolayer of urease on metal and glass plates with a method similar to the LB technique.[30] The LS technique, sometimes called horizontal deposition, deposits a lipid monolayer by dipping the substrate with a parallel orientation to the air-water interface through a compressed lipid monolayer (Figure 1.1B). Typically, the LS technique is used to deposit the outer leaflet of the membrane to create symmetric or asymmetric SLB, with the inner monolayer deposited by LB. LS is particularly useful for SLB formation on glass where the inner monolayer can delaminate from the substrate during vertical LB deposition.[31] In cases where the physiochemical interaction of the inner layer is insufficient to ensure the stability, the LS technique should be used to create the SLB.

Similar to the LB deposition method, the state of the lipid phase is also important for the LS technique. In works involving asymmetric SLBs, which are typically used for study of lipid flip-flop rate,[32-34] gel phase lipids should be used. Gerelli *et al*. demonstrated that deposition of fluid phase lipids induced mixing between the inner and outer leaflet due to mechanical shock from the LS method.[35] Dipping speed is not as crucial for achieving a quality bilayer. However, the orientation (that is, how level the substrate surface is relative to the water surface) is critical for successful LS deposition. When the substrate is at an angle, film material can be pushed away,

leading to a less well-packed transfer. A detailed comparison of the SLBs fabricated with LB-LS technique versus LB-LB technique is provided in section 4.

2.3. Vesicle Fusion Technique. The majority of SLB studies use the vesicle fusion method to prepare bilayers on solid substrates because of the ease and simplicity of this approach. To create an SLB, vesicles are incubated either on a monolayer of lipids deposited through LB technique to create an asymmetric bilayer (Figure 1.1C),[36] or on a clean hydrophilic surface to create a symmetric bilayer (Figure 1.1D). However, the quality of the asymmetric SLB deposited using LB/VF technique is lower compared to LB/LB or LB/LS deposited asymmetric bilayers (Figure 1.1E). In Langmuir trough techniques, the surface pressure of the monolayer is precisely controlled, which generally leads to few topological defects or variations in the SLB. Vesicle fusion relies on the instability of vesicles interacting with the support (and frequently, the extent of instability of the vesicles themselves in the dispersion), and attractive interactions of the vesicles with the support to yield spontaneous SLB formation. Osmotic stress, addition of divalent ions, and temperature cycling can also be done to aid SLB formation.[37-39] Similarly, the quality of the symmetric bilayer formed by vesicle fusion with a hydrophilic substrate is also lower in quality.[22] In one of the few direct comparison of LB deposited and vesicle fusion SLBs, Watkins *et al*.[27] established that DPPC membranes deposited by vesicle fusion mimic depositions by LB technique at surface pressures of 38±3 mN/m.

The first step in performing vesicle fusion is preparation of the vesicle solution. A small amount of concentrated lipid in organic solvent (~100 µL of 10 mg/mL lipid solution in chloroform or a chloroform:methanol mixture) is prepared in a vial or similar container. The solvent is then evaporated by a stream of nitrogen to leave a thin lipid layer on the wall of the

container. The amount of the lipid solution needed depends on the required volume of the vesicle solution. In general, the concentration of a vesicle solution used for SLB formation is between 0.2 to 1 mg/mL. After drying with nitrogen, the lipids are placed in a vacuum for at least 4 hours to fully remove all solvent before hydrating the lipids to create the vesicle solution. Applying a vacuum is essential as any solvent present upon addition of water will disturb the formation of vesicles. After drying, the lipids are hydrated with water or a salt buffer solution and vortexed to obtain multilamellar vesicles of heterogeneous sizes. Small unilamellar vesicles (SUVs) are preferable for vesicle fusion because they are more readily absorbed onto a substrate to form a single SLB. To make such small vesicles, the vortexed vesicles are probe-tip sonicated or extruded through a polycarbonate membrane to create SUVs of a small, homogeneous size distribution. Extrusion is the preferred method, as probe-tip sonication can release contaminant titanium particles into the vesicle solution, though these can be removed by centrifugation or an extra filtration step. The solid substrate is then incubated with the vesicle solution for at least 20 minutes based on surface plasmon resonance and quartz crystal microbalance studies.[40] Excess vesicles can be washed away after the incubation. Vesicle fusion usually results in a bilayer with topological defects or suboptimal surface coverage. However, there are a number of ways to increase the quality of membrane deposited via vesicle fusion technique.[23] Typical preparation methods include incubation of a fresh SUV dispersion with narrow size distribution, coupled with a freeze-thaw technique, and then rinsing with a solution of a different salt concentration to obtain higher bilayer surface coverage. In particular, the vesicle fusion must be performed with a fresh SUV solution because small unilamellar vesicles are unstable and will readily fuse to the clean hydrophilic substrate to make symmetric SLB, or

fuse with the monolayer to create asymmetric SLB.[41-42] Freeze-thaw cycling will rupture adsorbed vesicles through formation of ice crystals, so they can deform and cover the substrate.[43] After the incubation, excess and physisorbed vesicles are removed by exchanging the incubation solution with a vesicle-free buffer solution or water. If the rinsing solution has a different salt concentration than the vesicle solution, the concentration gradient creates osmotic flow which swells or shrinks and ruptures any excess vesicles stuck to the membrane or substrate, and thus results in a cleaner supported membrane. This washing step is typically repeated to ensure removal of excess vesicles. After the SLB is deposited on the substrate, thermal cycling/annealing can be done to increase the surface coverage after incubation.[38] However, the heating and cooling cycle must be done carefully to prevent loss of lipids into the subphase (Figure 1.2).

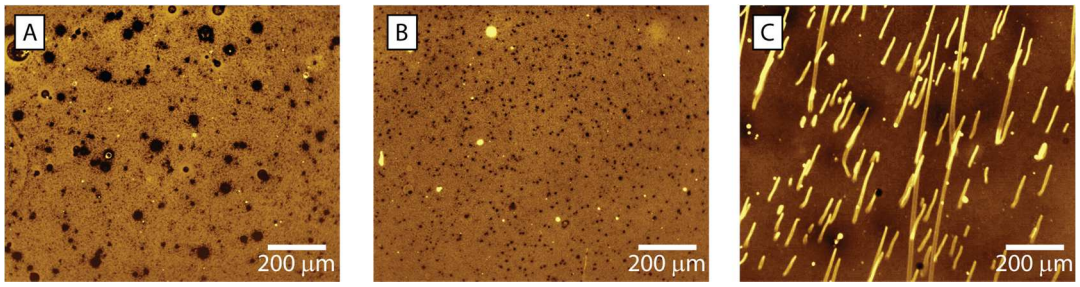

Figure 1.2. Fluorescence microscopy images of 2:2:1 DPPC-DOPC-cholesterol SLB formed on borosilicate glass using vesicle fusion of 100 nm SUV solution in 0.5mM $NaNO_3$. (A) SLB deposited on glass slide after 45 minutes incubation and 3 minutes rinsing with MilliQ water at 25°C. Membrane defects were observed before application of heat. (B) Membrane defects shrank with 15 minutes of heating at 45°C and a few vesicles and tubules started to form. (C) Longer heat application resulted in the formation of long tubules + vesicles and a significant loss of lipids into the subphase.

2.4. Spreading and Spin Coating Techniques. Spreading and spin coating are quick and easy techniques for deposition of solid supported lipid membranes. In spin coating, a lipid solution, with concentration ranging between 0.25 and 5 mM in a volatile solvent that wets the

substrate, is deposited on a clean substrate. After spreading, the substrate is rapidly accelerated to a certain rotation speed (e.g. 2000 rpm) to quickly remove the solvent, leaving a thin dry lipid film. In the spreading technique, one microliter of lipid solution with a similar concentration range is deposited on a clean substrate and the solvent is allowed to evaporate.[44] Once a thin, dry lipid layer is formed by either method on top of the solid substrate, the sample can then be partially or fully hydrated to create a stack of lipid membranes. Mennicke and Salditt[45] described parameters for the spin coating process in detail, such as lipid solution concentration and rotation speed, in order to deposit multiple bilayers (up to 22 layers). Excess floating bilayers can be subsequently removed by a fluid jet to leave a single supported bilayer in the treated region.[46] The fluid jet is typically water or buffer sprayed onto the substrate from a syringe or MilliQ water dispenser. While this technique can technically be used for solid supported membrane preparation, it is more suited for creating multiple bilayers on a solid substrate. This is due to the numerous topological defects and low stability of the sample as characterized by various methods such as X-ray reflectivity and electron microscopy.

3. CHARACTERIZATION OF SOLID SUPPORTED BILAYERS

A solid supported membrane created by any of the methods described above can be characterized by a variety of techniques. Characterization techniques provide information on SLB properties, and the results from one technique can corroborate data collected by another method. Typically used characterization techniques are described in greater detail below.

3.1. Fluorescence Microscopy (FM). Fluorescence microscopy is a basic but powerful technique that has been used since late 1960s that relies on doping in a small amount of

fluorescent lipids (usually 0.25 to 1 mole%) to characterize solid supported membrane systems. White light is directed through a bandpass (excitation) filter that only allows light with a specific wavelength range to pass through. The wavelength range is selected to match the absorption wavelength of the doping fluorescent dye molecule. A dichroic filter redirects this light to illuminate the dye molecule in the sample. Illumination excites the dye, resulting in the release of light with a higher wavelength that passes back through the dichroic mirror and an emission filter into the detector. FM enables the lateral organization, including phase separation and domains of the SLB, to be studied at the macro scale, since a given fluorescence dye will partition differently into the two phases.

FM also permits the analysis of membrane fluidity through fluorescence recovery after photobleaching (FRAP). FRAP enables the extraction of the 2-D diffusion coefficient of the fluorescently labeled lipid in the solid supported membrane. Loren *et al.* and Rayan *et al.* have published recent reviews of this method.[47-48] Figure 1.3 shows an example of FRAP measurement to extract diffusion coefficient from an SLB system. There are different configurations of fluorescence microscopy that can also be of use. For example, Forster resonance energy transfer (FRET) can be used to observe microdomains in a lipid raft[49] and the interaction between proteins in the membrane.[50-51] Total internal reflection microscopy (TIRF) and two-photon fluorescence microscopy (P2FM) can be utilized to study the directional alignment of the lipids in a gel phase domain.[52-53] Confocal fluorescence correlation microscopy, an improvement upon traditional FM, increases the resolution of lateral diffusivity measurements and can produce a three-dimensional structural scan of the solid supported membrane if there are features protruding out of the membrane plane.[54]

The fluorescent dyes used in FM have several key characteristics, such as their excitation/emission spectrum, quantum yield, and lifetime, which must be carefully considered against the demands of the experiment. For example, FRET requires two fluorescence dyes such that the absorption spectrum of one dye overlaps the excitation spectrum of the other dye. FRAP necessitates a dye with robust quantum yield and lifetime that is still easy to photobleach. Berezin and Achilefu qualified various fluorescence dyes in detail, including their spectra and lifetime.[55] Online tools from fluorescent dye vendors aid in determining the best dye for each specific use.[56]

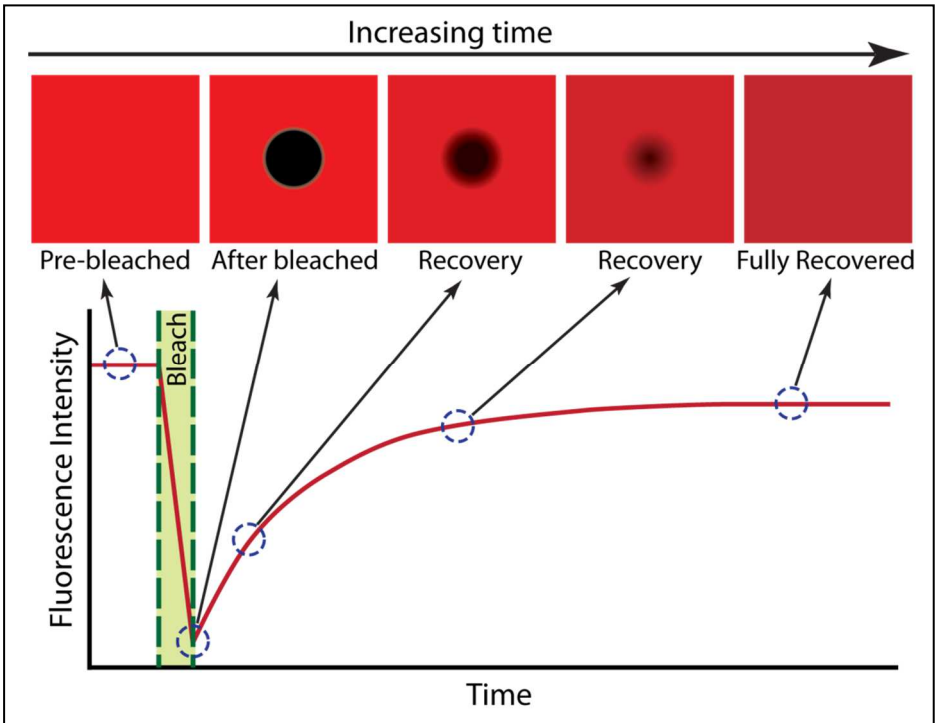

Figure 1.3. Schematic of FRAP technique showing the typical fluorescence intensity curve at the center of bleach spot with time. The diffusion coefficient is calculated from the fit of the intensity curve.

3.2. Atomic Force Microscopy (AFM). Atomic force microscopy can be used to characterize solid supported bilayer systems through information such as topography (as well as thickness),

interaction force, and visco-elastic properties of the surface film.[57-60] AFM measurements are based on an atomically sharp tip (colloidal particles are sometimes used to measure interaction force) on a cantilever with a known spring constant being brought into and out of contact or close proximity with the membrane surface during a raster-scan. Supported bilayers are primarily scanned using tapping mode, where the tip is vertically oscillated at or near the resonant frequency in the fluid while scanning the surface. The other AFM imaging mode is contact mode. In contact mode, as its name suggests, the tip is in physical contact with the surface to be scanned. Contact mode is not typically used to scan fluid membranes because it has high probability to damage the surface by the lateral force exerted by the tip. Condensed phase membranes are more resistant to the action of the tip and are much less affected by contact mode scans, resulting in a higher quality scan compared to the typical tapping mode used for SLB topography scan using AFM. The cantilever tip can be modified to control the surface chemistry or exposed groups by coating the tip with lipids or other molecules of interest, such as protein. The laser is reflected off the cantilever to the photodiode, and the cantilever deflects the laser when it interacts with the surface. Laser displacement is used to output the topography of the sample, among other information. The spring constant and deflection of the cantilever can be used to calculate the intermolecular forces between the tip and the sample. In terms of force measurements, AFM is used to quantify the non-specific interactions between chemically functionalized tips, polymers, and proteins with SLBs, as well as specific interactions such as ligand-receptor binding.[61-63]

The membrane sample used for an AFM scan can be prepared with any deposition technique described in the previous section. Once the membrane is deposited on a clean

surface, the substrate is transferred to a fluid cell specifically designed to hold the substrate under water and retain the native environment of the membrane. The design of the fluid cell is critical for obtaining optimal resolution in the scan. The fluid cell should not hinder the movement range of the cantilever stage and the cell should not couple external vibration to the cantilever. In addition, the cell should also be easy to use and clean. Details about fabrication of a simple fluid cell for SLB measurement are provided by Unsay *et al*.[64]

The resolution of the AFM scan depends on several factors, including tip geometry, tip cleanliness, tip spring constant, and the scanning speed. With correct technique, subnanometer resolution imaging can be obtained. Typically, a silicon nitride tip with a spring constant of about 0.1 N/m, slow scan speed (5 $\mu m^2/s$) and scanning force below 20 nN will improve the quality of the AFM images in contact mode. Higher spring constant tips (2 N/m) may be used in tapping mode, but the speed should still be kept under 5 $\mu m^2/s$. However, AFM is limited by tip convolution, which can be minimized through optimum tip geometry and image processing tools. It is therefore essential that the operator understand and optimize the parameters of the AFM scan for the specific SLB system. Figure 1.4 shows an example of a high resolution topography scans of phase-separated gel 1,2-dipalmitoyl-*sn*-glycero-3-phosphoethanolamine (DPPE) domains in a continuous fluid phase of 1,2-dioleoyl-*sn*-glycero-3-phosphocholine (DOPC) lipids. The DPPE domains are about 1.5 nm thicker.

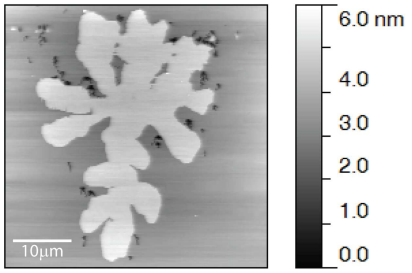

Figure 1.4. 45x45 µm AFM image of a gel phase DPPE domain in a 3:7 DPPE-DOPC SLB on mica. The SLB was asymmetric with an inner DPPE monolayer and outer 3:7 DPPE-DOPC monolayer LB deposited.

3.3. Surface Force Apparatus (SFA). Various direct force-measuring techniques has been developed which enable the interaction between membranes of various geometries to be measured.[61, 65] The SFA directly measures the full force profile between two SLBs at the angstrom (0.1 nm) level in liquids with a resolution of 10^{-8} N using a variety of (interchangeable) force-measuring springs. The solution in the SFA can be exchanged with SLBs in-situ to study their interactions under different conditions.[20, 26, 66-67] SFA characterization is very powerful because the interaction force profile, thickness and refractive index of the SLB can be determined unambiguously, and structural rearrangements can be observed when the SLBs are in contact.[19, 67] Figure 1.5 shows example interaction force-distance profiles between liquid-ordered SLBs, demonstrating the ability to measure nanoscopic structural rearrangement of the SLBs. A positive force indicates repulsion and a negative value indicates adhesion between the surfaces. The measured profile is the sum of any interactions present such as electrostatic, steric, van der Waals, depletion, and hydrophobic

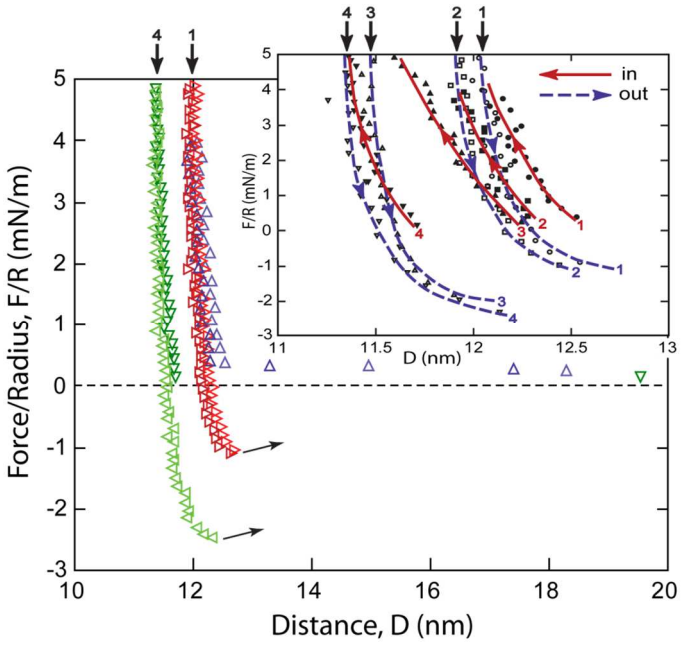

Figure 1.5. Force-distance profiles between asymmetric SLBs composed of an outer 1:1:1 DOPC-DPPC-cholesterol monolayer on an inner DPPE monolayer in ~0.5 mM $NaNO_3$ solution. D = 0 is defined as contact between bare mica surfaces. The inset shows four successively measured force profiles while allowing longer contact time between each distance displacement. There is an inward shift to smaller separations (decreasing membrane thickness) and greater adhesion due to lipid rearrangements in the contacting region (△,▽: approach ; ◁,▷ : separation).

forces. By careful experimental design, the contribution of the various interactions can be separated and quantified.

The substrate used in SFA is usually back-silvered, molecularly smooth mica which is glued onto a cylindrical disk (radius of ~1.5 cm). Once the mica is glued onto the disk, the desired SLB can be deposited, typically using the more controlled LB technique. After membrane deposition, the surfaces are transferred under water into the SFA box and the solution is saturated with lipid of the same composition as the membrane to minimize desorption of lipids from the surfaces. The two surfaces are positioned in a cross-cylindrical configuration which is locally equivalent to a sphere near a flat surface or two spheres close together. White light is passed through the opposing surfaces and the emerging beam is focused onto the slit of a grating spectrometer. The silver layer on each disk partially transmits light directed normally through the surfaces, which constructively interferes and produces fringes of equal chromatic order (FECO). The distance between the two surfaces can be adjusted using a motor connected to the lower surface or piezo connected to the upper surface. The separation between the surfaces is measured by monitoring the wavelength of the FECO. The lower surface is supported on a double cantilever spring with a known spring constant (typically around 2×10^5 mN/m for SLBs). Both repulsive and attractive forces can be measured and the force profile can be obtained over a large distance regime. Once the force F as a function of distance D is measured for the two surfaces (of radius R), the adhesion or interfacial energy E per unit area can be calculated using the Derjaguin approximation: $E = F/2\pi R$. Thus, for $R \sim 1$ cm, and given the measuring sensitivity in F of about 10^{-8} N, the sensitivity in measuring adhesion and interfacial energies is approximately to 10^{-3} mJ·m^{-2}

(erg·cm^{-2}). In addition to measuring interaction forces between two solid supported membranes,[20, 26, 66-67] the SFA has been used to probe the interaction between SLBs and substrates,[68] hemifusion of SLBs,[69-70] membrane mediated receptor-ligand interactions,[71-72] as well as the refractive index and thickness of supported monolayers and membranes.[19-20]

3.4. X-ray and Neutron Reflectivity. X-ray and neutron reflectivity are powerful surface-sensitive characterization techniques which provide information such as the thickness, density profile, and roughness down to the atomic scale of a thin-film deposited on solid substrate. Reflectivity, *R*, is defined as the intensity ratio of X-rays or neutrons (hereafter referred to as "particles") elastically and specularly scattered from the surface relative to the incident particle beam. The reflectivity is measured as a function of the wave vector transfer $q_z = \frac{4\pi sin\theta}{\lambda}$ perpendicular to the interface, where θ is the angle of the beam to the sample and λ is the wavelength of the particle beam. When measured this way, the reflectivity curve contains information regarding the average scattering length density of the sample normal to the interface and can be used to determine the concentration of atomic species at a particular depth in the film. Detailed theoretical descriptions of reflectivity measurements of SLBs can be found in the literature.[73-79] An example X-ray reflectivity profile from a DPPC SLB LB deposited on quartz is shown in Figure 1.6A.[22] The visible fringes in the reflectivity profile arise from interference between waves being reflected from the membrane-solution interface and membrane-substrate interface. The amplitude of the fringes relates to the scattering length density (SLD) contrast between the substrate, lipid headgroups, and acyl chains of the bilayer. While, the fringe spacing $\Delta q_z \approx \frac{2\pi}{d_{layer}}$ is related to the thickness of the film (d_{layer}). From the measured reflectivity profile, the SLD, thicknesses, and roughness of the various layers can be

determined by modeling the expected SLD profile and iterating to minimize the difference between the measured reflectivity profile and that obtained from the modeled SLD profile. However, as the majority of reflectivity measurements only provide intensity information, the structural information of interest is indirectly contained within the reflectivity data. The transformation of the data from inverse space to real space, in the absence of phase information, is mildly ill-posed and multiple solutions can be obtained. Limiting the possible solutions through constraints based on the known chemical identities of the layers, expected thickness, and other information. is extremely helpful. The corresponding scattering length density profile of the DPPC bilayer fitted to the measured reflectivity profile is shown in Figure 1.6B.

There are a number of key differences between neutron and X-ray scattering. Neutrons can penetrate large sample volumes and do not damage the sample as the beam is scattered by the atomic nuclei. Selective contrast can be achieved by deuteration of lipids/proteins and solvent contrast variation.[36] On the other hand, X-ray sources are much more brilliant. Because the beam is scattered by electrons in the sample, significant energy is deposited in the sample which can quickly degrade organic samples. Although contrast is limited to the electron density of the film, the high intensity of X-rays allows higher resolution measurements as shown in Figure 1.6A. The intensity also enables diffraction measurement from ordered SLBs, yielding molecular details such as tilt angle, packing parameters, and coupling between leaflets from the off-specular diffraction signals (grazing incidence X-ray diffraction or GIXD).[22, 27]

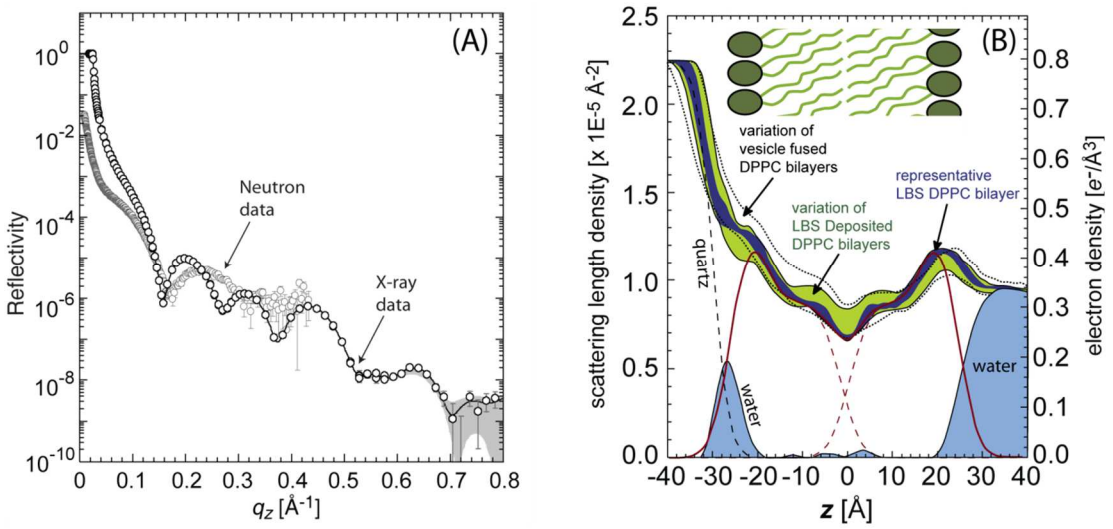

Figure 1.6. [A] Reflectivity data obtained from both neutron and X-ray scattering measurements of solid supported DPPC bilayers. The X-ray data covers a much larger q-range yielding higher resolution. [B] Density of DPPC bilayers deposited using LB-LS (LBS) and VF method obtained using X-ray reflectivity (scattering length density). From the density data, the thickness of the DPPC SLB and number of water molecules associated with the bilayer and substrate can be inferred.

SLBs for neutron and X-ray reflectivity are prepared on specifically ultra-polished smooth, single-crystal substrates (e.g. quartz, oxidized silicon, sapphire) using LB-LS or vesicle fusion. The sample is then mounted in a holder and the neutron/X-ray beam is reflected off the substrate through the SLB, which sits in a thin water layer. The scan area for neutron reflectivity is approximately 10-100 cm^2; a significantly smaller area of about 0.1 cm^2 can be used for X-ray reflectivity. The scattered signal and the quality of the data are dependent on a couple of factors, such as interfacial roughness (quality of the substrate and SLB), contrast of the various layers, and the level of incoherent scattering from the bulk liquid. For the purposes of obtaining basic structural information about an SLB with high resolution, higher fluxes of the X-ray source coupled with faster measurement times make X-ray reflectivity generally superior to neutron reflectivity. On the other hand, neutron reflectivity can take advantage of deuteration to enable measurements such as the flip-flop of lipids between the inner and outer leaflets of a bilayer.[35]

Details about neutron scattering characterization methods, including a discussion of advantages, limiting factors, recent works of SLB characterization, and extension of the use of neutron scattering on various platforms can be found in several recent publications.[74, 80-81]

3.5. Quartz Crystal Microbalance (QCM). QCM can be used to track the quantity of absorbed mass on a solid with time. The quartz crystal oscillates with a frequency dependent on crystal thickness. When films are deposited on the crystal, the frequency of the oscillation decreases and the change in the oscillation frequency can be correlated to the change in thickness. The thickness of the deposited layer can be calculated by an equation developed by Sauerbrey.[82] In the case of SLBs, QCM measurements have been used to study the process of vesicle fusion as a function of time. In-depth studies of the mechanics of vesicle fusion with various lipid mixtures have been performed to determine parameters that affect vesicle adsorption kinetics upon various substrates.[83-85] QCM can also be coupled with other techniques such as AFM and surface plasmon resonance to visualize the various stages of SLB formation via vesicle fusion.[86-87] In addition to obtaining information on the mechanism of vesicle fusion, QCM probes the interaction between various lipids with different types of substrates,[88] and the interaction between deposited SLBs and proteins[89] or nanoparticles.[90] An in-depth discussion of the specifics of QCM technique, including its diverse uses extending beyond SLB systems, can be found in following works by Cooper and coworkers.[82, 91]

4. EXPLORATION OF IDEAL SLB DEPOSITION CONDITIONS

In most cases, a clean, stable, and well-packed membrane is especially desirable for studies involving SLBs. Membrane topological defects, which span the outer monolayer or in some cases penetrate the inner monolayer, are typically present when SLBs are deposited with any commonly used preparation technique. In most cases, these membrane topological defects are nanoscopic and not visible through fluorescence microscopy.[70, 92-94] However, such nanoscopic features can be resolved by high-resolution AFM topography scans and play an important role in altering the molecular structure and behavior of the SLB. Both qualitative and quantitative comparisons of SLBs deposited by various techniques were performed to identify the best procedures and conditions for constructing an ideal system: a stable SLB with minimal topological defects. Important experimental deposition parameters such as lipid phase state, surface pressure during deposition, packing properties of the inner monolayer leaflet, substrate roughness, and other preparation conditions significantly affect the quality of the resulting SLB. All of these parameters were probed using qualitative observation of the SLB using FM, quantitative transfer ratio measurements conducted with LB deposition technique, and high-resolution AFM topography scan to quantify membrane topological defects (hereafter referred to as membrane defects).

4.1. Quantification of SLB quality by transfer ratio experiments. An important quantification of the quality of the deposited inner and outer monolayers is a transfer ratio measurement using LB deposition. The transfer ratio is defined as the ratio of area of lipids removed from the air-water interface to that of the substrate area coated during the deposition. Table 1.1 summarizes the transfer ratios of various lipid mixtures deposited with LB technique for inner

and outer monolayers at 25°C on different substrates.

4.1.1. Surface chemistry and substrate roughness. The studied substrates were mica, silicon wafers, and microscope slides (borosilicate glass) to quantify the effect of surface chemistry and substrate roughness on the deposition quality. In general, the transfer of lipid monolayers onto regular coverslip glass resulted in higher transfer ratios than onto mica or silicon wafers. This is likely the result of the significantly larger surface roughness of glass (root mean square height of 8-10 Å) compared to silicon wafers (2-3 Å) or mica (0.2 Å), creating a larger effective surface area on the glass. The transfer ratio of pure, fluid and transition phase lipids increased from about 95% surface coverage on mica to ~100% on borosilicate glass. Similar observations were seen for mixed lipid systems containing cholesterol, where the transfer ratio increased from less than 90% to about 100%. The only cases where the transfer onto mica was greater were for gel phase DPPE and DPPC. One hypothesis formulated from these observations is that the greater stiffness of the gel phase monolayer prevents good conformity and physisorption onto rough glass slides. Conversely, mica's and silicon's ultra-smooth surfaces are especially well suited for transfer of gel phase monolayers. When the monolayer contains cholesterol, or exists at fluid or transition phases, it can conform to the roughness of the glass substrate and result in a higher transfer ratio. We also examined the transfer ratio of various lipid mixtures transferred onto DPPE and DPPC monolayers on both mica and borosilicate glass. However, the inner monolayer always delaminated when it was deposited on borosilicate glass, again reinforcing the need for the LS method for the outer leaflet. Thus, outer layer transfer ratios were only done using mica substrates.

4.1.2. Lipid phase state. The phase state of the inner lipid monolayer, which is controlled by the lipid composition and temperature, also greatly affected the transfer ratio of the outer leaflet. The transfer ratio of fluid onto fluid (DTPC on DTPC) and transition onto transition (DMPC on DMPC) were below 80%. However, the transfer of gel onto gel (DPPC on DPPC), gel onto fluid (DPPC on DTPC), and fluid onto gel (DTPC on DPPC) was significantly higher. In addition, gel phase lipids provided a good base for LB deposition of outer monolayers of various phases. In some cases, interleaflet lipid coupling enhanced the transfer ratio of the outer layer, as can be seen on transfer of DPPC onto DPPC.[22, 27] The coupling condensed the DPPC SLB and resulted in a transfer ratio above 100%. These findings, based on transfer ratio experiments about the importance of lipid phase and interleaflet coupling, are corroborated using AFM topography scans described in detail in section 4.2.

4.1.3. Effect of drying the inner monolayer. Further characterization of outer leaflet deposition was performed on LB deposited DPPE at 45 mN/m with a dipping speed of 1 mm/min. We measured transfer ratios of freshly deposited DPPE inner monolayers and monolayers that were dried overnight. If the outer layer deposition was delayed for at least 8 hours after deposition of the inner monolayer, the transfer ratio of outer leaflets were increased for the various types of lipid monolayers. We hypothesize that the drying time between the deposition of the inner and outer monolayer helped to remove trapped moisture on the inner monolayer and trapped between the monolayer and substrate, which would reduce the transfer ratio of the outer monolayer. However, further characterization must be conducted.

Table 1.1. Transfer Ratio Summary of Various Lipid Mixtures deposited with the LB technique

	Lipid	Deposited on	Phase	Transfer Ratio
Inner Layer	DTPC	Borosilicate Glass	Fluid	102.8 ± 0.7
	DMPC	Borosilicate Glass	Transition (Gel to Fluid)	100.5 ± 0.8
	DPPC	Borosilicate Glass	Gel	89.9 ± 1.0
	DPPE	**Borosilicate Glass**	**Gel**	**92.0 ± 3.6**
	92:8 DPPC-chol.	Borosilicate Glass	Gel	100.1 ±0.3
	1:1:2 BSM-POPC-chol.	Borosilicate Glass	Liquid Ordered	102.3 ±3.2
	DTPC	Mica	Fluid	93.4 ± 1.3
	DMPC	Mica	Transition (Gel to Fluid)	95.7 ± 1.1
	DPPC	Mica	Gel	97.2 ± 1.8
	DPPE	**Mica**	**Gel**	**98.2 ± 1.3**
	92:8 DPPC-chol.	Mica	Gel	88.8 ± 3.0
	1:1:2 BSM-POPC-chol.	Mica	Liquid Ordered	80.1 ± 1.8
	DTPC	Silicon Wafers	Fluid	93.7 ± 2.0
	DMPC	Silicon Wafers	Transition (Gel to Fluid)	96.5 ± 0.5
	DPPC	Silicon Wafers	Gel	96.2 ± 0.7
	DPPE	**Silicon Wafers**	**Gel**	**95.9 ± 1.7**
Outer Layer (substrate: mica)	DTPC	DTPC	Fluid	61.7 ± 5.6
	DPPE	DTPC	Gel	96.2 ± 0.4
	DMPC	DMPC	Transition (Gel to Fluid)	75.1 ± 1.8
	DPPC	DPPC	Gel	102.1 ± 0.6
	DTPC	DPPC	Fluid	98.4 ± 0.7
	DTPC	DPPE	Fluid	97.5 ± 1.6
	DMPC	DPPE	Transition (Gel to Fluid)	96.0 ± 1.6
	DPPC	DPPE	Gel	90.5 ± 1.2
	92:8 DPPC-chol.	DPPE	Gel	95.8 ± 0.7
	1:1:1 DPPC-POPC-chol.	DPPE	Liquid Ordered	96.0 ± 1.4
	1:1:2 BSM-POPC-chol.	DPPE	Liquid Ordered	98.6 ± 1.1
	DTPC	Dried DPPE	Fluid	99.0 ± 2.1
	DMPC	Dried DPPE	Transition (Gel to Fluid)	97.3 ± 0.5
	DPPC	Dried DPPE	Gel	97.7 ± 2.1
	92:8 DPPC-chol.	Dried DPPE	Gel	97.8 ± 0.8
	1:1:1 DPPC-POPC-chol.	Dried DPPE	Liquid Ordered	98.3 ± 0.3
	1:1:2 BSM-POPC-chol.	Dried DPPE	Liquid Ordered	99.5 ± 1.8

4.2. AFM Characterization of Membrane Defects to assess SLB Quality. Another quantification method to assess the quality of the deposited SLB is high-resolution AFM topography scans to quantify nanoscopic membrane defects, which are not resolvable using FM technique. Some of the AFM probed deposition parameters, such as lipid phase state, surface roughness, surface chemistry, and interleaflet couplings, corroborate the results from transfer ratio measurements, as detailed in the following subsections.

4.2.1. Lipid phase state and substrate roughness on the quality of inner monolayer. First, the quality of LB deposited inner monolayers was determined for various lipids in different phase states at a dipping speed of 1 mm/min. The monolayers were scanned using AFM in air to reveal the presence of defects in the inner monolayer (Figure 1.7). The surface pressure of the LB deposition for each monolayer was chosen to be where the slope of the isotherm was the steepest for each respective lipid mixture. For monolayers in

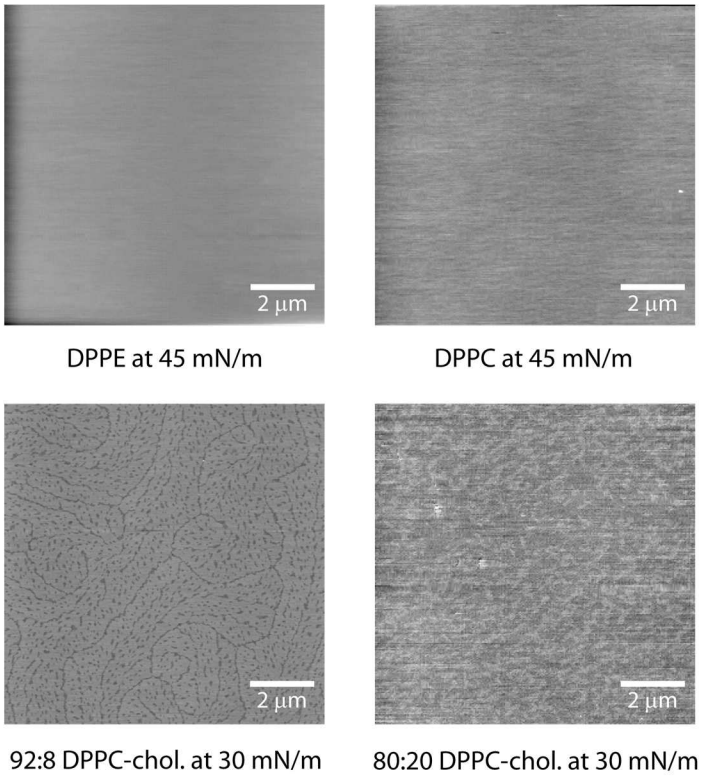

Figure 1.7. Representative 10x10 μm AFM topography scans of various monolayers LB deposited with dipping speed of 1 mm/min on mica. The DPPE and DPPC monolayer were deposited at surface pressure of 45mN/m and the 92:8 DPPC-chol. and 80:20 DPPC-chol. were deposited at surface pressure of 30 mN/m.

the gel phase, AFM scans showed that DPPE and DPPC monolayers had almost no defects across the sample, ≤0.5% and ≤1% respectively. AFM scans of DPPC-cholesterol mixtures showed topographical features with 3-5 Å differences in height corresponding to coexisting gel and liquid-ordered phase, but no topological defects greater than 2 nm in depth. High quality AFM topography scan of fluid phase DMPC and DTPC monolayers were not obtainable as these fluid lipids were constantly stuck to the AFM tip during contact or tapping mode scans. Many studies use gel phase inner leaflets to minimize exchange between leaflets. When both leaflets are in the fluid state, exchange between them is rapid.[32, 35] Delamination of the inner monolayer during deposition of the outer layer can also occur if the physisorption of the inner monolayer is not strong enough. This is the main motivation for choosing LS over LB deposition of outer monolayer leaflets. In the case of mica substrates, the physisorption strength is sufficient to allow LB deposition of both leaflets. With glass, silica, oxidized silicon wafers, and quartz, the inner leaflet delaminates when attempting to deposit the outer leaflet and LS transfer must be used. Figure 8 shows the quality of LB deposited DPPC monolayers on various substrates. Because of mica's low roughness (RMS of ~0.2 Å), DPPC monolayers deposited on mica have fewer defects compared to DPPC monolayers on silicon wafers (RMS of 3-4 Å). Highly polished quartz and silicon wafers (RMS of 2-4 Å) are typically used in ellipsometry and X-ray and neutron reflectivity experiments.

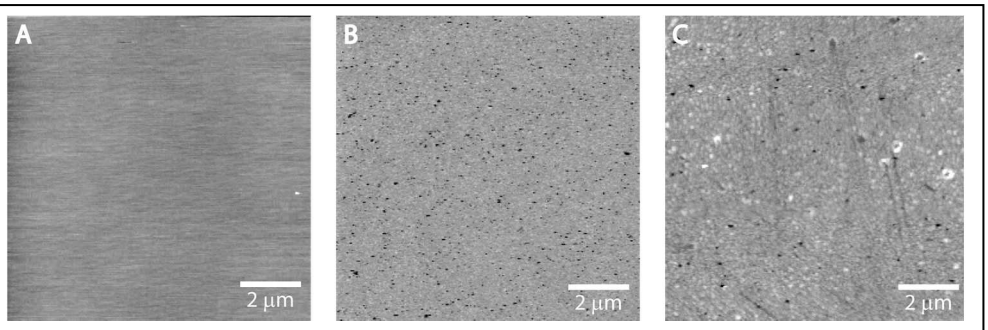

Figure 1.8. Representative 10x10 μm AFM topography scans of DPPC monolayers LB deposited at surface pressure of 45mN/m on mica (A), silicon wafer (B), and glass slide (C).

4.2.2. Significance of interleaflet coupling and packing of inner monolayer on SLB quality. A previous study by Watkins *et al*.[27] used X-ray diffraction to demonstrate the importance of interleaflet coupling between the inner and outer monolayer in the SLB. Thus, the quality of the outer leaflet may, in fact, depend on the completeness of the inner monolayer.[92] Inter-leaflet coupling and the importance of a well-packed inner leaflet were quantified by characterizing the resulting SLB with a series of symmetric and asymmetric SLB compositions. To minimize the parameter space, two gel phase compositions were studied, DPPC and 92:8 DPPC-cholesterol, which were also scanned as monolayers (Figure 1.7). The symmetric SLBs were prepared using LB-LB deposition at 30 mN/m and a dipping speed of 1 mm/min for both the inner and outer monolayers. These symmetric SLBs were compared to asymmetric SLBs where the outer monolayer was deposited on a near defect-free DPPE inner monolayer. Figure 1.9 shows the AFM topography scans of the symmetric and asymmetric SLBs. The symmetric SLBs contain more defects than the asymmetric SLBs, clearly demonstrating the importance of a strongly physisorbed, defect-free inner leaflet. As demonstrated in numerous measurements of bilayer interactions, the exchange between the inner and outer gel

phase leaflet is minimal on mica, enabling the interaction of the outer leaflet composition membranes to be precisely determined.[20, 66-67, 69, 71]

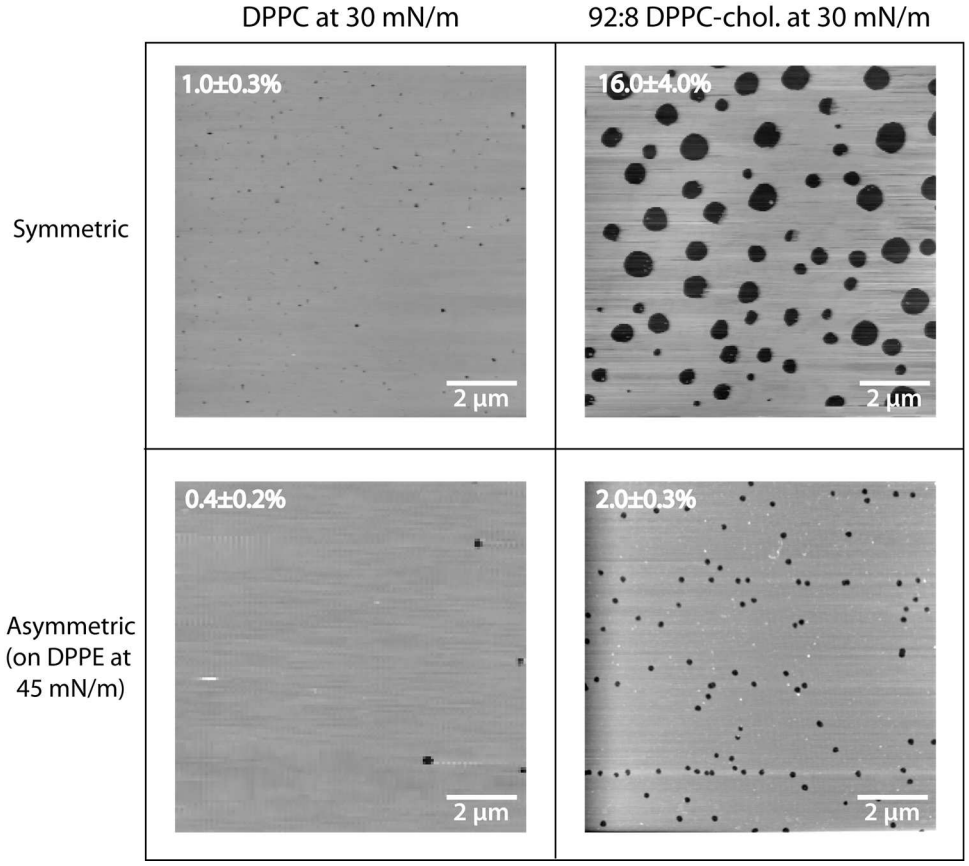

Figure 1.9. Representative 10x10 µm AFM topography scans of DPPC and 92:8 DPPC-chol. deposited as symmetric or asymmetric (on DPPE monolayer) bilayer showing varying amount of membrane topological defects.

4.2.3. Preparation technique and quality of SLBs. Recent studies of biomimetic "raft" membranes typically involve mixtures of high melting temperature lipids (saturated or sphingomyelin), low melting temperature lipids (unsaturated), and sterols. Depending on the ratio of the components and the temperature, the mixture could exist in gel, liquid order (L_o), liquid disorder (L_d), or multiple phases (i.e. co-existence between L_o/L_d phases) which mimic the liquid-liquid immiscibility region thought to exist in cellular

membranes. One frequently studied system is 1:1:1 DOPC-DPPC-cholesterol, which makes a uniform fluid phase biomimetic membrane. Using this system, the impact of preparation technique and deposition parameters on the quality of the deposited SLB was investigated. In the first case, we compared asymmetric bilayers where the first or inner monolayer was DPPE monolayer LB deposited on mica (45 mN/m) and the outer monolayer (or leaflet) was deposited by LB, LS, or vesicle fusion. AFM scans of the resulting SLBs clearly demonstrated that LB and LS yield more well-packed, complete membranes than does vesicle fusion (Figure 1.1E). The outer layer of fluid phase 1:1:1 DOPC-DPPC-cholesterol was LB deposited at surface pressure of 30 mN/m and dipping speed of 4 mm/min, LS at surface pressure of 30 mN/m, or formed by VF technique 45 minutes incubation using 1 mg/mL SUV solution. In all cases, AFM scans of the resulting SLBs showed nanoscopic monolayer defects down to the inner DPPE monolayer (Figure 1.1E). However, the distribution/density and the uniformity of the defects varied depending on the deposition technique. SLBs with an LB-deposited outer layer showed the fewest defects. The quantity of defects increased when LS was used. In LB, the substrate is slowly dipped vertically through the lipid monolayer at air-water interface while maintaining a constant surface pressure. We hypothesize that small lateral defects form either during the deposition process or from a small condensation of the lipids when contacted with the DPPE layer. For the LS technique, the substrate is stamped through the monolayer at the air-water interface. Alignment of the substrate parallel to the monolayer (minimizing monolayer film displacement) is critical to obtain a high quality transfer. In the case of a VF-deposited outer layer, the quality of the SLB was

much worse than an SLB constructed with LB or LS technique. Even though LB and LS showed better quality SLBs, a majority of studies use vesicle fusion as the preparation technique. Qualitative observation with FM revealed that the VF deposited membranes contained microscopic defects (>1 μm) and generally were less homogeneous, particularly in preparing asymmetric SLBs (Figure 1.1). Moreover, the quality of the asymmetric SLB form when vesicles fused to an LB deposited monolayer had significantly less uniformity then when vesicles were fused to a bare substrate. In addition, nanoscopic membrane defects also exist. Finally, excess vesicles are hard to completely remove from the system, and the lack of control over the deposited membrane's surface pressure makes VF inferior to the LB and LS techniques. Still, VF is the most straightforward method to make SLBs and the only method that can be used to perform backfilling for membrane lithography (filling up defects or areas with no bilayer or only a monolayer on the surface).[95] Figure 1.10 provides an example of UV photolithography to create a membrane pattern of DMPC squares enclosed by backfilled Bovine Serum Albumin (BSA). Details for how to UV pattern SLBs are provided in the following references.[96-97] Importantly, VF can also be used to insert polypeptides[98] or membrane proteins into SLBs.

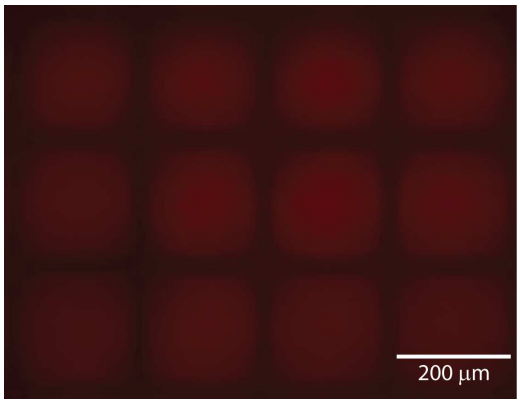

Figure 1.10. 200x200 μm squares of DMPC SLB enclosed by BSA created using UV photolitography technique. The BSA was backfilled after the UV patterning of the SLB.

4.2.4. Cholesterol in altering the phase state and SLB quality. Cholesterol, a specific type of sterol, is known to alter the packing or phase of 1,2-dipalmitoyl-sn-glycero-3-phosphocholine (DPPC) monolayers. The transition between the gel and liquid order phase occurs at ~15 mol% cholesterol.[99] In order to study the effect of cholesterol and phase state on the quality of LB deposited SLBs, binary mixtures composed of DPPC with various cholesterol concentrations were deposited on a robust, near defect-free DPPE inner monolayer (Figure 1.11). As the amount of cholesterol increased from 0-20 mole%, the mixed monolayer gradually transitions from a pure gel phase to a binary coexisting phase of gel and L_o. AFM scans showed that as the gel phase monolayer became more fluid, more defects were observed. Similar effects of increasing defect density with higher fluidity can be observed for any mixture of lipids, and thus LB and LS deposition are typically performed with the lipid mixture in the gel or solid phase state. Another advantage of deposition with gel phase systems is a lower flip-flop rate between the inner and outer leaflet, and a slower equilibration process (lipid dissolution into the subphase). Presaturating the working solution with lipids in the outer leaflets minimizes

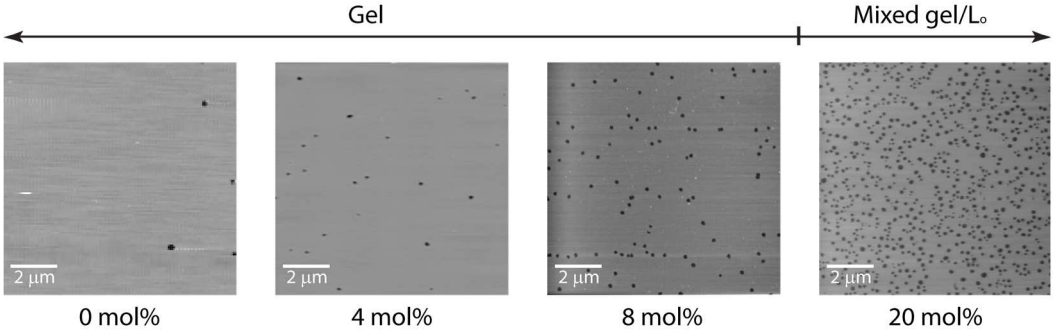

Figure 1.11. 10x10 μm AFM topography images showing defect density as function of cholesterol concentration in a DPPC outer leaflet at 25°C. The outer monolayers were deposited on a near defect-free DPPE inner monolayer on mica.

desorption for longer time experiments.

4.2.5. Surface pressure/area per molecule. Another important deposition parameter that dictates the quality of the resulting SLB is the surface pressure during deposition. The surface pressure-area (Π-*A*) isotherm depends on the lipid mixture and temperature, and can be used to select the desired lipid packing (area per molecule) of the deposited monolayer. Typically, deposition using LB or LS technique is conducted with a surface pressure where the slope of the Π-*A* isotherm curve is at its steepest (largest change in the surface pressure with small shift in area per molecule). The surface pressure is held constant during the deposition by decreasing the area of the monolayer film as material is transferred from the air-water interface to the substrate. Better uniformity and transfer occurs when the change in pressure is large for a small change in area. For this reason, layers cannot be transferred well in the coexisting regions and better transfers are typically obtained in the solid or gel phase state. The relationship between the surface pressure (or area per molecule) and amount of membrane defects in the deposited monolayer can be observed experimentally by AFM topography scans of LB-deposited 92:8 DPPC-cholesterol mixtures at various surface pressures. Figure 1.12 shows the pressure-area isotherm of 92:8 DPPC-cholesterol at 25°C and AFM scans of the asymmetric SLB composed of 92:8 DPPC-cholesterol deposited on DPPE at various surface pressures. In all cases, the dipping speed was 1 mm/min and the DPPE inner leaflet was deposited at 45 mN/m on mica. The SLB deposited at 30 mN/m shows the smallest defect size and lowest defect density. The higher total defect density and larger defect size at 40 mN/m is attributed to the lower

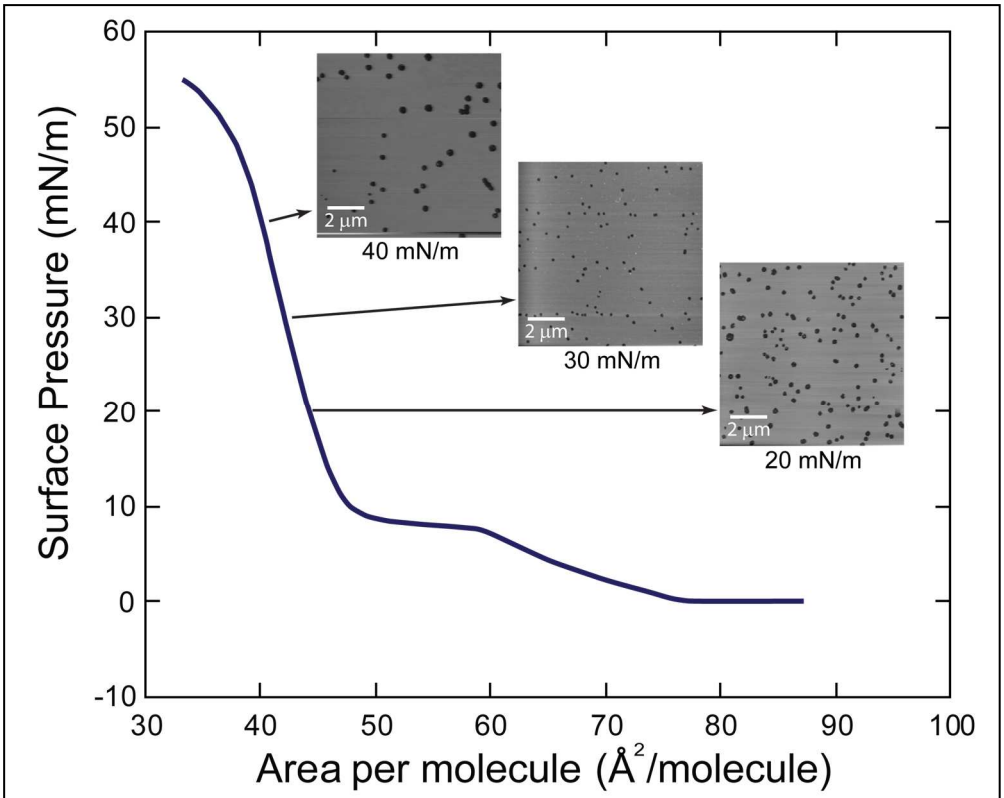

Figure 1.12. Effect of surface pressure on defects in LB deposited 92:8 DPPC-cholesterol on DPPE. Insets are 10x10 μm AFM topography images at surface pressure of 20, 30, and 40 mN/m. The outer leaflet was deposited at dipping speed of 1 mm/min and 25°C.

stability of the monolayer at this surface pressure where the slope of the Π-*A* curve is beginning to decrease. At the lower surface pressure of 20 mN/m, again a larger defect size and density occurs. One might hypothesize that the greater defect density at 20 mN/m compared to 30 mN/m is due to condensation of the deposited film and potentially driving to a more equilibrated state. However, a careful GIXD of pure DPPC membranes LB/LS deposited as a function of surface pressure on quartz demonstrated that these gel phases SLBs for the most part tracked and maintained the conditions under which they were deposited.[22, 27] Subtle changes were observed between monolayers and bilayers because of coupling between the leaflets, but to first order the packing and structure of the SLB followed the deposition pressure consistently.

5. CONCLUSION

The solid supported bilayer is a simple and robust platform which is extensively used to obtain biomimetic lipid membrane properties such as lateral topography, lipid mixing and phase state, dynamics/diffusion, as well as a base system for studies with proteins and other molecules of interest using various complementary characterization techniques. This instructional review discussed different preparation techniques to create SLBs with an emphasis on parameters and conditions that yield the highest quality bilayer. Membrane topological defects, which span the outer monolayer or in some cases penetrate the inner monolayer, were characterized. Some experiments using the SLB platform require a specific type of lipid mixture. Optimal deposition parameters such as lipid phase, surface pressure, inner leaflet packing, and substrate roughness were described in detail to aid in creating the best quality SLB for the desired studies. Comparisons of SLBs prepared with different methods were performed qualitatively by fluorescence microscopy, and quantitatively by transfer ratio measurements and high-resolution AFM topography scans. In general, SLBs prepared by LB-LB and LB-LS techniques are superior compared to vesicle fusion because of the lower defect density and absence of residual vesicles, which are undesirable for some characterization or subsequent measurement techniques. In addition, LB and LS deposition are further preferred as the surface pressure and packing area can be controlled. The SLB can also be modified by incorporating various molecules such as membrane proteins, and used to probe the inserted molecules. However, the study of membrane proteins on SLBs is limited to peripheral membrane proteins or integral membrane proteins that do not protrude out from membrane. The absence of a water cushion between the SLB and substrate frequently denatures trans-membrane proteins resulting in their

loss of function. The optimal deposition parameters for SLB are also relevant for polymer-cushioned SLBs, which are an extension of the SLB platform used for trans-membrane protein study.

ACKNOWLEDGEMENT

We would like to thank Yeeun Kim for the assistance with AFM sample preparations; Amanda Dang, Hilary Chan, Gregory Kittleson, and Shawn Mattathil for assistance with transfer ratio and fluorescence microscopy experiments.

Chapter II

Characterization of Solid-Supported Dipalmitoylphosphatidylcholine Membranes Containing Cholesterol

James Kurniawan[†] *and Tonya L. Kuhl**[†‡]
[†]Department of Chemical Engineering, University of California Davis, 95616, USA
[‡]Department of Biomedical Engineering, University of California Davis, 95616, USA
Corresponding Authors: *E-mail: tlkuhl@ucdavis.edu

Reproduced with permission from J. Kurniawan and T.L. Kuhl, *Characterization of Solid-Supported Dipalmitoylphosphatidylcholine Membranes Containing Cholesterol*. Langmuir, 2015. **31** (8), pp 2527–2532.

ABSTRACT

The incorporation of cholesterol into dipalmitoylphosphatidylcholine (DPPC) membranes, even in small amounts, has been shown to significantly alter the properties of the membrane. In this work, force-distance interaction profiles of DPPC membranes containing 8 mole% cholesterol obtained using the surface force apparatus are analyzed in the context of high resolution structural characterization by atomic force microscopy and neutron reflectometry. The adhesion between the mixed membranes was greater than that for pure DPPC and was variable – depending on the number of defects in the outer membrane leaflets. These defects were only detectable by atomic force microscopy and had an average size of 230±30 nm and 1-5% surface density in the outer leaflet. The adhesion between the membranes monotonically increased as the thickness of the membrane decreased – in direct correlation with the number of defects present (exposed hydrophobic groups) in the

membrane contact region. Due to the low diffusion rate of gel phase membranes, the interaction force profiles were stable and no membrane restructuring was observed.

INTRODUCTION

Cholesterol is an important building block in biological membranes and is found in every cell in the human body. Cholesterol's ubiquitousness underlines its important role in altering the physical[100-101] and thermodynamic properties of membranes by changing the packing or the ordering of lipids, reducing membrane permeability,[102-104] and in the formation of lipid rafts.[105-109] In particular, cholesterol is known to have a condensing effect on fluid phase lipids and to conversely fluidize solid phase lipids which helps maintain the integrity of cell membrane when stressed.[110-111] The concentration of cholesterol varies between different cell types and organelles with concentrations ranging from 5% [112] to as high as 50% [113] of the membrane. A plethora of studies have looked at the function of cholesterol in cell membranes and the effect of the addition of cholesterol in altering the intermolecular interactions in biomimetic membrane systems.[102, 114-116] For example, phase diagrams of binary and ternary lipid mixtures containing cholesterol are well-documented,[99, 117-118] and studies have also looked at the alteration of membrane mechanical properties due to preferential segregation of cholesterol.[101, 107] In terms of high resolution structural characterization, Mills *et al*.[119] quantified changes in the lamellar repeat distance in multilamellar DPPC vesicles with cholesterol using wide angle X-ray scattering. They found that, in general, addition of cholesterol resulted in the tighter packing of DPPC lipids which induced an increase in membrane thickness and lamellar spacing. Further, 8 mole% cholesterol had the largest effect on altering the packing of DPPC as the

mixture remains in the gel phase. Higher cholesterol concentrations result in coexisting gel and liquid ordered phases.

The alteration of lateral intermolecular interactions by cholesterol is well-established from an array of earlier work. However, much less is known regarding how the presence of cholesterol modifies the interactions between membranes. In this work, DPPC membranes with 8 mole% cholesterol were studied to quantify and understand how the addition of cholesterol to a DPPC membrane impacts supported membrane structure and membrane-membrane interactions in the gel phase. A comparison is made between measured membrane interaction force-distance profiles by surface force apparatus (SFA), neutron scattering structural characterization, vesicle zeta-potential (ZP), and membrane structure/topology as determined by atomic force microscopy (AFM).

MATERIALS AND METHODS

Chemicals. 1,2-dihexadecanoyl-*sn*-glycero-3-phosphoethanolamine (DPPE, melting point, T_M = 63°C), 1,2-dipalmitoyl-*sn*-glycero-3-phosphocholine (DPPC, T_M = 41°C), and cholesterol (ovine wool, >98%, T_M = 148°C) were purchased from Avanti Polar Lipids, Inc. (Alabaster, AL) and used as received. 2-(4,4-Difluoro-5,7-Diphenyl-4-Bora-3a,4a-Diaza-*s*-Indacene-3-Pentanoyl)-1-Hexadecanoyl-*sn*-Glycero-3-Phosphocholine (β-BODIPY® 530/550 C_5-HPC) was purchased from Life Technologies (Carlsbad, CA). Electrolyte solutions used $NaNO_3$ 99.995% (Sigma, St. Louis, MO). Water was purified with a MilliQ gradient water purification system to a resistivity of 18 MΩ·cm.

Sample Preparation. Mica substrate supported lipid bilayers were used in SFA, fluorescence microscopy (FM), and AFM studies. Neutron scattering studies used ultra smooth, single crystal quartz. The membranes were constructed using Langmuir-Blodgett (LB) deposition (Nima Coventry, U.K.). The inner monolayer for SFA, AFM and FM experiments was DPPE LB deposited at 45 mN/m and dipping speed of 1 mm/min. Mixtures for FM imaging contained 0.5% of Bodipy-HPC. Previous studies show that LB deposited DPPE forms an almost defect free, robust and strongly physisorbed monolayer on mica with transfer ratios of 0.997 ± 0.004 [66] with a thickness of 2.56 ± 0.05 nm under these conditions.[19] The tight packing and stability of the gel phase DPPE inner monolayer minimizes molecular exchange between the two leaflets and provides an ideal base for the 92:8 monolayer, which is the primary interest of this study. In all cases, the outer monolayer was 92:8 DPPC-cholesterol deposited at 30mN/m. For the SFA, FM, and AFM work, the outer leaflet was LB deposited with a dipping speed of 4 mm/min. The transfer ratio of the outer monolayer was 0.843±0.057. For neutron scattering measurements, a symmetric membrane of 92:8 DPPC-cholesterol was used for ease of modeling and analysis. The inner leaflet was deposited by LB at 30 mN/m and dipping speed of 1

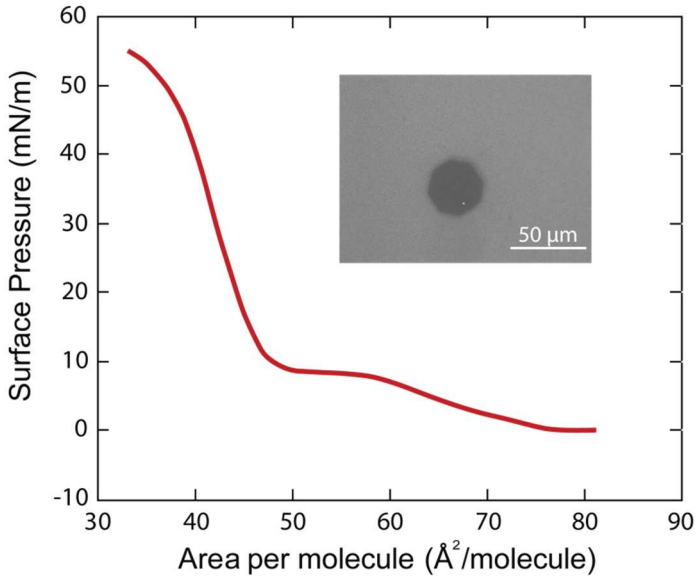

Figure 2.1. Isotherm of 92:8 DPPC-cholesterol at 25°C. (Inset) FM image of the 92:8 DPPC-cholesterol membrane at 40x magnification with a photobleached spot. The diffusivity of the DPPC-cholesterol mixtures was very low (almost no recovery observed after 3 hours).

mm/min on quartz substrates. Because of the weaker adhesion of the membrane to quartz vs. mica, the outer leaflet was deposited by Langmuir-Schaefer (LS) method where the monolayer coated quartz was stamped horizontally through the lipid monolayer on the air-water interface to form the symmetric bilayer. The isotherm for 92:8 DPPC-cholesterol is shown in Figure 2.1.

Vesicle solutions for zeta potential measurements were prepared using the extrusion method. 92:8 DPPC-cholesterol mixtures were prepared in chloroform, dried under nitrogen and then placed under vacuum for at least 4 hours. The dried lipids were hydrated with 0.5mM $NaNO_3$ solution prepared in MiliQ-water to a concentration of 0.4 mg/mL, heated to a temperature of 50°C, and then extruded through a 100 nm pore size polycarbonate membrane for 10 passes while maintaining the temperature around 50°C. After the extrusion process, the vesicle solution was placed in a warm water bath (~50°C) and then cooled down slowly to 25°C by placing the bath with the vesicle solution in a temperature controlled room at 25°C.

Surface Force Measurements (SFA). The SFA technique has been used extensively to measure the interaction forces between surfaces and details of the technique can be found in the following references.[120-122] Based on multiple-beam interferometry (MBI), the SFA provides a definitive reference for the surface separation (±0.2 nm in this work). Briefly, one of the membrane coated mica surfaces was mounted on a fixed stage and the other on a double cantilever spring of known stiffness (~$2.6x10^5$ mN/m) which can be displaced vertically. The back of the mica substrates was coated with a 55 nm thick, evaporated silver layer. The silver layer on each disk partially transmits light directed normally through the surfaces which constructively interferes producing fringes of equal chromatic order (FECO). The distances between the surfaces can be measured by observation of the position and displacement of

FECO peak wavelengths within a spectrometer. A custom automated SFA Mark-II was used for data collection.[72] The system enables constant and/or variable surface displacements via a computer-controlled motor system. A sensitive CCD camera (Princeton SPEC-10:2K Roper Scientific, Trenton, NJ) was interfaced with the spectrometer and computer acquisition system to allow automated FECO wavelength determination, which was used to determine the separation distance.

After lipid bilayer deposition, the surfaces were transferred and mounted into the SFA under water. The water in the SFA was saturated with 92:8 DPPC-cholesterol to minimize desorption from the surface during the course of the measurements. After the surfaces were mounted, the SFA was placed in a temperature-controlled room at 25.0°C for at least two hours to allow equilibration. The membrane thickness was determined using the FECO wavelength shift from membrane contact relative to bare mica substrates after completing each experiment. As the membranes were asymmetric with inner leaflets of DPPE and outer leaflets of DPPC containing 8 mole% cholesterol, we treat the two outer leaflets, which we are primarily interested in, as an equivalent membrane of the mixture composition. Force profiles shown in the results section are from three independent experiments which represent the range of typical force profiles obtained from six completely independent SFA experiments.

Atomic Force Microscopy (AFM). AFM images were acquired using a MFP3D-SA system (Asylum Research, Santa Barbara, CA). A silicon nitrite cantilever (model AC240, Bruker, Santa Barbara, CA) with force constant of 1 N/m was used for imaging. All the images were acquired in contact mode in MilliQ gradient water with a force of 37nN. AFM images were analyzed using Gwyddion Version 2.31 (http://gwyddion.net/).

Fluorescence Microscopy (FM). FM images were acquired using a Nikon Eclipse E600 microscope connected with CoolSNAP-Pro CCD camera at 10x and 40x magnification.

Zeta Potential Measurements (ZP). ZP was used to quantify the magnitude of the electrical charge based on measurements of vesicle mobility in an electric field (Brookhaven Zeta Plus, Holtsville, NY). Small amount of the vesicle dispersion (2.5 mL) was transferred into standard disposable polystyrene cuvette. ZP measurements were performed using NanoBrook 90Plus Zeta (λ = 659.0 nm) at 25°C, with an initial equilibration time of 15 minutes. The values of the viscosity and refractive index were set at 0.890 cP and 1.330, respectively. The mean ZP values were evaluated using Smoluchowski equation and the results were obtained from six independent samples with at least 10 measurements per sample. Although not identical with the surface charge or surface potential determination from force profile measurements by SFA, ZP provides the sign of the electrical charge and its relative magnitude referenced between the hydrodynamic shear plane at the vesicle surface and the bulk solution.

Neutron Reflectivity (NR). Reflectivity, R, is defined as the ratio of the number of neutrons elastically and specularly scattered from a surface to that of the incident beam. When measured as a function of the wave-vector transfer, $Q_Z = \left|k_{out} - k_{in}\right| = \frac{4\pi \sin\theta}{\lambda}$, where θ is the angle of incidence and λ is the wavelength of the neutron beam, the reflectivity curve contains information regarding the sample-normal profile of the in-plane averaged scattering length density (SLD) and is therefore most suited for studies of interfacial, layered films. From the measured reflectivity profile, the thickness, SLD, and roughness of the membrane normal to the substrate can be determined by minimizing the difference between the measured reflectivity profile and that obtained from a modeled SLD profile of the membrane.[123]

NR experiments were performed on the SPEAR beamline at the Manuel Lujan Neutron Scattering Center (Los Alamos National Laboratory). Neutron reflectivities down to R ≈ $1x10^{-6}$, and momentum transfers out to Q_z = ~0.2 $Å^{-1}$ were obtained. The uncertainty of the Q_z resolution, $\sigma Q_z/Q_z$, including instrumental resolution, was approximately 3% for the entire range of scattering vectors. NR data was modeled using Motofit (Rev. 409), a module in IgorPro 6.31. All measurements were done in D_2O at room temperature which varied between 24-28°C, well below the melting point of the membrane. Three independent experiments were done and about the same membrane thickness was obtained from each of the experiments. The NR profile shown in the results section is the data set from the most complete (highest quality) membrane.

RESULTS AND DISCUSSIONS

Force – distance profiles of 92:8 DPPC-cholesterol membranes. Figure 2.2 shows three independently measured force–distance profile between opposing 92:8 DPPC–cholesterol membranes in 0.5mM $NaNO_3$. The three different profiles capture the variation in measurements from six independent experiments. The average thickness obtained across all the measurements for an equivalent 92:8 DPPC-cholesterol bilayer was 5.9±0.3nm. A weak, long-range electrostatic repulsion was apparent in the force profiles with a decay length consistent with the electrolyte concentration. The electrostatic repulsion was fitted using the non-linear Poisson-Boltzmann with constant charge approximation. A constant surface charge density of 1.0±0.5 mC/m^2 or surface potential of 19±3 mV with the origin of charge at the membrane surface was obtained.[124] Although the ionization constant of cholesterol and PC

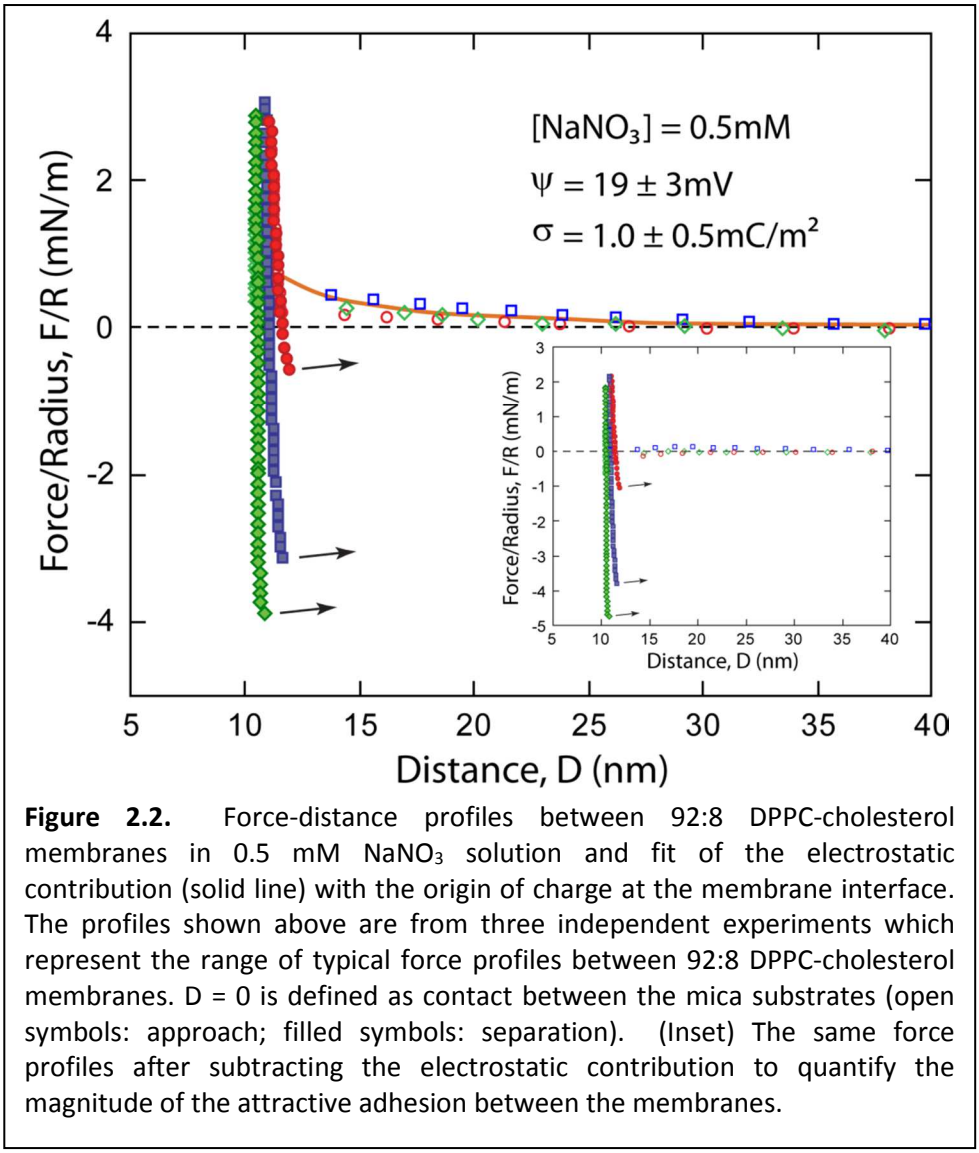

Figure 2.2. Force-distance profiles between 92:8 DPPC-cholesterol membranes in 0.5 mM $NaNO_3$ solution and fit of the electrostatic contribution (solid line) with the origin of charge at the membrane interface. The profiles shown above are from three independent experiments which represent the range of typical force profiles between 92:8 DPPC-cholesterol membranes. D = 0 is defined as contact between the mica substrates (open symbols: approach; filled symbols: separation). (Inset) The same force profiles after subtracting the electrostatic contribution to quantify the magnitude of the attractive adhesion between the membranes.

lipids[125-126] would suggest an overall neutral charge for the membranes, the presence of charged lipid impurities has been previously reported.[66, 127] The measured surface charge density corresponds to 1 negative charge per 400 lipids, or 0.25 mole% of impurities present in the mixture. In order to corroborate and further quantify the electrostatic repulsion in the 92:8 DPPC-cholesterol system, the zeta potential of vesicle suspensions was measured. The zeta potential of 92:8 DPPC-cholesterol vesicles was -9.8±3.8 mV,[32] which is in good agreement with the electrostatic charge measured in the SFA and our previous zeta potential measurements of

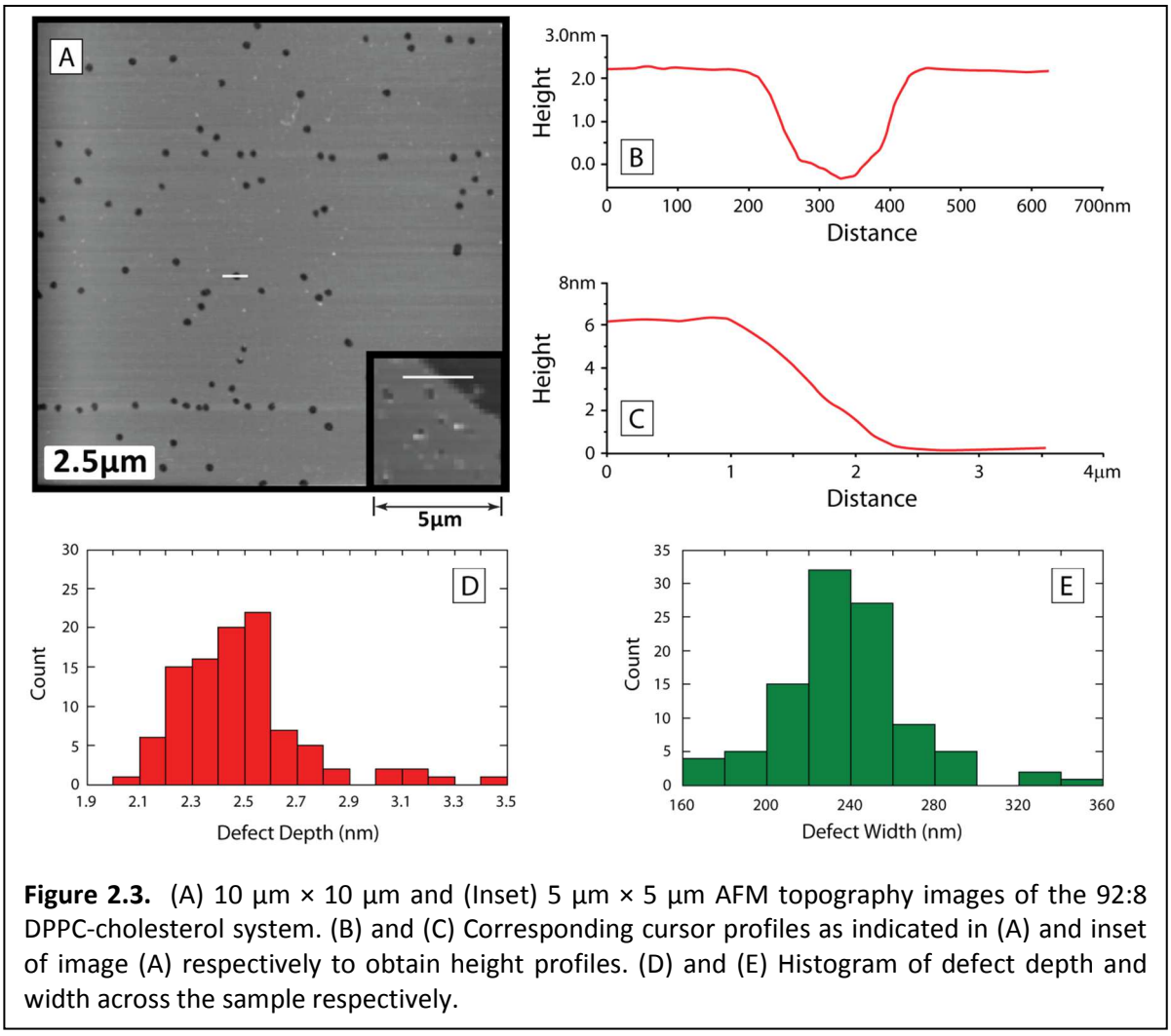

Figure 2.3. (A) 10 µm × 10 µm and (Inset) 5 µm × 5 µm AFM topography images of the 92:8 DPPC-cholesterol system. (B) and (C) Corresponding cursor profiles as indicated in (A) and inset of image (A) respectively to obtain height profiles. (D) and (E) Histogram of defect depth and width across the sample respectively.

similar lipid compositions.[66] The zeta potential and low incidence of membrane spanning defects observed from AFM scans, as described below, are consistent with the source of the electrostatic repulsion being due to the presence of lipid impurities with the origin of charge at the membrane surface. A more in-depth discussion about the source of electrostatic repulsion can be found in chapter III.

To better quantify the adhesion between the membranes, the electrostatic repulsion was subtracted from the force profile as shown in the inset of Figure 2.2. The adhesion between the 92:8 DPPC-cholesterol membranes varied from -1.1±0.1 to -4.7±0.1 mN/m and

was reproducible for a given contact region between the membranes. The strength of adhesion at the low end is comparable to pure gel phase DPPC membranes.[20,26] The higher adhesion values of some membrane contact positions are attributed to hydrophobic attraction due to membrane defects. Specifically, AFM scans of the 92:8 DPPC-cholesterol membrane (Figure 2.3) revealed nanoscopic monolayer defects in the outer 92:8 monolayer that extend down to the inner DPPE monolayer. The average depth of the defects was 2.5±0.2 nm. The lateral size of the defects was remarkably uniform, diameter = 230±30 nm. AFM scans of membranes devoid of cholesterol (a pure DPPC leaflet on an inner DPPE leaflet) showed an order of magnitude fewer defects strongly suggesting that the incorporation of cholesterol correlates with more defects (Figure 2.4).[37] These defects expose hydrophobic moieties resulting in a commensurate increase in the measured adhesion between the opposing membranes due to hydrophobic attraction. The variability in the adhesion is attributed to inhomogeneities in the membrane defect density, which ranged from 1 to 5% surface coverage,[36] rather than structural rearrangements as observed in fluid phase systems.[66] In one case, a membrane spanning hole that reached the mica substrate was detected by AFM (Figure 2.3B). The height scan thickness of the membrane was ~6 nm, which is in good agreement with the membrane thickness obtained from SFA measurements.

In all cases, membrane restructuring or thinning of the membrane was negligible during the course of an experiment, even under increased loads at contact. Reproducible force profiles and adhesive minima for a given contact position strongly suggests that the system does not rearrange during the time scale of the experiment. This observed trend is consistent with the small size of the defects and the gel phase behavior of the membrane (see Figure 2.1).

Hemifusion was not observed in any of the experiments due to the low diffusion and relatively low applied force during the course of the experiments. Conversely, fluid phase membranes containing defects have been shown to restructure in contact resulting in adhesion that depends on the applied load and contact time of the opposing membranes.[66]

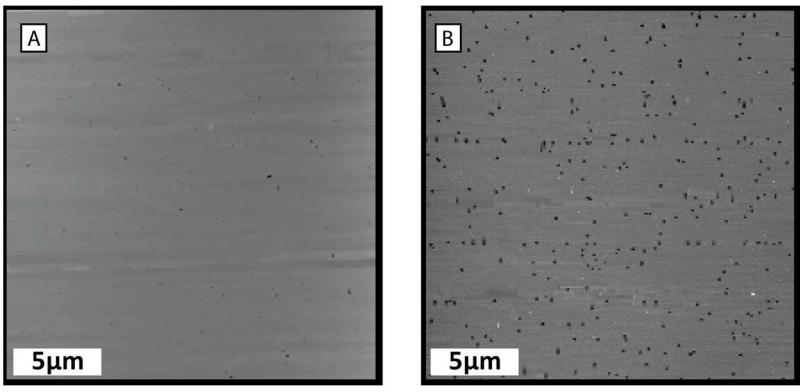

Figure 2.4. Representative 20x20 µm AFM images of membranes composed of (A) DPPC and (B) 92:8 DPPC-cholesterol outer monolayers respectively on inner DPPE monolayers. In the cholesterol devoid DPPC membrane, the defect density in multiple 10x10 µm AFM scans ranged between 0.1-0.5% surface coverage. In contrast, the 92:8 DPPC-cholesterol system had an order of magnitude larger defect surface density ranging from 1-5%.

Neutron Scattering Studies. The structure of supported 92:8 DPPC-cholesterol membranes on quartz was also characterized using NR and Figure 2.5 shows the best data set from three independent experiments. The thickness of the membrane was consistent between the three measurements, but the scattering length density (SLD) of the hydrocarbon region was somewhat higher for the other two cases. The hydrocarbon region SLD is indicative of membrane defects as the presence of D_2O in the defects increases the SLD. Due to the resolution of the NR data, which was primarily sensitive to the hydrocarbon region (acyl chains) of the bilayer, a simple 1-layer model of the membrane was used to represent the hydrocarbon

region and fit the data. The thickness of the box was 4.15±0.10 nm with an SLD of -0.3±0.2 x10^{-6} Å^{-2}. This value is in excellent agreement with the SLD of pure gel phase PC hydrocarbon tails of -0.41 x10^{-6} Å^{-2} obtained by Fragneto *et al*.[128], given that the neutron SLD of cholesterol is 0.21 x10^{-6} Å^{-2} and defect density of less than 5%.[35, 129] The other samples had somewhat higher hydrocarbon region SLDs indicative of higher defect densities. The uniform thickness of the hydrocarbon region for all the samples is also consistent with nanoscopic rather than macroscopic defects.

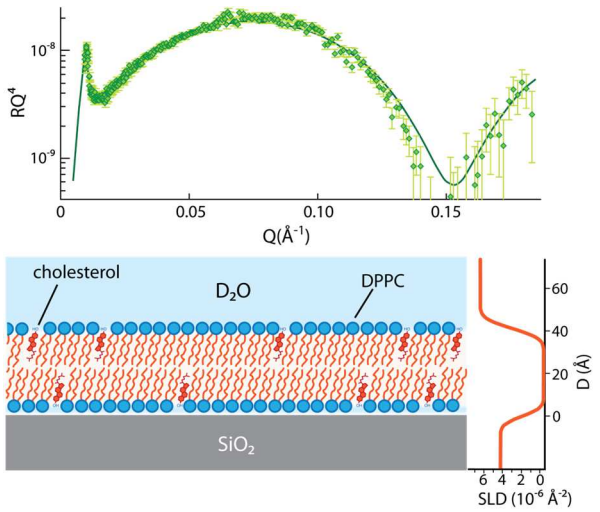

Figure 2.5. (Top image) Fit of RQ^4 vs Q from the neutron reflectivity data. (Bottom image) Schematic of the supported membrane and corresponding neutron scattering length density profile of the membrane obtained from fitting the data.

CONCLUSIONS

As one of the major components in biological membranes, the functions and properties of cholesterol have been widely studied and documented. In this work, a simplified system of a substrate supported membrane was used to measure the interaction forces between two cholesterol containing membranes and the structure of the membranes with ultra-high resolution. The interaction force-distance profiles between DPPC-cholesterol membranes measured using SFA and AFM imaging of the membrane revealed the presence of nanoscopic defects, which was attributed to an enhanced hydrophobic attraction between the membranes in contact. The non-homogeneity in the lateral defect distribution across the membrane, as

demonstrated by AFM and neutron scattering studies, leads to variation in the thickness of the membrane and membrane-membrane adhesion. A weak electrostatic repulsion, plausibly due to the presence of charged lipid impurities, was detected and further quantified by vesicle zeta potential measurements. Such studies demonstrate that cholesterol alters the intersurface interaction and membrane structure in complex and important ways.

ACKNOWLEDGEMENTS

This work was primarily supported by the NSF chemistry division through grant CHE-0957868 and completed under CHE-1413745. This work benefited from the neutron research facilities of the Manual Lujan Jr. Neutron Scattering Center which is supported by DOE under Contract No. W7405-ENG-36. We thank Joao Ventrici for assistance with atomic force microscopy, Araceli Munaier Almeida for assistance with transfer ratio measurements, and Christy Michelle Turcios for assistance with fluorescence microscopy measurements.

Chapter III

Interaction Forces between Ternary Lipid Bilayers Containing Cholesterol

James Kurniawan,† Nai-Ning Yin,‡ Gang-yu Liu,‡ and Tonya L. Kuhl†*
†Department of Chemical Engineering, University of California Davis, 95616, USA
‡Department of Chemistry, University of California Davis, 95616, USA
Corresponding Authors: *E-mail: tlkuhl@ucdavis.edu

ABSTRACT

Interaction force-distance profiles between substrate supported membranes composed of equimolar ternary mixtures of unsaturated phosphotidylcholine (PC) lipid, saturated PC lipid, and cholesterol were determined using the surface force apparatus. Both doubly and single unsaturated PC lipids were studied. In all cases, the membranes were slightly negatively charged resulting in a weak, long-range electrostatic repulsion. Corroborative atomic force microscopy, zeta potential, and fluorescence microscopy measurements were used to establish that a small level of charged lipid impurities (~1/400 lipid molecules) were responsible for the repulsive electrostatic interaction between the membranes. At contact, the membranes were adhesive. The magnitude of the adhesion was greater than the van der Waals interaction between pure PC membranes without cholesterol. The enhanced adhesion was primarily attributed to hydrophobic attraction due to the presence of nanoscopic membrane defects which exposed the underlying membrane leaflet. The interaction force-distance profiles also demonstrated that the nanoscopic defects enabled membrane restructuring in the contact region.

INTRODUCTION

Biological membranes are complex, self-organized structures that define boundaries and compartmentalize volumes in living matter. Composed primarily of cholesterol and a wide variety of lipid and protein molecules, a typical mammalian membrane contains hundreds of different constituent molecules. Biophysical studies seek to recapitulate the fundamental thermodynamic and physical attributes of biological membranes using simpler systems of a few components with well-defined compositions. Importantly, model systems still exhibit a variety of properties and different ordered states ranging from the tightly packed gel phase to the fluid like liquid ordered (L_o) and liquid disordered (L_d) phases. Although binary lipid mixtures can display coexistence of gel and fluid phases, cholesterol is necessary for L_d and L_o fluid phase coexistence.[102-103] Lateral heterogeneities within model membranes have been widely used to study lipid domain formation and as analogs for lipid rafts.[105,130] In particular, the phase behavior of ternary mixtures of saturated lipids, unsaturated lipids, and cholesterol are considered the simplest model of biological membranes in so far as their fluidity and coexistence of L_d and L_o phases.[131-133] As a result, there have been a plethora of studies focused on elucidating the specific interactions and condensed complexes of cholesterol – lipid mixtures, including determination of ternary phase diagrams and alterations of membrane mechanical properties on the macro-scale[104,110-111,117,119] to temporal, composition fluctuations, and preferential segregation of different membrane constituent moieties on the nano-scale.[134-135] However, less is known regarding how the presence of cholesterol modifies the interactions between membranes.

The majority of investigations of ternary mixtures have focused on monolayers at the air water interface or on unilamellar vesicles in solution.[105, 130-133] In both cases, incorporation of lipid based dyes enables the use of fluorescence microscopy (FM) to measure domains as a function of surface pressure, composition, and temperature.[132-133] Similar investigations with substrate supported membranes can be carried out and also allow for atomic force microscopy (AFM) measurements of domain height or frictional differences due to alterations in packing and composition of the domains. More detailed thermodynamic information including the elucidation of tie-lines in the two phase region has been extracted from NMR and X-ray scattering measurements.[133]

In this work, we investigate the interactions between membranes containing ternary mixtures of saturated lipids, unsaturated lipids, and cholesterol using the surface force apparatus (SFA). A comparison is made between measured membrane interaction force-distance profiles, vesicle zeta-potential, and membrane structure/topology as determined by AFM to reveal the contributions of van der Waals, hydration, hydrophobic and electrostatic interactions as well as subtle differences in the interactions when the fluid lipid component is singly or doubly unsaturated.

MATERIALS AND METHODS

Chemicals. 1,2-dihexadecanoyl-*sn*-glycero-3-phosphoethanolamine (DPPE, melting point, T_M = 63°C), 1,2-dioleoyl-*sn*-glycero-3-phosphocholine (DOPC, T_M = -20°C), 1-palmitoyl-2-oleoyl-*sn*-glycero-3-phosphocholine (POPC, T_M = -2°C), 1,2-dipalmitoyl-*sn*-glycero-3-phosphocholine (DPPC, T_M = 41°C), 1,2-dimyristoyl-sn-glycero-3-phosphocholine (DMPC, T_M =

23°C), 2-(4,4-Difluoro-5,7-Diphenyl-4-Bora-3a,4a-Diaza-*s*-Indacene-3-Pentanoyl)-1-hexadecanoyl-*sn*-Glycero-3-Phosphocholine (β-BODIPY® 530/550 C_5-HPC) and cholesterol (ovine wool, >98%, T_M = 148°C) were purchased from Avanti Polar Lipids, Inc. (Alabaster, AL) and used as received. Electrolyte solutions used $NaNO_3$ 99.995% (Sigma, St. Louis, MO). The water used was purified with a MilliQ gradient water purification system with a resistivity of 18 MΩ·cm.

Atomic Force Microscopy (AFM). AFM images were acquired using a MFP3D-SA system (Asylum Research, Santa Barbara, CA) with closed loop capability. A silicon cantilever (model MSNL, Bruker, Santa Barbara, CA) with force constant of 0.1 N/m was used for imaging. All the images were acquired in tapping mode in MilliQ gradient water. The cantilever was modulated by a driving frequency of 61 kHz and the imaging set point was adjusted to 70-80% damping of the free amplitude. The AFM images were acquired and analyzed using Asylum MFP3D software developed on the Igor Pro 6.12 platform and Gwyddion Version 2.33 (http://gwyddion.net/). Three independent samples for each lipid composition were scanned. The statistics of each composition were obtained from at least 100 measurements over multiple images.

Fluorescence Microscopy (FM). FM images were acquired using a Nikon Eclipse E600 microscope connected with CoolSNAP-Pro CCD camera at 10x, 40x, and 60x magnification.

Zeta Potential Measurements (ZP). The details about ZP measurements can be found in chapter II. ZP measurements were done in 0.45 mM $NaNO_3$ electrolyte solutions (Brookhaven Zeta Plus, Holtsville, NY). ZP results summarized in Table 3.1 were obtained from at least three independent samples with ten measurements per sample for each vesicle composition.

Sample Preparation. The mica substrate supported lipid bilayers were constructed using Langmuir-Blodgett (LB) deposition (Nima Coventry, U.K.). The inner monolayer was DPPE deposited at 45 mN/m. DPPE forms an almost defect free, robust and strongly physisorbed monolayer on mica.[136] The dipping speed used to deposit the inner monolayer was 1 mm/min and the monolayer transfer ratio was 0.997±0.004 on freshly cleaved mica. The tight packing and stability of the gel phase DPPE inner monolayer minimizes molecular exchange between the two leaflets. The outer monolayer consisted of a 1:1:1 (mole %) mixture of either DOPC/DPPC/cholesterol or POPC/DPPC/cholesterol. Two different methods were used to deposit the outer leaflet. The main method in the reported work was to deposit the outer monolayer using a second Langmuir-Blodgett deposition. In this case the outer leaflet was deposited at 30 mN/m with a dipping speed of 4 mm/min. The transfer ratio of the outer monolayer was 0.982±0.007 for the 1:1:1 DOPC-DPPC-cholesterol on DPPE and 0.983±0.004 for the 1:1:1 POPC-DPPC-cholesterol on DPPE. The duration of entire process for deposition of the outer leaflet was less than 30 minutes, which minimized oxidation of cholesterol and the unsaturated lipid component. Figure 3.1 shows the pressure-area isotherm of the mixtures used as the outer leaflet of the supported lipid bilayer. These isotherms are in agreement with the condensation effect of cholesterol on PC lipids observed by Smaby *et al*.[110] At 33 mole% of cholesterol, the average molecular area is about 40 – 45 $Å^2$/molecule at surface pressure of 30 mN/m.

The second method used to construct the supported membrane was vesicle fusion.[59] Lipid-cholesterol mixtures were prepared in chloroform, dried under nitrogen and then placed under vacuum for at least 4 hours. Mixtures characterized by fluorescence microscopy imaging contained 1% of bodipy-HPC. The dried lipids were hydrated with MiliQ-water to a concentration of 0.5 mg/mL, sonicated using a probe tip sonicator for 1 minute, and then extruded through a 100 nm pore size polycarbonate membrane for 10 passes. Vesicle solutions for ZP were extruded and not probe tip sonicated to prevent titanium contamination. In some studies, a DPPE monolayer was incubated with the extruded vesicle solution for one hour to create an asymmetric bilayer as in the Langmuir deposited case. In others, a freshly cleaved mica substrate was incubated with the vesicle solution to form the entire membrane by vesicle fusion. After incubation, excess vesicles were removed by extensively rinsing the sample with MilliQ water. However, formation of a uniform supported membrane using either vesicle fusion approach was problematic. High resolution fluorescence microscopy and surface force measurements revealed the presence of tubules and tethered vesicles extending from the

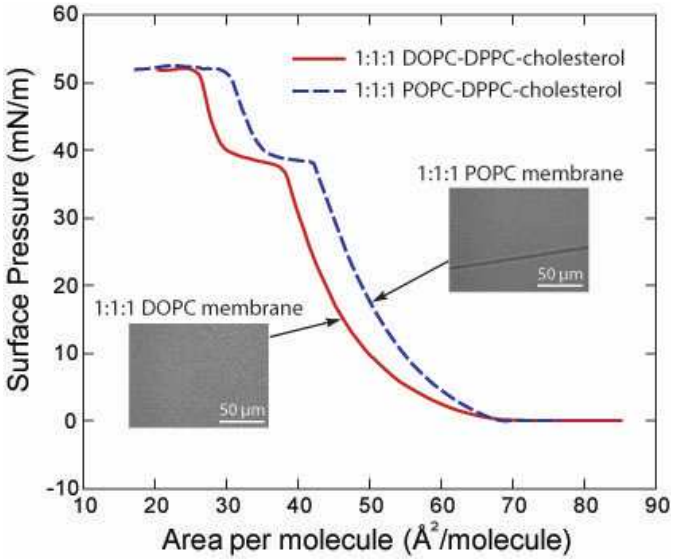

Figure 3.1. Isotherms of the lipid mixtures used to make the outer monolayer of the membrane bilayer at 25°C. When both acyl chains in the fluid phase lipid component are unsaturated (DOPC vs. POPC), a larger condensation with cholesterol is observed. Top right inset is FM image of the 1:1:1 POPC-DPPC-cholesterol membrane and bottom left is the FM for 1:1:1 DOPC-DPPC-cholesterol membrane at 40x magnification. The dark stripe on the image was a scratch made to better visualize the homogeneity of the membrane.

membrane surface, rather than a uniform membrane. As a result, a significant repulsion was observed during the force measurements due to confinement and compression of tubules and tethered vesicles between the supported membranes. In addition, the vesicle fusion method on either bare mica or a supported DPPE monolayer did not yield as complete membranes, as demonstrated by a greater number of defects in the membranes. Further, membranes formed entirely by the vesicle fusion method onto a bare mica substrate were of even lower quality in terms of uniformity and surface coverage compared to membranes formed by fusion to a DPPE monolayer.

Surface Force Measurements (SFA). The details about SFA technique can be found in chapter II. The stiffness of the double cantilever spring was 2.16×10^5 mN/m. Three independent SFA experiments were carried out for each of the membrane compositions. Force profiles shown in the results section are for one set of experimental measurements, but were consistent between the three independent experiments.

RESULTS

1:1:1 DOPC-DPPC-cholesterol membranes. Figure 3.2 shows the measured force-distance profile between opposing membranes with 1:1:1 DOPC-DPPC-cholesterol as the outer monolayer in 0.5 mM $NaNO_3$ solution. As the membranes were asymmetric with inner leaflets of DPPE and outer leaflets composed of mixtures of unsaturated lipid, saturated lipid, and cholesterol, we treat the two outer leaflets, which we are primarily interested in, as an equivalent membrane of the mixture composition. The force profile distance is based on mica-mica contact (D = 0 nm). The thickness of the two opposing bilayers was determined from the

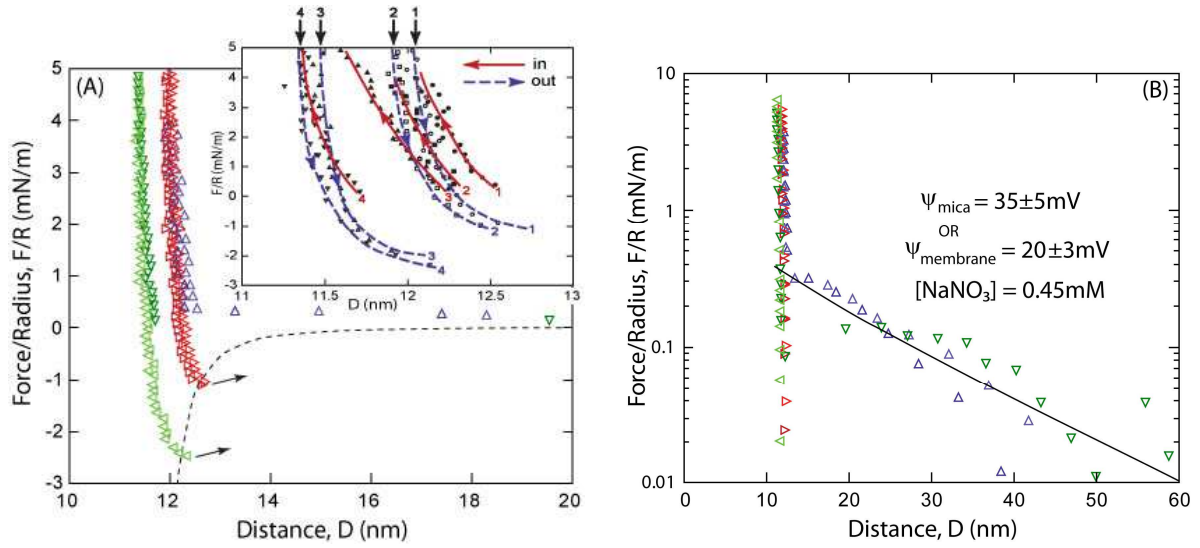

Figure 3.2. (A) Force-distance profiles between opposing 1:1:1 DOPC-DPPC- in ~0.5mM $NaNO_3$ solution. D = 0 is defined as contact between bare mica-mica surfaces. The dashed line is the predicted van der Waals interaction $F = \frac{-AR}{6D^2}$ with $A = 7 \times 10^{-21}$ with van der Waals plane 0.7 nm inward from distance of membrane contact at zero force. The shift of 0.7 nm was estimated from data on DPPC membranes by Marra and Israelachvili (Biochemistry 1985). The inset shows four successively measured force profiles while allowing longer contact time between each distance displacement. There is an inward shift to smaller separations (decreasing membrane thickness) and greater adhesion due to lipid rearrangements in the contacting region. (B) Semi-logarithmic plot of the force profile and fit of the electrostatic contribution (solid line) using either the mica or membrane as the charged interface (△,▽: approach ; ◁,▷ : separation).

shift of the contact FECO wavelength before and after deposition of the bilayers on the mica substrates as well as after removal of the deposited membranes at the end of the measurements.[36] The average thickness of the two DPPE/1:1:1 bilayers including the hydration layer was 11.7±0.6 nm. The thickness of a DPPE monolayer on mica deposited at 45 mN/m has been established to be 2.56±0.05 nm using the method of UV light exposure.[70, 136] Therefore, the thickness of a single outer 1:1:1 DOPC-DPPC-cholesterol monolayer, including the hydration layer, is ≈3.3±0.7 nm.

Figure 3.2B displays the data on a semi-log plot to aid in ascertaining the source of the weak repulsive contribution to the force profile. As can be seen, the decay length of the repulsion is determined by the electrolyte concentration in the solution (~0.5 mM $NaNO_3$ or κ^{-}

[1]~14 nm), indicating that the force is electrostatic. An electrostatic repulsion between the membranes was unexpected given that the membranes should be overall neutral in charge. The headgroups of PC and PE lipids are zwitterionic but neutral at pH 6; and cholesterol is not charged under these conditions. However, in the case of unsaturated lipids, there are reports that a small amount of the lipid (contaminant lipid) is charged, resulting in a weakly charged membrane. In the absence of other charges in the system, the effect of these lipid contaminants can be measureable as observed here.[127, 137]

On the other hand, the underlying mica substrate is also negatively charged. AFM images of a representative and identically prepared 1:1:1 DOPC-DPPC-cholesterol membrane are shown in Figure 3.3A-C. As can be seen, membrane defects (which reach the underlying DPPE monolayer) are present, although the membrane appears homogeneous under fluorescence microscopy imaging (Figure 3.1 bottom left inset). Figure 3.3E is a representative profile across a defect. The average depth of the defects was 3.0±0.4 nm (Figure 3.3G), which is in very good agreement with the thickness of the outer monolayer as measured by SFA (3.3±0.7 nm). Similar defects were previously observed on solid supported, one component bilayer system using AFM at low deposition pressure.[70] Holes in the membrane, that penetrate all the way to the mica surface were also present, but at a much smaller fraction, precluding a definitive measure of the total membrane thickness by AFM. Thus, the electrostatic repulsion measured between the opposing membranes could arise from two different sources: (1) charged lipid contaminants in the membrane, or (2) exposed regions of the negatively charged mica substrates. The non-linear Poisson-Boltzmann (P-B) equation with constant charge approximation was used to fit the electrostatic contribution to the force profile for both

scenarios. Assuming the origin of charge was at the mica substrate, the best electrostatic fit was obtained for a salt concentration of 0.45 mM with surface charge of 1.8 mC/m^2 or surface potential of 35 mV. If the origin of charge was instead at the membrane interface, a lower charge density of 1 mC/m^2 or a surface potential of 20 mV is obtained. The slightly lower salt concentration used in the electrostatic fit (0.45 vs 0.50 mM) is due to dilution during the transfer of the membrane coated substrates from the Langmuir trough into the SFA.

Upon separation of the membranes a substantial adhesion was measured. The magnitude of the adhesion with 1:1:1 DOPC-DPPC-cholesterol membranes ranged from -1.1 mN/m to -2.5 mN/m as shown in Figure 3.2A (arrows). A Hamaker constant of $7x10^{-21}$ J was used as previously determined by Marra and Israelachvili[20] to estimate the van der Waals contribution (dashed curve with the VdW plane located at D = 11.5 nm). The measured adhesion between the two membranes is comparable to the prediction, but the magnitude of the adhesion is actually significantly greater than predicted, once the repulsive electrostatic contribution is accounted for. Effectively, the adhesion is approximately 0.3-0.4 mN/m greater in magnitude – significantly greater than the VdW prediction. The enhanced adhesion suggests that hydrophobic contributions due to defects in the membrane also contribute to the adhesion.[54] A clear signature of some hydrophobic character to the adhesion was indicated by an increase in the magnitude of the adhesion with increasing contact time and compression of the membranes. As depicted in the inset of Figure 3.2A (run 2 vs. run 3), increased contact time allowed structural rearrangements of the membrane and an enhancement in the adhesion. It seems likely that this is due to alignment of hydrophobic defects in the opposing membranes.[138-140] The structural rearrangement can be observed from the inward shift of the

contact separation distance and thinning of membranes (Figure 3.2A inset). The number of defects or holes and the magnitude of force applied were apparently insufficient to result in complete hemifusion between the membranes containing cholesterol. Previously, Benz *et al*.[70] reported hemifusion between single component membranes with a high number of defect under high loads.

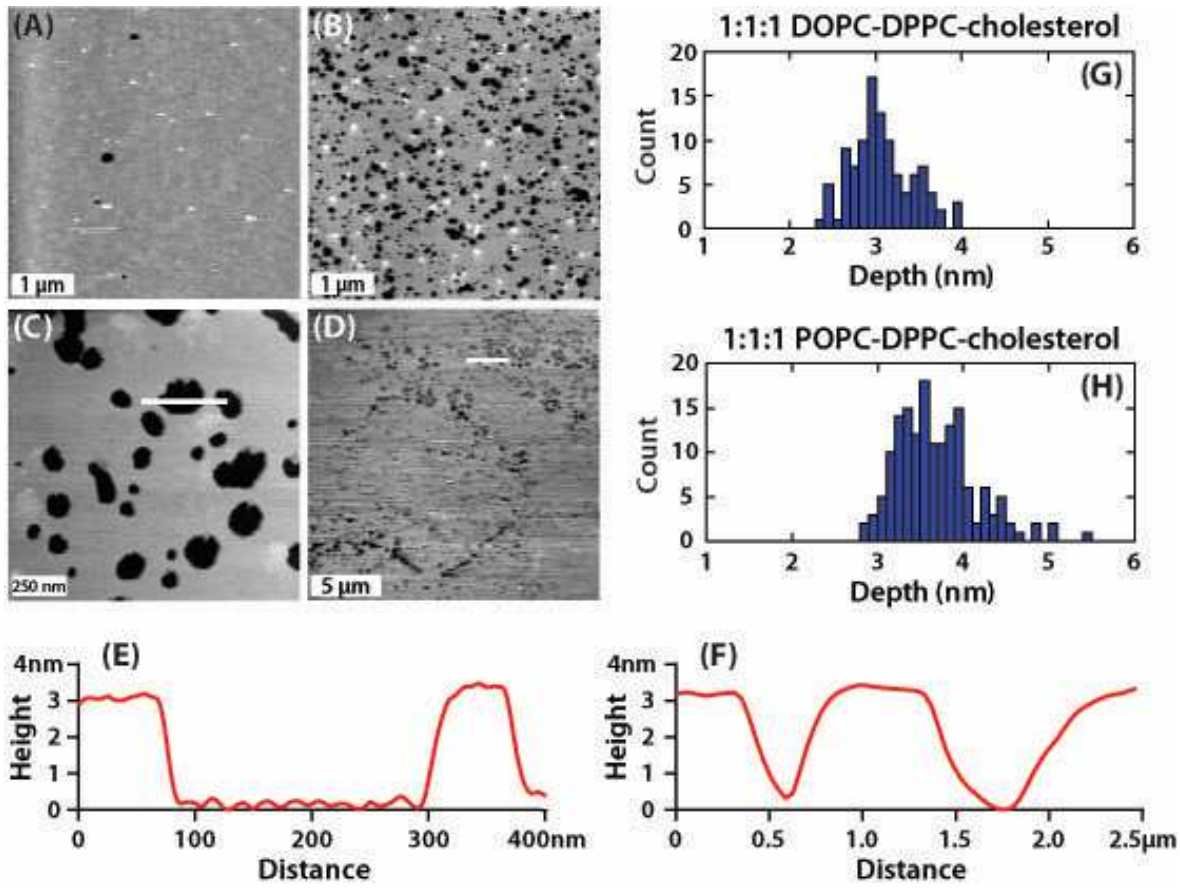

Figure 3.3. [A] 5 µm × 5 µm AFM topography image of the DOPC:DPPC:cholesterol system showing that there are regions that are relatively defect free. [B] 5 µm × 5 µm AFM topography image of the DOPC:DPPC:cholesterol system showing that there are regions that have defects. [C] 1.5 µm × 1.5 µm AFM zoom-in image of the DOPC:DPPC:cholesterol system with a representative cursor measuring the depth of the defect. [D] 20 µm × 20 µm AFM topography image of the POPC:DPPC:cholesterol system. [E, F] Corresponding cursor profiles as indicated in [C] and [D], respectively to obtain defect depth profiles. [G,H] Histogram of defect depths for the DOPC:DPPC:cholesterol system and POPC:DPPC:cholesterol system, respectively.

POPC-DPPC-cholesterol membranes. Figure 3.4 shows the measured force-distance profile between opposing membranes with 1:1:1 POPC-DPPC-cholesterol as the outer monolayer in ~0.5 mM $NaNO_3$ solution. The force-distance plot was based on mica-mica contact (D = 0 nm). The average thickness of two DPPE/1:1:1 bilayers was 13.5±0.6 nm, yielding a thickness of 4.2±0.7 nm for a single, hydrated 1:1:1 monolayer containing POPC. AFM images for the 1:1:1 POPC-DPPC-cholesterol membrane (figure 3.3D) also demonstrated that defects and holes were present in the membranes similar in size to the 1:1:1 DOPC-DPPC-cholesterol system. Figure 3.3F is a representative profile across a defect. The average depth of the monolayer defects was 3.6±0.4 nm (Figure 3.3H), consistent with the thickness of the 1:1:1 POPC-DPPC-cholesterol monolayer obtained via SFA measurements.[46]

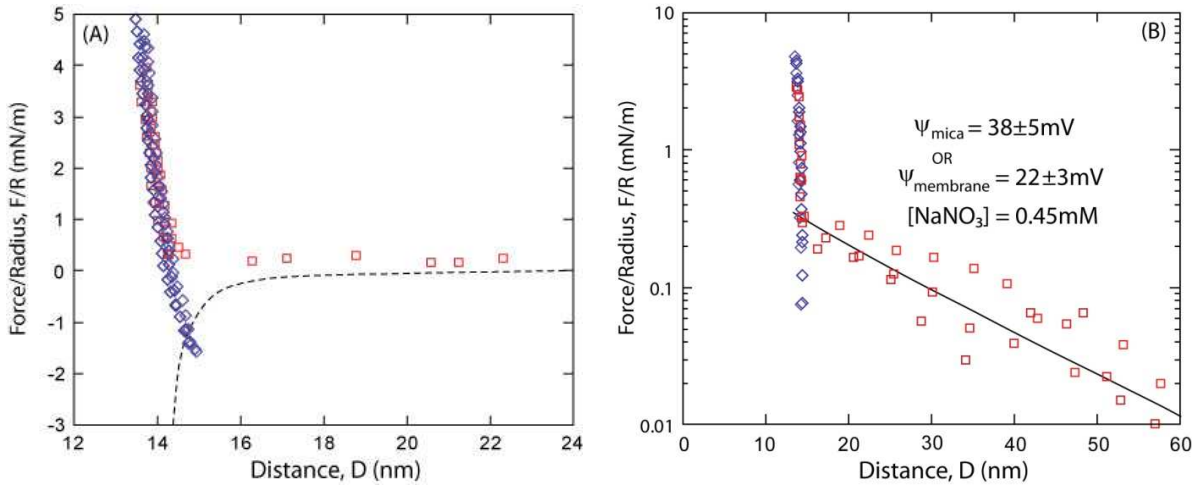

Figure 3.4. (A) Force-distance profiles between 1:1:1 POPC-DPPC-cholesterol membranes in ~0.5mM $NaNO_3$ solution. D = 0 is defined as contact between bare mica-mica surfaces. The dashed line is the van der Waals interaction $F = -AR/6D^2$ with $A = 7 \times 10^{-21}$ J with van der Waals plane 0.7 nm inward from distance of membrane contact at zero force. The shift of 0.7 nm was estimated from data on DPPC membranes by Marra and Israelachvili (Biochemistry 1985). (B) Semilogarithmic plot of the force profile and fit of the electrostatic contribution (□: approach ; ◇ : separation).

Fluorescence imaging of the 1:1:1 POPC-DPPC-cholesterol membrane mixture revealed a macroscopically uniform membrane, as was the case with the doubly unsaturated DOPC-DPPC-cholesterol mixture. An electrostatic repulsion was also observed, detectable from a distance of about 50 nm from bilayer-bilayer contact. The electrostatic repulsion for this membrane composition was very similar to that obtained with the doubly unsaturated DOPC-DPPC-cholesterol membrane. With the origin of charge at the mica surface, a constant surface charge of 2 mC/m^2 or surface potential of 38 mV were obtained. If the origin of charge was at the membrane interface due to inclusion of a small level of charged lipids in the membrane, lower values of 1.1 mC/m^2 or 22 mV were obtained. Finally, the magnitude of the membrane adhesion, about -1.6 mN/m, was similar to that measured between membranes with doubly unsaturated DOPC-DPPC-cholesterol. The magnitude of the adhesion is again greater than the predicted van der Waals attraction between the membranes (VdW plane at D=13.7 nm). In the case of POPC-DPPC-cholesterol membranes, longer contact times did not result in a significant change in the force profile or decrease in membrane thickness due to lipid rearrangements $(\Delta D \leq 5\ nm)$.

DISCUSSION

Electrostatics:

The general features of the measured interaction force-distance profiles of the two membrane compositions are quite similar. In both cases a long range but weak electrostatic repulsion was measured with a short-range, predominantly van der Waals attraction resulting in adhesion of the membranes at contact. We first discuss the electrostatic repulsion. Previous

measurements of single component membranes on mica have indicated that saturated PC and PE lipids form relatively defect free, uncharged supported membranes on mica.[140] Ionization constant or pKa of PC and PE lipids[125-126, 141] at the experimental pH of ~6 also suggest an overall neutral charge for PC and/or PE membrane.[53] In contrast, unsaturated lipids have been reported to contain a small amount of charged, contaminant lipid that renders the membrane weakly charged.[127] With the origin of charge at the membrane interface, the resulting 1 mC/m^2 charge density corresponds to about one charge per 400 lipids for both 1:1:1 membrane compositions. If the origin of charge is at the mica surface due to membrane spanning holes, the measured surface charge density of about 2 mC/m^2 corresponds to one negative charge per 80 nm^2. In comparison, the basal plane of mica has a much greater negative charge of about one per 5 nm^2. [142] Thus, the underlying mica substrate is relatively well screened by the membrane. AFM scans of the membranes reveal that most of the features are monolayer defects (depth <3.6 nm) and not membrane spanning holes. This finding and the fact that in some cases, no electrostatic repulsion were not observed in overall neutral system (see Chapter V) suggest that charged lipid impurities are the dominant source of electrostatic repulsion. In the case of defects, the underlying mica substrate is still coated by a DPPE monolayer. The low dielectric constant of the inner DPPE monolayer ($\epsilon \approx 3 - 5$) greatly inhibits charge dissociation and screens any charge at the mica surface.

To unequivocally establish that charged lipid contaminants were present in the membrane, zeta potential measurements were carried out with various compositions of POPC, DOPC, DPPC, DMPC, and cholesterol containing vesicles. Table 3.1 reports the measured zeta potential for the various compositions in 0.45 mM $NaNO_3$ solution to match the SFA force

profile measurements. The zeta potential of the 1:1:1 compositions was -15 to -20±5 mV, consistent with the SFA measurements of an electrostatic charge being present in the membrane. To establish the source of the negatively charged lipid contaminant, a variety of mixtures were studied. In all cases, the vesicles were negatively charged. The zeta potential for pure saturated lipid vesicles was done using DMPC to enable room temperature measurements (DMPC, T_M = 23°C). The higher melting temperature of 41°C for DPPC requires that the vesicle solution temperature be maintained above T_M throughout the course of the zeta potential measurement. The difference in the length of the acyl chains should not affect the charge of the vesicle. The findings suggest that charged lipid contaminants are present in both saturated and unsaturated lipid samples. Moreover, zeta potential measurements of the surface potential at the hydrodynamic plane of the 1:1:1 vesicles were in good agreement with the SFA measured force profiles between supported 1:1:1 membranes.

Table 3.1. Summary of zeta potential of various lipid compositions

Lipid	Solution	Ψ (mV)
Pure DMPC	0.45mM $NaNO_3$	-7.1±4.5
Pure DMPC	Water	-22.3±4.3
Pure DOPC	0.45mM $NaNO_3$	-10.1±5.4
Pure DOPC	Water	-21.8±4.0
Pure POPC	0.45mM $NaNO_3$	-10.9±4.9
2-1 DOPC-Cholesterol	0.45mM $NaNO_3$	-12.1±4.7
2-1 DOPC-Cholesterol	Water	-21.8±4.6
2-1 POPC-Cholesterol	0.45mM $NaNO_3$	-13.9±4.5
2-1 DPPC-Cholesterol	0.45mM $NaNO_3$	-10.6±4.1
1-1-1 DOPC-DPPC-cholesterol	0.45mM $NaNO_3$	-14.9±4.5
1-1-1 DOPC-DPPC-cholesterol	Water	-24.2±4.5
1-1-1 POPC-DPPC-cholesterol	0.45mM $NaNO_3$	-19.5±5.4

Adhesion:

We now discuss the differences in adhesion between the two membrane compositions. As detailed in the result section, the adhesion between the 1:1:1 DOPC containing membranes varied from -1.1 to -2.5±0.3 mN/m and the adhesion of 1:1:1 POPC containing membranes was about -1.6±0.2 mN/m. Although we believe hydrophobic nanoscale defects in the outer 1:1:1 monolayer are the source of the enhanced adhesion over VdW, we also consider the effect of cholesterol and potential differences in membrane hydration for completeness. Cholesterol is known to induce a "condensation effect" on various PC membranes which increases the lateral interaction between the components. Huang and Feigenson[143] suggested that the PC lipid headgroups shield the adjacent hydrophobic body of cholesterol to create an umbrella structure. Since the van der Waals plane of a predominantly lipid membrane is expected to be located at the plane of the lipid headgroups and the membrane mixtures only have one phase, the umbrella model suggests a similar Hamaker constant for PC membranes with or without cholesterol. As both membranes had PC lipids and cholesterol in the same ratios, our expectation was to measure a similar adhesion between the two membrane compositions. Moreover, as PC lipids were the predominant constituent of both membranes, we further expected that the measured adhesion would be similar to previous measurements of van der Waals adhesion between pure PC membranes.

Marra and Israelachvili[20] measured and reported that the VdW adhesion between fluid phase DMPC and DPPC membranes was about -0.6 mN/m and extracted a Hamaker constant of $A = 7 \pm 1 \text{ x } 10^{-21}$ J based specifically on measurements of DPPE and DPPC membranes. In both cases the membrane was deposited by Langmuir-Blodgett method, presumably on an

inner leaflet of DPPE as in our studies. Subsequent studies found similar values for pure DPPC membranes[26] and for DMPC on DPPE,[140] and confirm this adhesive range. In contrast, the measured VdW adhesion between phosphotidylethanolamine membranes in the gel phase is significantly greater (-5 mN/m).[20] As the Hamaker constant for PC and PE lipids should be very similar, Marra and Israelachvili[20] suggested that the difference in adhesion was due to differences in the level of hydration and contact separation between the membranes , where $\frac{F_{vdW}}{R} = \frac{-A}{6\pi D^2}$ and $D = 0$ corresponds to the van der Waals plane of origin, which varies for different lipids based on their hydration.[144] Refractive index measurements of DPPC and DPPE monolayers also support that their Hamaker constants are within 10%.[136] Thus, variations in membrane hydration due to cholesterol, lipid composition, and/or van der Waals plane of origin could potentially account for the differences in the measured adhesion in this work.

Due to the possible presence of a significant dependence on hydration, we next comment on the 0.9 nm difference in thicknesses of the 1:1:1 POPC-DPPC-cholesterol membrane versus the 1:1:1 DOPC-DPPC-cholesterol membrane, as measured by SFA. In SFA experiments, the wavelength shift of the FECO fringes before and after removing the membranes was used to determine the average membrane thickness over the ≈20 x 10 μm^2 contact region. Defects or holes in the membrane below a few microns in lateral dimension are not resolvable, and only an average measure of the membrane thickness can be obtained. In addition, the water of hydration of the headgroups is intrinsically part of the membrane thickness. In our studies, the ratio of fluid lipid to saturated lipid to cholesterol, and the deposition pressure were maintained between the two membrane compositions. Thus, it is likely that the difference in membrane thickness is due to packing differences of these tri-

component mixtures with doubly or singly unsaturated acyl chains in the fluid phase lipid (DOPC vs POPC), including any present defects or holes, and any intrinsic difference in hydration, if present. In regards to packing in the mixtures, cholesterol is known to have condensing effect on fluid phase lipids and to conversely fluidize solid phase lipids, here DPPC. Molecular dynamic simulations by Pitman and coworkers[134] have also indicated that cholesterol has a higher affinity for saturated versus unsaturated acyl chains due to better packing of the hydrophobic core. As POPC contains one more saturated acyl chain than DOPC, the POPC-DPPC-cholesterol membrane may have a tighter packing, leading to an increased thickness compared to the DOPC-containing membrane. In contrast to this assessment, the isotherms and area per molecule measurements at the air-water interface (Figure 3.1) indicate that POPC-containing monolayers have a slightly higher average area per molecule compared to the DOPC-containing monolayers. Assuming an incompressible system, this would suggest a decrease in the thickness of the POPC containing membrane compared to the one with DOPC. However, isotherm measurements may not be sensitive to differences in hydration or molecule protrusions out of the membrane plane which affect the overall thickness. Thickness measurements of multi-component lipid mixtures should be able to resolve these differences, especially if they are of substrate supported membranes. Our AFM measurements of the two membrane compositions are consistent with an increase in thickness of the POPC containing membrane, but only by approximately 0.6 nm, versus a value of 0.9 nm as found by SFA. Rawicz *et al*.[145] showed that vesicles have very similar bending moduli for lipid mixtures of two unsaturated, two saturated, and mixed saturation acyl chain lipids with similar chain length. Although bending rigidity is not a direct measure of protrusions out of the membrane plane,

the similarity in the compressibility of the membrane as measured by SFA suggests that any difference in thickness due to lipid protrusions out of the membrane plane between the two membrane compositions would be very modest. Although we cannot rule out an increase in VdW adhesion due to subtle changes in hydration and lipid packing in membranes containing cholesterol, we believe the primary cause is increased hydrophobic attraction as described below.

In support of hydrophobic interactions as the main cause of the increased adhesion and variation in membrane thickness in the mixed membrane systems, AFM scans indicated that there were defects in both the membrane mixtures, which exposed the inner DPPE monolayer of the membrane. Although the level of defects in the two mixtures was relatively similar, there was significant variation in the number of defects across the membrane, especially in the case of the 1:1:1 DOPC containing membrane, which showed a greater variation in the magnitude of the adhesion. Defects which exposed regions of the inner leaflet would lead to an additional hydrophobic interaction between the two membranes. These defects were relatively few in number of area, as hemifusion between the two membranes was not observed. Instead, the presence of defects is reflected by a decrease in the average membrane thickness in the SFA measurements, which averaged over about 100 μm^2 areas. Further, in the case of 1:1:1 DOPC membranes, lipid membrane restructuring was observed with increased contact time (Figure 3.2A inset). The role of hydrophobic interactions between membranes has been well documented by Helm *et al*.[138] who showed a linear increase in adhesion with decreasing lipid density in the outer membrane leaflet. Taken together, the data and analysis strongly suggest

that the increased adhesion in these mixed lipid systems primarily arises from membrane defects and their hydrophobic contributions.[55]

CONCLUSIONS

The interactions between lipid membranes include electrostatics, van der Waals, hydration, hydrophobic and in free standing systems significant protrusion/undulation repulsion. A large body of work has focused on recapitulating complex membrane behavior with greatly simplified systems. In particular, substrate supported membrane systems are used extensively due to their ease of handling, compatibility of study with numerous surface sensitive techniques, and potential applications in biotechnology and biosensing. In this work, the force profiles between 1:1:1 DOPC-DPPC-cholesterol membranes and also between 1:1:1 POPC-DPPC-cholesterol membranes were measured using SFA and coupled to structural and chemical information to highlight the presence of lipid contaminants and role of defects in dictating the resulting interactions. The membranes were found to carry a distinct and non-negligible negative charge due to the presence of lipid contaminants resulting in a long range electrostatic repulsion. In contact, an increase in adhesion between membranes containing cholesterol compared to a pure PC membrane was observed. The greater than expected adhesion was attributed to hydrophobic interactions between membrane defects. The presence of an unexpected membrane charge and membrane defects could be important in other supported membrane studies and biosensor applications where the selective binding of ligands or proteins to membranes is important.

ACKNOWLEDGEMENTS

This work was supported by the NSF chemistry division through grant CHE-0957868. Nai-Ning was supported by NSF (CHE-0809977 and DMR-1104260). We also thank Daniel Kienle for assistance with SFA measurements, Emily Parry for assistance with zeta potential measurements, Easton Groves and William Chan for assistance with fluorescence microscopy measurements.

Chapter IV

Interaction Forces between Lipid Rafts

James Kurniawan[†], Gregory Kittleson[†] and Tonya L. Kuhl[†‡]*
[†]Department of Chemical Engineering, University of California Davis, 95616, USA
[‡]Department of Biomedical Engineering, University of California Davis, 95616, USA
Corresponding Authors: *E-mail: tlkuhl@ucdavis.edu

ABSTRACT

Cellular membranes containing sphingolipids and cholesterol have been shown to self-organize into lipid rafts, specialized domains which host integral membrane proteins. In this work, force-distance profiles between raft membranes consisting of singly-unsaturated 1-palmitoyl-2-oleoyl-sn-glycero-3-phosphocholine (POPC), a complex mixture of brain sphingomyelin (BSM), and cholesterol were measured using the surface force apparatus (SFA). Two distinct force profiles were detected corresponding to homogeneous (low defect density) or heterogeneous (higher defect density) raft membranes as corroborated by AFM scans. In all cases a weak, long-range electrostatic repulsion was observed with some variation in the surface charge density. The adhesion between the homogeneous raft membranes was comparable to our previous work with pure component, liquid-ordered POPC:DPPC (1,2-dipalmitoyl-*sn*-glycero-3-phosphocholine):cholesterol membranes. Raft membranes with more defects adhered more strongly due to hydrophobic attraction between exposed acyl chains. The small variations observed in electrostatic repulsion were attributed to the heterogeneity of the BSM constituent lipids. Even though the rafts were in the liquid-ordered phase and membrane defects were present in the contact region, the raft membranes were stable and no

structural rearrangement was observed throughout the measurements. Our findings demonstrate that liquid ordered membranes are stable to mechanical loading and not particularly sensitive to compositional variation.

INTRODUCTION

Biological membranes are sophisticated structures that provide boundaries between discrete volumes in all life forms. They are composed of a myriad of different molecular species including various lipids, sterols, and proteins. These constituents are thought to segregate dynamically into nanoscale lateral domains called lipid rafts, which influence vital bioactivity such as signaling events and transport across biological membranes.[4, 105, 115, 146-147] Due to the complexity of cell membranes, numerous studies have mimicked raft domain properties and phase state using simple model systems comprised of a high melting point (T_m) lipid, a low T_m lipid, and sterol.[146, 148-150] Such ternary mixtures can form coexisting liquid ordered (L_o) / liquid disordered (L_d) phases, exhibiting phase separation analogous to liquid-liquid immiscibility in cellular membranes and raft formation.[131-133, 151] Ternary mixtures of sphingomyelin (SM), phosphatidylcholine (PC), and cholesterol, in particular, are similar to the predominant lipid species in the outer membrane leaflet of eukaryotic cells.[109, 148, 152-154] Most investigations of ternary SM/PC/cholesterol mixtures have focused on the importance of lateral, molecular level interactions in nanodomain formation. For example, the immiscible L_o/L_d coexistence phases of ternary SM/PC/cholesterol mixtures were mapped by thermodynamic analysis of differential scanning calorimetry (DSC) scans and fluorescence resonance energy transfer (FRET) to construct the ternary mixture phase diagram.[148-149, 152] The mechanisms responsible for lipid

raft stability and domain size have also been studied by small angle neutron scattering (SANS) coupled with Monte-Carlo simulations.[146]

Despite the plethora of research on these more biologically relevant systems, little is known about intermembrane interactions between ternary mixed membranes containing SM, PC and cholesterol that purportedly better mimic native lipid rafts. BSM is a natural pseudo-mixture of sphingolipids which contains at least 6 different SM lipid species. Biophysical studies of membranes containing more complex mixtures are becoming more common. The major lipid acyl chains are octadecanoyl (18:0) and nervonoyl (24:1). Previous nuclear magnetic resonance (NMR) and molecular dynamic simulation studies have proposed that the variety in saturation and length of the SM amide-linked acyl chains mediate coupling between membrane leaflets through interdigitation of the long amide-linked acyl chain with the inner cytoplasmic leaflet.[155-157] In addition, the mismatch of acyl chain length has been suggested to hold an important role in the regulation of membrane protein partitioning in cellular membranes.[147, 156, 158] In this work, we measured the interactions between lipid raft membranes composed of a pseudo-mixture BSM, POPC and cholesterol. The composition was selected due to their abundance in the outer leaflet of plasma membranes and greater relevance to biological systems.[159-160] The resulting SFA force-distance profiles were corroborated with high-resolution AFM topography scans to reveal the contributions of van der Waals, electrostatic, hydration, and hydrophobic interactions. Due to its importance in controlling various cellular functions and bioactivity of cells, a more fundamental understanding of raft membranes is crucial. This work provides direct measurements of intermembrane interactions in this complex system.

MATERIALS AND METHODS

Chemicals. 1,2-dihexadecanoyl-*sn*-glycero-3-phosphoethanolamine (DPPE, melting point, T_M = 63 °C), 1-palmitoyl-2-oleoyl-*sn*-glycero-3-phosphocholine (POPC, T_M = -2 °C), N-(octadecanoyl)-sphing-4-enine-1-phosphocholine (BSM porcine brain, T_M = ~45 °C) and cholesterol (ovine wool, >98%, TM = 148 °C) were purchased from Avanti Polar Lipids, Inc. (Alabaster, AL) and used as received. BSM is a mixture of various acyl chain length: 50% 18:0, 21% 24:1, 7% 22:0, 5% 20:0, 5% 24:0, 2% 16:0 SM and 10% unknown lipid species. Sodium nitrate ($NaNO_3$ 99.995%) was purchased from Sigma-Aldrich (St. Louis, MO). Water was purified with a MilliQ gradient water purification system to a resistivity of 18 MΩ·cm.

Sample Preparation. Asymmetric supported lipid bilayers on mica were used in the SFA and AFM studies. The membranes were constructed using Langmuir-Blodgett (LB) deposition (Nima Coventry, U.K.). The inner monolayer for all the experiments was DPPE deposited at 45 mN/m and a dipping speed of 1 mm/min. The outer monolayer was 1:1:2 POPC-BSM-cholesterol LB deposited at 30 mN/m and dipping speed of 4 mm/min under low-oxygen environment (<1 vol% O_2). The asymmetry mimics plasma membranes which are enriched in PE lipids on the cytoplasmic side and enriched in SM on the exoplasmic leaflet. The transfer ratio of the outer monolayer was 0.995 ± 0.018. The deposition of the outer layer was performed within 30 minutes under inert nitrogen or argon gas to minimize oxidation of cholesterol and lipid components. After lipid bilayer deposition, the surfaces were transferred underwater and mounted into the SFA.

Surface Force Measurements (SFA). The details about SFA technique can be found in chapter II. The stiffness of the double cantilever spring was about 2.8×10^5 mN/m. Force profiles

shown in the results section are representative force-distance profiles of seven independent experiments. The force profiles shown are typical for experiments with homogeneous low defect lipid raft membranes and lipid raft membranes with a higher defect density. At least five repeatable force measurements were taken for each independent experiment. The reported error propagation in the results section was based on the average of the five force runs for each independent measurement and showed the range of the observed experimental parameters for the two different conditions. Two additional independent SFA experiments were carried out to determine the thickness of a 1:1:2 POPC-BSM-cholesterol monolayer on mica. These measurements in air were used to determine the "dry" thickness of a POPC-BSM-cholesterol monolayer and quantify the hydration between the 1:1:2 POPC-BSM-cholesterol raft membranes in water.

Atomic Force Microscopy (AFM). AFM images were acquired using an MFP3D-SA system (Asylum Research, Santa Barbara, CA). A silicon cantilever (model MSNL-10, Bruker, Santa Barbara, CA) with force constant of 0.6 N/m was used for imaging. All the images were acquired in contact mode with a force of 12 nN. AFM images were analyzed using Gwyddion Version 2.31 (http://gwyddion.net/).

RESULTS

Table 4.1. Summary of SFA results showing the ranges of various extracted parameters

Lipid Raft Membrane	Equivalent Thickness (nm)*	σ (mC/m^2)	Ψ (mV)	F_{ad}/R (mN/m)	$\|F_{ad}/R\|_{vdw}$ (mN/m)	Hydration (nm)**
Homogeneous (low defect density)	6.5±0.2	2.6±0.6 to 4.3±0.4	25±6 to 43±4	-0.5±0.2 to -0.9±0.2	1.3±0.2 to 1.5±0.2	2.1±0.2
Heterogeneous (higher defect density)	5.7±0.2	4.5±0.5 to 5.9±0.6	60±5 to 70±5	-1.8±0.2 to -3.0±0.2	3.8±0.2 to 4.3±0.2	1.4±0.2

* The equivalent thickness is the thickness of the two outer monolayers including their hydration layer
** The amount of hydration is the total thickness of water between the membranes in contact

Force – distance profiles. The measured force profiles between opposing 1:1:2 POPC-BSM-cholesterol lipid raft membranes are shown in Figure 4.1. Seven independent experiments were carried out and two distinct force profiles were observed. The force-distance profiles shown using the square and diamond symbols were from experiments with homogeneous (low defect) lipid raft membranes. In this case, the equivalent membrane thickness of the two outer leaflets including the hydration was 6.5±0.2 nm. A weak, long-range electrostatic repulsion with decay length consistent with the electrolyte concentration was observed. The electrostatic repulsion was fitted to the non-linear Poisson-Boltzmann equation, yielding a range of constant surface charge densities from 2.6±0.6 to 4.3±0.4 mC/m^2 or surface potentials between 25±6 and 43±4 mV for the various experiments. Although there was variation in the electrostatic repulsion between independent experiments, the electrostatic repulsion for a given membrane contacting region was reproducible. It was therefore straightforward to fit the electrostatic contribution to the measured force profile for a given series of measurements. As the electrostatic and van der Waals attraction should be additive, the electrostatic interaction was

subtracted from the total force profile to deduce the attractive component of the membrane raft – membrane raft interaction. After removing the electrostatic contribution, the magnitude of the adhesion between the more homogeneous lipid rafts ranged between 1.3±0.2 and 1.5±0.2 mN/m.

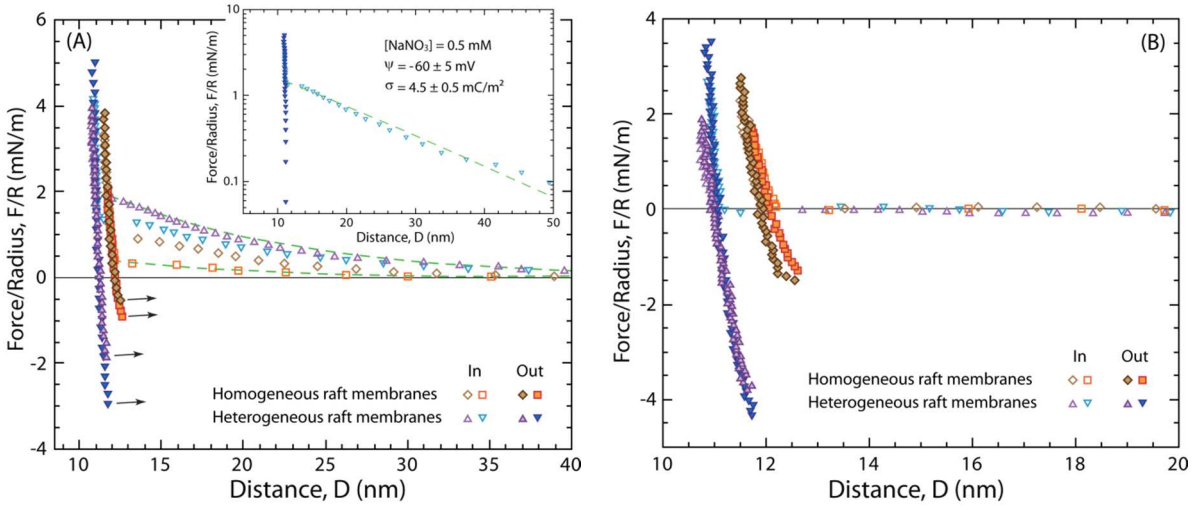

Figure 4.1. (A) Force–distance profiles between lipid raft membranes composed of 1:1:2 POPC-BSM-cholesterol membranes of two different thicknesses in 0.5mM $NaNO_3$ solution were obtained (Diamond and squares: homogeneous raft membranes; triangle and inverted triangle curves: heterogeneous raft membranes). Dashed lines represent the range of observed long-range electrostatic repulsion. Inset: an exemplar semi-logarithmic plot of a force profile and fit of the electrostatic contribution (dashed line) with origin of charge at the membrane surface. D = 0 is defined as the contact between bare mica–mica surfaces. (B) Force-distance profiles after subtraction of the electrostatic contribution. Open and filled symbols represent approach and separation respectively.

The force-distance profile of more heterogeneous (higher defect density) lipid rafts are shown as triangles in Figure 4.1. In these cases, the equivalent membrane thickness was less, namely 5.7±0.2 nm. As with the homogeneous bilayers, electrostatic repulsion was observed and consistent with a constant surface charge density ranging from 4.5±0.5 to 5.9±0.6 mC/m^2, or a constant surface potential between 60±5 and 70±5 mV. After subtracting the electrostatic contribution, a higher magnitude of adhesion between 3.8±0.2 to 4.3±0.2 mN/m was apparent. With both homogeneous and more heterogeneous lipid raft membranes, some variation in the

measured range of interaction behavior was observed. Even though POPC-BSM-cholesterol mixtures are usually considered to be ternary, BSM itself is a mixture of more than 6 different sphingolipids with saturated 18:0 SM as the major constituent in the mixture (~50%). Indeed, 10% of the BSM is unidentified lipid. We hypothesize that the experimental variations in the measured electrostatic repulsion between various raft membranes was due to subtle dissimilarity in the molecular concentrations of the charged species.[43, 66] In comparison, in pure liquid-ordered 1:1:1 POPC-DPPC-cholesterol membranes, there was little to no variation in the adhesion or electrostatic repulsion in the measured interaction force profiles.[66] The consistency in the force-distance profiles in this case was attributed to the uniform composition, while more physiological lipid rafts containing BSM show more variation.

Adhesion magnitude and presence of membrane defects. A significant difference in membrane adhesion was found between the more homogeneous and heterogeneous lipid raft membranes. High-resolution AFM scans of the raft membranes (Figure 4.2) revealed the presence of variable-sized nanoscopic defects in the outer membrane leaflet that reached the underlying inner leaflet. Most of the defects were below a few hundred nanometers in diameter. In a few cases with the heterogeneous membranes, defects about a micron in diameter were detected. Based on a typical contact area of ~50 μm^2 for the SFA measurements, the defect density across the samples varied between 0.5 to 8%. Hence, only a small variation in the adhesion was found for more homogeneous raft membranes, which also had a correspondingly larger membrane thickness. In contrast, the higher adhesion in the more heterogeneous raft membranes was attributed to additional hydrophobic attraction due to exposed acyl chains in the contact region. The reference frame for $D = 0$ in the force profiles

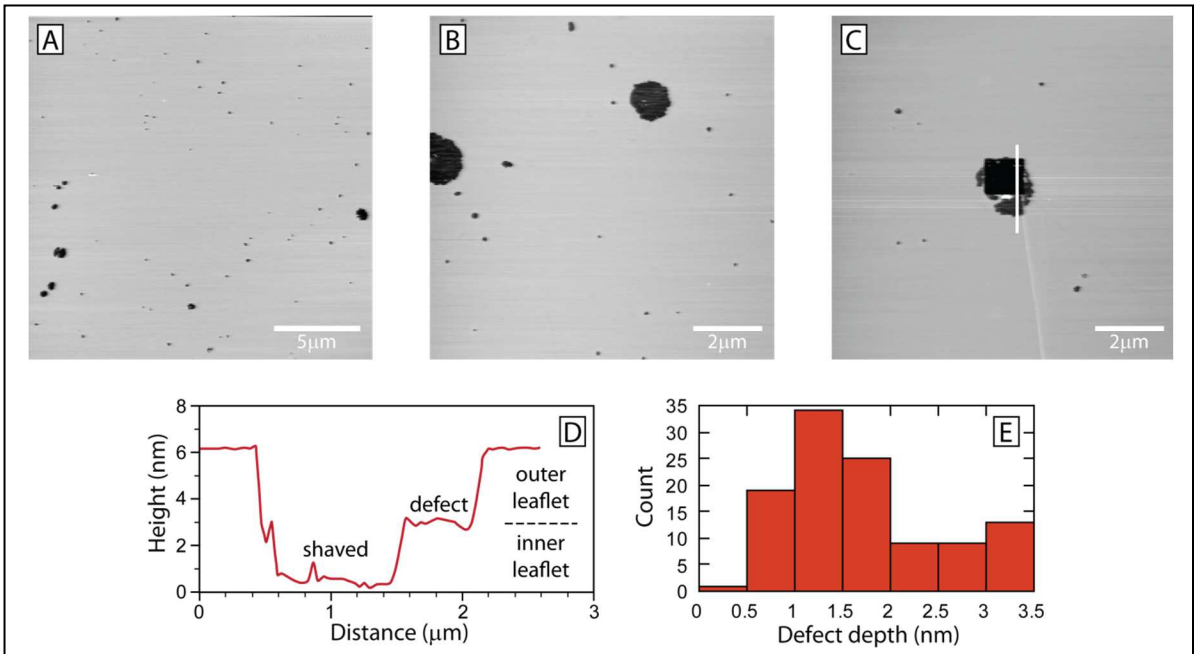

Figure 4.2. [A] Typical AFM topography scans of lipid raft membranes composed of 1:1:2 POPC-BSM-cholesterol in 0.5 mM $NaNO_3$ solution. [B] Scan of a membrane with micron diameter defects. [C] Membrane defect with diameter of ~1.5 μm. The center of the defect was shaved off using the AFM tip. Removal of the inner leaflet in the defect allowed the total thickness of the membrane to be measured. [D] Histogram of the defect depths. [E] The corresponding cursor profile (vertical line on [C]) is shown.

(Figure 4.1) is contact between bare mica substrates and therefore corresponds to the total membrane thickness. At a small applied force of 1 mN/m, the combined opposing raft membranes thicknesses were 11.9±0.3 and 11.1±0.3 nm for the two cases. In comparison, the AFM was used to obtain the membrane thickness by "shaving" away the inner DPPE monolayer leaflet in one of the large micron sized defects. The shaved thickness of about 6 nm or equivalently 12 nm for two membranes is consistent with that measured by SFA. Importantly, no structural rearrangement was observed throughout the SFA experiments even though the raft membranes were in the liquid-ordered phase and membrane defects were present in the contact region. Likewise, the contact mode AFM scans were stable and no change in defect shape was observed when scanning. Similar stability behavior was observed for pure

component liquid-ordered 1:1:1 POPC-DPPC-cholesterol membranes. The adhesion magnitude was also comparable to the homogeneous raft membranes.[66]

Equivalent thickness and hydration of raft membranes. The equivalent raft membranes thickness was defined as the thickness of the two outer monolayers including their water of hydration. The equivalent thicknesses of the raft membranes were 6.5±0.2 and 5.7±0.2 nm for the homogeneous and heterogeneous membranes, respectively. In order to determine the thickness of the hydration layer between the raft membranes, two independent measurements of raft monolayers on mica in air were carried out. The dry monolayer thickness was 2.2±0.1 nm. With this value, the hydration layer is 2.1±0.3 nm (6.5 nm minus two dry monolayers), which is comparable to a previous study by Marra and Israelachvili on hydration between pure PC bilayers.[20]

DISCUSSION

The primary goal of this work was to obtain a better understanding of properties and interactions between lipid raft membranes in a more complex biomimetic system. A composition of 1:1:2 BSM-POPC-cholesterol was selected to ensure the raft membrane was in the L_o phase and thus comparisons could be made to our previous work of pure component liquid-ordered ternary mixtures of DPPC-POPC-cholesterol without the complication of phase separation. As mentioned previously, BSM is a pseudo-mixture lipid with a variety of amide-linked acyl chain lengths. Studies have suggested that the long chained SM lipids in the outer membrane leaflet might interdigitate and affect the overall structure or phase state of the bilayer membrane.[156-157, 161-162] For example, fluorescence experiments of asymmetric bilayers indicated that domains on the outer leaflet and the coupling between the membrane leaflets

can induce formation of domains in the inner leaflet.[160, 163] In this work, the raft membrane mixture of 1:1:2 BSM-POPC-cholesterol was deposited onto an almost defect-free, gel phase DPPE monolayer immobilized on mica. Phase separation or formation of nanodomains was not observed by high-resolution AFM topography scans and confirmed that the raft membranes existed as a single L_o phase. Likewise, no evidence of interdigitation of the long amide-linked acyl chain SM lipid between the leaflets was detected.

The observed behavior of these more biological raft membranes revealed similar properties to well-studied pure component systems. In terms of adhesion magnitude, the homogeneous well-packed raft membranes had comparable van der Waals attraction (1.3±0.2 to 1.5±0.2 mN/m) to the ternary mixed membranes containing pure DPPC (1.8±0.2 mN/m).[66] The adhesion of these L_o supported membranes was higher than previously measured values for fluid and gel phase PC membranes (0.5-1.0 mN/m)[20, 26, 140] and significantly lower than adhesion between gel phase PE membranes (5-6 mN/m).[20] Both PC and PE membranes are expected to have similar Hamaker constants based on the SFA[20] and refractive index measurements.[19] Thus, the differences in the measured adhesion between the ternary L_o phase membranes can be attributed to the variation in the lipid composition, contact separation and hydration thickness between the membranes. Even though the adhesion magnitude is similar in both L_o systems, the raft membrane equivalent thickness was lower compared to the thickness of 1:1:1 ternary mixed membrane. The main difference between the two systems was the saturated lipid component in the mixture (BSM *vs.* DPPC). In comparison to glycerol lipids, SM can both hydrogen bond donate and accept. This difference in intermolecular hydrogen

bonding structure could account for the reduced hydration and thinner equivalent thickness of the BSM raft membranes.[156]

In both the homogeneous and heterogeneous raft membrane experiments, as well as in recent studies with supported lipid membranes of different lipid compositions, a small electrostatic repulsion has been observed.[66-67, 137] As reported previously, the electrostatic repulsion is due to a small fraction of charged lipid species in the membrane.[137] AFM scans of our raft membranes revealed that membrane-spanning holes were not present. Thus, the measured charge was not due to the underlying support, further confirming that charged lipid species are the source of the electrostatic repulsion. This conclusion is also consistent with the previously studied pure component 1:1:1 system. Despite the dramatic difference in the cholesterol concentration (33 *vs.* 50 mole%) and lipid constituents, the L_o membranes had very similar compressibility and stability. Although cholesterol is known to fluidize membranes, biomimetic raft membranes in the L_o phase are highly stable and do not show structural rearrangements such as thinning or higher adhesion with increased contact time or load. This stability is surprising given the hypothesized fluctuations of lipid raft domains. Continued investigations with more biologically complex systems are needed to further address this issue.

CONCLUSION

This study determined the interaction behavior between liquid-ordered biomimetic lipid raft membranes composed of 1:1:2 POPC-BSM-cholesterol. The force-distance profiles showed a small variation in the long-range electrostatic repulsion and raft membrane adhesion, which was attributed to the heterogeneity of the sphingolipids used in the mixture and the presence

of non-uniform sized nanoscopic membrane defects of densities varying between 0.5 to 8%. In comparison, no variation in interaction behavior was observed in our previous work with liquid-ordered ternary mixtures of pure POPC-DPPC-cholesterol membranes. Nevertheless, these more complex raft membranes exhibited an adhesion magnitude and compressibility similar to the ternary mixed membranes containing pure components.[66] The similarity in behavior of liquid-ordered membranes suggests that their physical properties are not very sensitive to the molecular details of the saturated lipid species. The variation in hydrogen bonding structure due to amine linkages and hydration shell only led to subtle changes in the overall interaction forces in the liquid-ordered BSM *vs*. DPPC ternary mixed membranes. The insensitivity in the interaction behavior over the range of components and compositions (*i.e*. the high concentration of cholesterol and complex mixture of BSM) suggest that membranes in liquid ordered phases have well defined properties. If cellular membranes rafts are liquid ordered phases, it may be possible to reasonably simulate their properties with synthetic mixtures.

ACKNOWLEDGMENTS

This work was primarily supported by the NSF chemistry division through grant CHE-1413745. We thank Joao Ventrici for assistance with atomic force microscopy and Shawn Mattathill for assistance with transfer ratio measurements.

Chapter V

Interaction Forces of 7:3 DPPC-oleic acid membranes in different pH conditions

James Kurniawan[†], Keishi Suga[#‡] and Tonya L. Kuhl[†¥]*
[†]Department of Chemical Engineering, University of California Davis, 95616, USA
[‡]Division of Chemical Engineering, Graduate School of Engineering Science, Osaka University, 1-3 Machikaneyamacho, Toyonaka, Osaka 560-8531, Japan
[¥]Department of Biomedical Engineering, University of California Davis, 95616, USA
Corresponding Authors: *E-mail: tlkuhl@ucdavis.edu [#]E-mail: keishi.suga@cheng.es.osaka-u.ac.jp

ABSTRACT

Oleic acid is known to interact with saturated lipid molecules and increase the fluidity of gel phase lipid membranes. In this work, the thermodynamic properties of mixed monolayers of 1,2-dipalmitoyl-*sn*-glycero-3-phosphocholine (DPPC) and oleic acid at the air-water interface were determined using Langmuir isotherms. The isotherm study revealed an attractive interaction between oleic acid and DPPC. The incorporation of oleic acid also monotonically decreased the elastic modulus of the monolayer indicative of higher fluidity with increasing oleic acid content. Using the surface force apparatus, intermembrane force–distance profiles were obtained for substrate supported DPPC membranes containing 30 mol% oleic acid at pH 5.8 and 7.4. Three different preparation conditions resulted in distinct force profiles. Membranes prepared in pH 5.8 subphase had a low number of nanoscopic defects ≤1% and an adhesion magnitude of ~0.6 mN/m. A slightly higher defect density of 1-4% was found for membranes prepared in a physiological pH 7.4 subphase. The presence of the exposed hydrophobic moieties resulted in a higher adhesion magnitude of 2.9 mN/m. Importantly, at pH

7.4, some oleic acid deprotonates resulting in a long-range electrostatic repulsion. Even though oleic acid increased the DPPC bilayer fluidity and the number of defects, no membrane restructuring was observed indicating that the system maintained a stable configuration.

INTRODUCTION

Biologically occurring fatty acids have been extensively studied due to their strong link to numerous health benefits.[164-165] Fatty acids, which are found in foods such as fruits, seeds, nuts, vegetable oils, animal fats, and fish oils, can be categorized into saturated, monounsaturated, polyunsaturated, and *trans* fats. Both saturated and *trans* fatty acids has been shown to increase the risk of cardiovascular diseases.[166-169] In contrast, unsaturated fatty acids have been shown to have a potentially therapeutic benefit for patients with type-2 diabetes,[170] dementia,[171] cystic fibrosis,[172] and arguably to reduce the risk of coronary heart diseases.[173-176] In particular, polyunsaturated fatty acids (PUFAs) such as α-linolenic acid (omega-3) and linoleic acid (omega-6) have received the most attention as humans cannot synthesize either of these molecules. As a result, the importance of the monounsaturated fatty acids (MUFAs) has been somewhat overshadowed.

Oleic acid is an example of monounsaturated omega-9 free fatty acid and is a major constituent in vegetable oil derived from olive, rapeseed, and sesame seeds. Free fatty acids, such as oleic acid can intercalate into lipid membranes and alter their physicochemical properties.[177-178] Specifically, due to the kinked *cis*-double bond structure, oleic acid has been shown to alter the structure, fluidity, and permeability of saturated phospholipid monolayers and bilayers.[179-181] Based on monolayer studies, Gonçalves *et al.* reported attractive lateral

interactions between oleic acid and DPPC based on a decrease in the area per molecule in their mixtures at the air-water interface.[182] Thermodynamic analysis using differential scanning calorimetry (DSC) revealed the melting temperature of DPPC-oleic acid mixtures decreased up to ~50 mol% oleic acid content.[183] Additional measurements indicated that the fluidity of DPPC membranes concomitantly increased with the presence of oleic acid.[184] The miscibility of oleic acid in DPPC membranes and fluidization of the membrane was corroborated by molecular dynamics simulation studies performed by Cerezo and coworkers.[185] Their simulations also found an increase in lateral diffusivity in the mixed system and enhancement in membrane permeability. The interaction between oleic acid and DPPC molecules is also likely to affect the deprotonation of the oleic acid's carboxyl headgroup. The pKa of an isolated carboxyl group in water is ~4.8,[186] while the apparent pKa of oleic acid's carboxyl headgroup tends to be higher depending on the type of co-existing molecules in the mixture and structure of the assembly (*i.e.*, pKa of ~6.1 in the hexagonal phase of oleic acid and monoolein mixtures[187]; pKa of ~6.5 in 4:6 oleic acid-DPPE vesicles[188]; pKa of ~8.0-8.5 in pure oleic acid vesicles[186]; and, an even higher pKa of ~9.85 for oleic acid monolayers at air-water interface[189]). The deprotonation of oleic acid in the system consequently alters molecular level lateral interactions and phase behavior of the mixture.[186, 190] Likewise, deprotonation would significantly impact the interaction between membranes and oleic acid can be used to induce pH-dependent membrane fusion or membrane repulsion in model systems.[188, 191-192] The ability to alter the charge of oleic acid through pH enables switching between attractive, null and repulsive electrostatic interactions in membranes. For example, positively charged vesicles will spontaneously fuse with negatively charged vesicles containing oleic acid under alkaline conditions. Beyond the ability to tailor the

charge of membranes containing oleic acid through pH, incorporation of oleic acid may alter membrane structure, fluidity, permeability as well as water of hydration and entropic motion such as membrane protrusions and undulations.

In this work, the lateral interaction between oleic acid and DPPC molecules in monolayers were examined using Langmuir isotherms at the air-water interface as a function of oleic acid concentration. The isotherm studies were used to determine the Gibbs free energy of mixing and changes in monolayer compressibility, which are indicative of constituent molecule interactions and membrane fluidity. The interaction forces between 7:3 DPPC-oleic acid membranes were investigated at different pH conditions using the surface force apparatus (SFA) technique.[120] Force profiles were measured and compared at physiological pH 7.4, where full deprotonation is expected, and at pH 5.8. The force profile measurements also enabled the membrane thickness, adhesive minimum and surface charge density to be directly determined.

MATERIALS AND METHODS

Chemicals. 1,2-dihexadecanoyl-*sn*-glycero-3-phosphoethanolamine (DPPE, melting point, T_M = 63°C) and 1,2-dipalmitoyl-*sn*-glycero-3-phosphocholine (DPPC, T_M = 41°C) were purchased from Avanti Polar Lipids, Inc. (Alabaster, AL) and used as received. Oleic acid (*cis*-9-octadecanoic acid, T_M = 13-14°C), monosodium phosphate (NaH_2PO_4 99.999%), disodium phosphate (Na_2HPO_4 99.95%) and sodium nitrate ($NaNO_3$ 99.995%) were purchased from Sigma-Aldrich (St. Louis, MO). Water was purified with a MilliQ gradient water purification system to a resistivity of 18 MΩ·cm.

Isotherm of DPPC-oleic acid at the air-water interface. Pressure-area isotherms (Π-*A*) of various DPPC-oleic acid mixtures were obtained on a pure water subphase at 25°C under an inert environment, depleted of oxygen, which inhibits oxidation of carbon-carbon double bonds. The isotherms were obtained without prior compression cycles with a compression ratio of about 17 cm^2/min, which corresponds to a compression rate of 2-3 $Å^2$ per molecule per min. The lateral interaction between DPPC and oleic acid molecules such as the monolayer elastic modulus, C_s^{-1}, excess area, A_{ex} and Gibbs excess free energy of mixing, ΔG_{mix} were calculated from the isotherm data. The elastic modulus is defined as the product of the average area per molecule (A) and the slope of the Π-*A* isotherm at a specific surface pressure:

$$C_s^{-1} = -A\frac{\mathrm{d}\Pi}{\mathrm{d}A} \qquad \text{(Eq. 5.1)}$$

Excess area was calculated using the area per molecule data from the pure component and mixture isotherms given by

$$A_{ex} = A_{12} - (x_1A_1 + x_2A_2) \qquad \text{(Eq. 5.2)}$$

where A_{12}, A_1, A_2 are area per molecule of the DPPC-oleic acid mixture, DPPC, and oleic acid, respectively, and x_1 and x_2 are molar fractions of DPPC and oleic acid, respectively. The total Gibbs excess free energy of mixing is defined as

$$\Delta G_{mix} = \Delta G_{ex} + \Delta G_{ideal} \qquad \text{(Eq. 5.3)}$$

where the excess Gibbs free energy, ΔG_{ex}, was obtained by integrating A_{ex} with respect to the surface pressure, $\Delta G_{ex} = \int A_{ex} d\Pi$, and the ideal Gibbs free energy of mixing was calculated by

$$\Delta G_{ideal} = kT\big(x_1 ln(x_1) + x_2 ln(x_2)\big) \qquad \text{(Eq. 5.4)}$$

where *k* is the Boltzmann constant and *T* is absolute temperature.

Membrane Preparation. Mica substrate supported lipid membranes were used in SFA and AFM studies. The membranes were constructed using Langmuir-Blodgett (LB) deposition (Nima Coventry, U.K.). The inner monolayer for all the experiments was DPPE deposited using Langmuir-Blodgett (LB) method at 45 mN/m and dipping speed of 1 mm/min with a MilliQ water subphase (pH = 5.8). Previous studies have shown that LB deposited DPPE forms an almost defect free, robust and strongly physisorbed monolayer on mica with transfer ratios of 0.997±0.004[66] and a thickness of 2.56±0.05 nm under these conditions.[19] As the underlying mica support is negatively charged, this near perfect DPPE inner monolayer minimizes any charge originating from the substrate. In addition, the tight packing and stability of the gel phase DPPE inner monolayer minimizes molecular exchange between the two leaflets. The outer monolayer was 7:3 DPPC-oleic acid LB deposited at 35 mN/m and dipping speed of 1 mm/min on MilliQ water (pH = 5.8) or 0.5 mM phosphate buffer (pH = 7.4) subphase. The average molecular areas for the 7:3 DPPC-oleic acid outer monolayer were 34.2±1.0 $Å^2$ at pH 5.8 and 33.7±1.5 $Å^2$ at pH 7.4.

Surface Force Apparatus Measurements (SFA). The details about SFA technique can be found in chapter II. The stiffness of the double cantilever spring was $2.6x10^5$ mN/m. Force profiles shown in the results section are representative force-distance profiles of three independent experiments at three different experimental conditions. The experimental conditions were (i) both the inner and outer monolayers LB deposited on MilliQ water subphase at pH 5.8 and the force profiles measured in 0.5 mM $NaNO_3$ solution at pH 5.8; (ii) membrane deposited on MilliQ water subphase at pH 5.8, but with the force profiles measured in 0.5 mM phosphate buffer at pH 7.4; (iii) outer membrane leaflet deposition and force measured in 0.5

mM phosphate buffer at pH 7.4. At least five repeatable force measurements were taken for each experimental condition and the reported error propagation in the results section was based on the average of the five force runs for each condition.

Atomic Force Microscopy (AFM). AFM images were acquired using a MFP3D-SA system (Asylum Research, Santa Barbara, CA). A silicon cantilever (model MSNL-10, Bruker, Santa Barbara, CA) with force constant of 0.6 N/m was used for imaging. All the images were acquired in contact mode with a force of 12 nN. AFM images were analyzed using Gwyddion Version 2.31 (http://gwyddion.net/).

RESULTS

Monolayer properties of DPPC-oleic acid mixtures. Pressure-area (Π-*A*) isotherms of DPPC-oleic acid mixtures were measured on a pure water subphase (Figure 5.1A). In general, the area per molecule at each pressure decreased with increasing oleic acid molar ratio.[182] Isotherm data were used to calculate the elastic moduli and excess Gibbs free energy of mixing of the mixtures (Eq. 5.1). The elastic moduli of pure DPPC plateaued at a surface pressure range of 28-37 mN/m (Figure 5.1B). Due to the noise in the data, a moving average value was used to obtain the average elastic moduli. As shown in Figure 5.1C, a trend of decreasing elastic moduli with increasing oleic acid was observed. To estimate the miscibility of oleic acid in DPPC, the excess Gibbs free energy of mixing was determined (Eq. 5.3).[193-194] The excess Gibbs free energy of mixing values were negative for all DPPC-oleic acid mixtures which indicates a favorable interaction between DPPC and oleic acid (Figure 5.1D). It has been reported that hydrogen bonding between oleic acid molecules and DPPC could alter the apparent pKa value of oleic

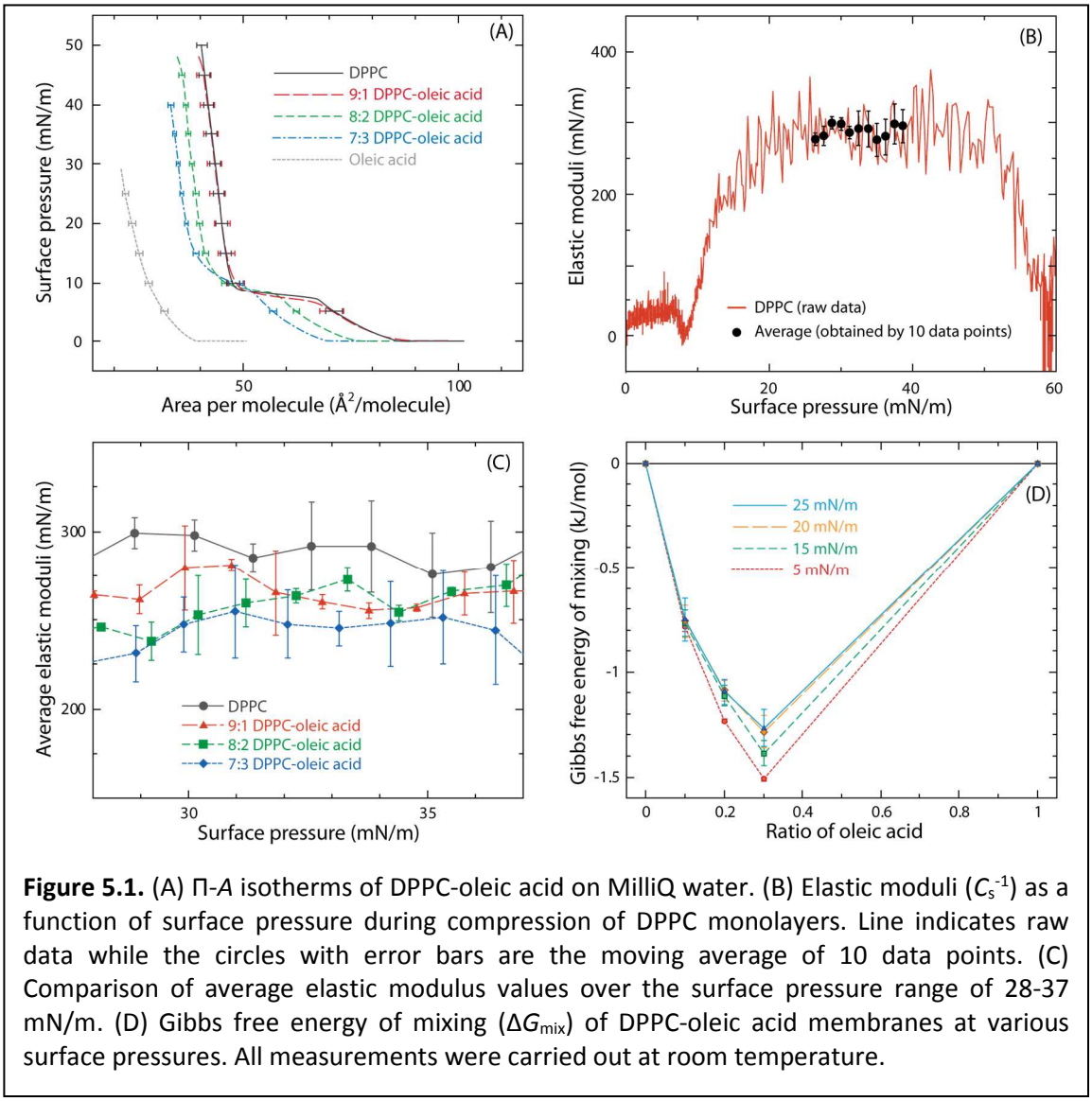

Figure 5.1. (A) Π-*A* isotherms of DPPC-oleic acid on MilliQ water. (B) Elastic moduli (C_s^{-1}) as a function of surface pressure during compression of DPPC monolayers. Line indicates raw data while the circles with error bars are the moving average of 10 data points. (C) Comparison of average elastic modulus values over the surface pressure range of 28-37 mN/m. (D) Gibbs free energy of mixing (ΔG_{mix}) of DPPC-oleic acid membranes at various surface pressures. All measurements were carried out at room temperature.

acid.[195] To further elucidate the impact of lateral interactions and embedding of oleic acid in a phospholipids membrane on deprotonation, membrane thickness, and adhesion, the interaction force profiles between 7:3 DPPC-oleic acid membranes were directly measured with an SFA under the various deposition and solution conditions listed previously.

Force – distance profile of 7:3 DPPC-oleic acid at different pH. Figure 5.2 shows the measured force profiles between opposing membranes with 7:3 DPPC-oleic acid as the outer monolayer at three different experimental conditions. When both the inner and outer

monolayers were LB deposited on MilliQ water subphase at pH 5.8, and the force profiles measured in 0.5 mM $NaNO_3$ solution at pH 5.8, the thickness of the equivalent of 7:3 DPPC-oleic acid membrane was 7.8±0.2 nm. This equivalent thickness is defined as the thickness of the two outer monolayers including the water of hydration between the bilayers. The magnitude of adhesion between the membranes was 0.6±0.1 mN/m and no electrostatic repulsion was observed. The lack of electrostatic repulsion is consistent with a very low-degree of deprotonated oleic acid at pH of 5.8 (pKa of oleic acid >6.1).[187]

Using the same membrane preparation method (where the membrane was LB deposited in MilliQ water at pH 5.8), but force profile measurements were done in 0.5 mM pH 7.4 phosphate buffer subphase, the thickness of the equivalent 7:3 DPPC-oleic acid membrane was 7.4±0.2 nm. The force profiles clearly showed a long-range electrostatic repulsion with decay length consistent with the electrolyte concentration and a short-range attraction. The electrostatic contribution was fitted using the non-linear Poisson–Boltzmann equation with constant charge approximation. A constant surface charge density of 1.3±0.3 mC/m^2 or surface potential of -25±3 mV was obtained with the origin of charge at the membrane surface. The thickness and adhesion of the equivalent 7:3 DPPC-oleic acid membranes at pH 5.8 and 7.4 were similar due to the identical deposition conditions. As the electrostatic and van der Waals attraction should be additive, the electrostatic interaction was subtracted from the total force profile to extract the attractive contribution to the membrane-membrane interaction. After removing the electrostatic contribution, the membrane adhesion magnitude was 0.7±0.1 mN/m (Figure 5.2C).

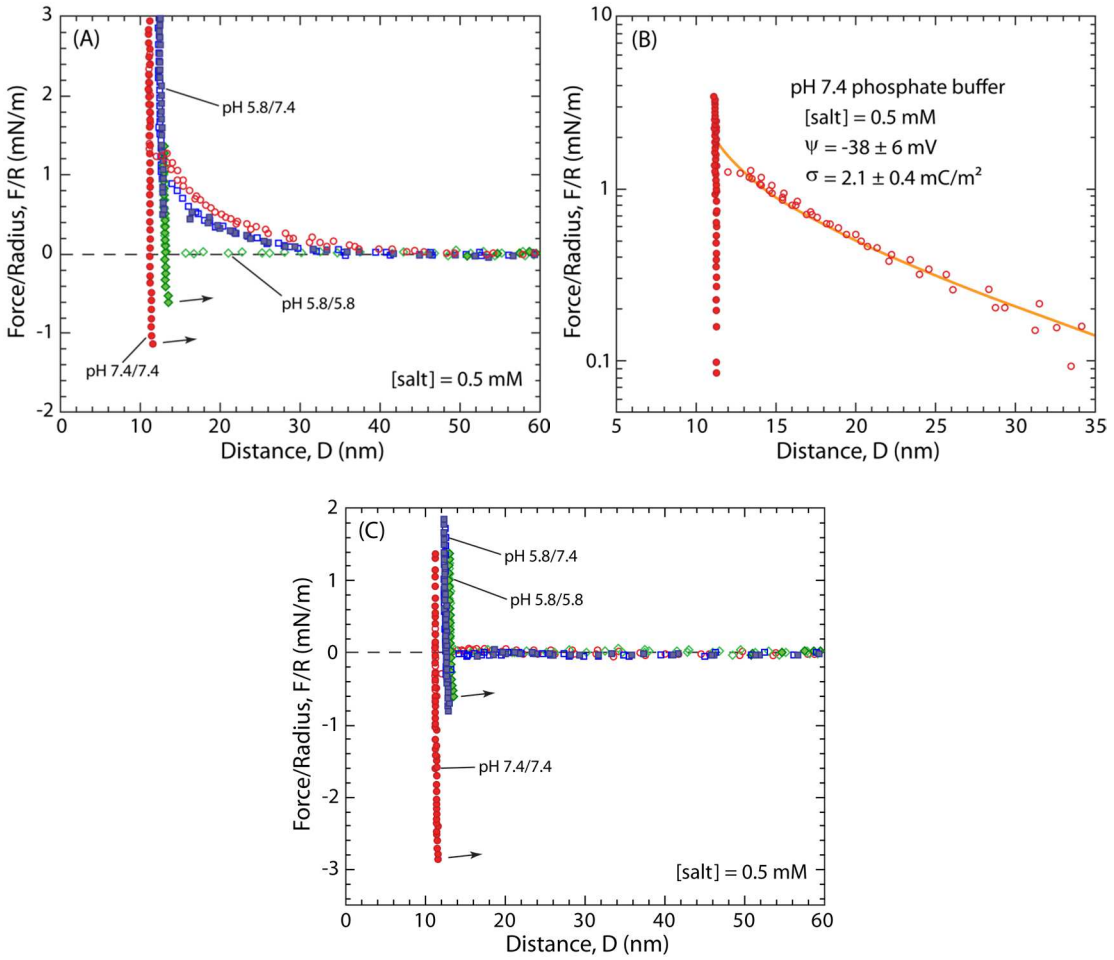

Figure 5.2. (A) Force–distance profiles between 7:3 DPPC-oleic acid membranes under three different experimental conditions. The pH during the membrane deposition is shown as the first value and the pH during force profile measurements is shown as the second value, where diamonds pH 5.8/5.8, squares pH 5.8/7.4, and circles pH 7.4/7.4. Open and filled symbols indicate approach and separation respectively. (B) Semi-logarithmic plot of the force profile of 7:3 DPPC-oleic acid membranes prepared and measured in 0.5 mM pH 7.4 phosphate buffer (pH 7.4/7.4). The solid line is the fitted electrostatic contribution with the origin of charge at the membrane surface. D = 0 is defined as the contact between bare mica–mica surfaces. (C) Subtraction of the electrostatic contribution and corresponding attractive contribution to the force profile.

When both the deposition of the outer monolayer and the force measurement were done in 0.5 mM pH 7.4 phosphate buffer, a significantly thinner 7:3 DPPC-oleic acid membrane with equivalent thickness of 6.0±0.2 nm was obtained. Again, because of the higher pH, the oleic acid molecules were partially deprotonated resulting in a long-range electrostatic

repulsion. The surface charge density was slightly higher than it was in the case of depositing the membrane at pH 5.8 and measuring the force profiles at pH 7.4. At pH 7.4 conditions, a constant surface charge density of 2.1±0.4 mC/m^2 or surface potential of -38±6 mV was obtained. After subtracting the electrostatic contribution, the magnitude of the membrane adhesion was substantially greater at 2.9±0.1 mN/m (Figure 5.2C). Results for the SFA measurements are summarized in Table 5.1.

Table 5.1. Summary of SFA Results at three different experimental conditions.

pH during deposition	pH for force run	Equivalent Thickness (nm)*	σ (mC/m^2)	Ψ (mV)	$\|F_{ad}/R\|_{VdW}$ (mN/m)
5.8	5.8	7.8±0.2	N/A	N/A	0.6±0.1
5.8	7.4	7.4±0.2	-1.3±0.3	-25±3	0.7±0.1
7.4	7.4	6.0±0.2	-2.1±0.4	-38±6	2.9±0.1

* The equivalent thickness is the thickness of the two outer monolayers including their hydration layer

In order to corroborate the resulting force profiles with membrane structure under different preparation conditions, high-resolution AFM topography scans were done on LB deposited 7:3 DPPC-oleic acid membranes at pH 5.8 and 7.4 (Figure 5.3). No phase separated domains were observed, but the AFM scans revealed topological membrane defects that extended down to the inner DPPE monolayer in both cases. When 7:3 DPPC-oleic acid was prepared in MilliQ water at pH 5.8, more uniform, well-packed membranes were obtained. Based on image analysis of four independent samples with at least five different regions scanned per sample, the average defect depth was 2.0±0.7 nm with surface coverage area between 0-1% of the supported membrane.[50] In one case, multiple membrane spanning holes that penetrated the DPPE inner monolayer were detected (Figure 5.3). When the outer membrane leaflet was deposited from an 0.5 mM phosphate buffer at pH 7.4, significantly more topological defects were found. Based on analysis of two independent samples with at

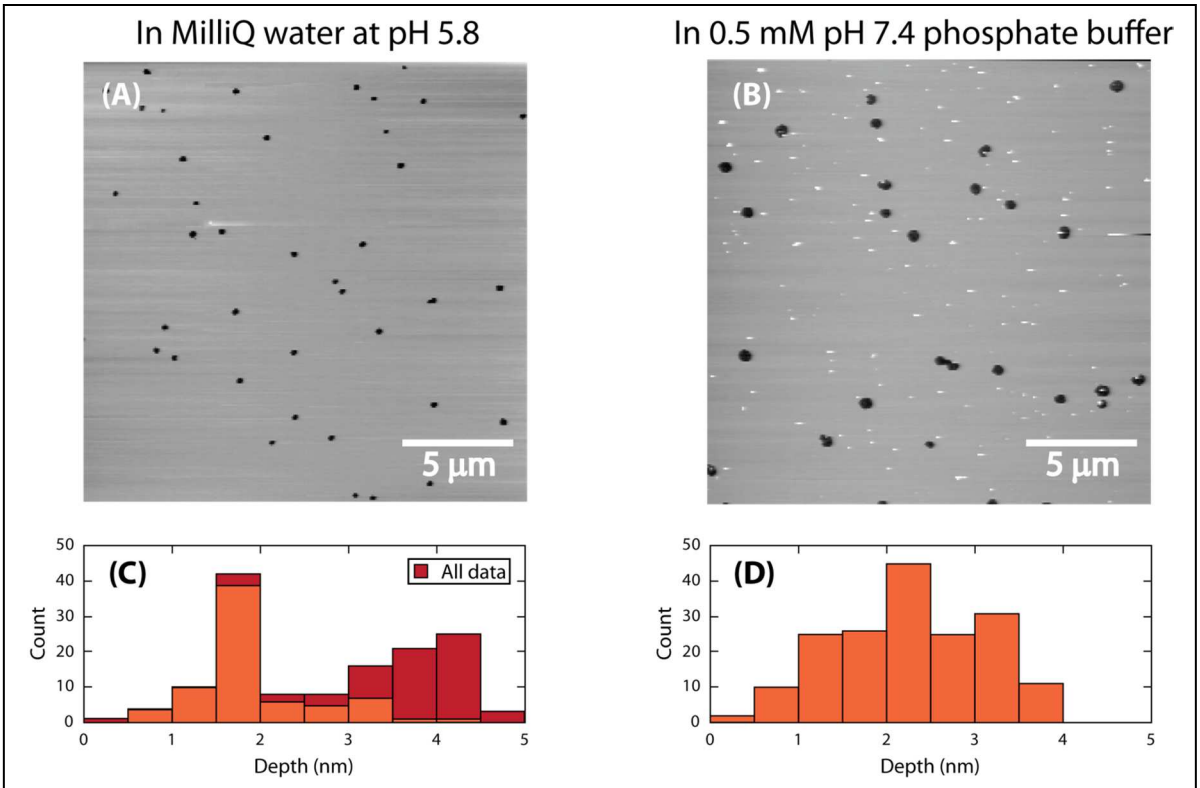

Figure 5.3. 20x20 µm AFM scan of 7:3 DPPC-oleic acid on DPPE membrane LB deposited on mica in pH 5.8 MilliQ water [A] and in 0.5 mM pH 7.4 phosphate buffer [B]. [C] Histogram of the defect depth for 7:3 DPPC-oleic acid on DPPE membrane in pH 5.8 MilliQ water (orange) and histogram of defects+holes that reached the underlying mica substrate found in one scan (red). [D] Histogram of the defect depth for 7:3 DPPC-oleic acid on DPPE membrane in 0.5 mM pH 7.4 phosphate buffer. The histograms were constructed based on 2-4 independent samples with at least 5 different regions scanned per sample yielding 10-20 analyzed images. The average depths and defect density area were statistically analyzed with error bars as standard deviation: in pure water, depth = 2.0±0.7 nm, defect area = 0.6±0.4%; in pH 7.4 buffer, depth = 2.3±0.8 nm, defect area = 1.5±0.7%.

least five different regions scanned per sample, the surface coverage of the defects ranged between 1-4% [50] and the average defect depth was 2.3±0.8 nm.

DISCUSSION

Langmuir monolayer analysis of DPPC-oleic acid lateral interaction. Isotherms of various DPPC-oleic acid mixtures revealed that the fluid to gel phase transition of DPPC was maintained in DPPC-oleic acid mixtures, indicating that DPPC still formed the continuous phase.

The absence of phase separation in the 7:3 DPPC-oleic acid membranes was corroborated by the high resolution AFM topography scan (Figure 5.3). The isotherm of the DPPC-oleic acid mixtures also indicated stabilization of oleic acid by the lateral interaction with DPPC lipids. For all oleic acid concentrations studied, the DPPC-oleic acid monolayer was able to compress beyond the collapse pressure of a pure oleic acid monolayer (~30 mN/m) and there was no indication of oleic acid squeezing out from the air-water interface at a surface pressure of 35 mN/m. These results demonstrate that DPPC and oleic acid are miscible with each other, and the interaction between DPPC and oleic acid molecules is favorable under the experimental conditions studied. Additionally, one of the roles of unsaturated fatty acid in membranes is to destabilize ordered structures such as raft domains. Onuki *et al*. reported that 30% of oleic acid significantly fluidized DPPC membranes, resulting in a decrease of detergent-insolubility.[196] The monolayer elastic modulus is a measure of the membrane stiffness and correlated to the fluidity of the membrane. The experimental data showed that incorporation of oleic acid into DPPC monolayers decreased the film stiffness (Figure 5.1C). Although the differences of elastic modulus in DPPC and DPPC-oleic acid mixture were small, the averaged values show a decreasing trend with increasing oleic acid in the monolayer. Thus, incorporation of oleic acid decreases the stiffness of DPPC monolayers and correspondingly increases monolayer fluidity.[184]

Adhesion between 7:3 DPPC-oleic membranes. When the membranes were deposited in MilliQ water at pH 5.8, the effective membrane adhesion due to attractive van der Waals interactions was consistent and matched well with the measured adhesion between pure fluid phase PC membranes of 0.6±0.1 mN/m reported by Marra and Israelachvili.[20] In addition, the

fluidization effect of oleic acid incorporation into DPPC membrane observed by Langmuir monolayer analysis is consistent with the lower adhesion compared to gel phase DPPC.[20] However, the mixed oleic acid-DPPC membrane was thicker at 7.4-7.8 nm compared to the thickness of gel phase DPPC presumably deposited on DPPE of 5.5±0.3 nm[20] and our own measurements of DPPC on DPPE membrane thickness of 6.0±0.2 nm using the SFA. Similar values were obtained from X-ray reflectivity measurements of supported DPPC membranes on quartz.[22] Possible, even coexisting, reasons for the increase in apparent membrane thickness include (i) a larger hydration shell of charged oleic acid in the DPPC membrane, (ii) greater protrusions of the single acyl chain fatty acid out of the membrane plane and/or (iii) a decrease in tilt of the DPPC lipids from surface normal. Further studies such as high-resolution X-ray scattering and NMR hydration studies could help quantify these different contributions. In contrast, the higher level of defects on the 7:3 DPPC-oleic acid membranes deposited at pH 7.4 led to a thinner membrane and significantly higher adhesion. The difference in the adhesion magnitude of about 2 mN/m was attributed to hydrophobic attraction due to the higher amount of exposed inner monolayer acyl chains or hydrophobic moieties in the contact regions.[138]

Dissociation of oleic acid in mixed 7:3 DPPC-oleic acid membranes. Fatty acid molecules self-assemble into micelles, vesicles, and other closed structures in aqueous media. Their deprotonation depends on the surrounding pH and the type of any associated lipids or molecules in the assembled structure. Previous studies have shown that the apparent pKa of oleic acid in different surfactant and lipid mixtures ranges from 6.0 to 9.5. For example, the pKa

of pure oleic acid vesicles is 8.0-9.5.[190, 197-198] While when mixed with monoolein, the pKa was 6.0-7.0.[187] A similar pKa of 6.5 was found for 4:6 oleic acid-DPPE vesicles.[188]

The force profile measurements and determination of the surface charge density of 7:3 DPPC-oleic acid SLBs under various pH conditions enable the deprotonation level of oleic acid in DPPC membranes to be extracted precisely. At pH 5.8, no electrostatic repulsion was measured, indicating that oleic acid does not dissociate (deprotonate) under these conditions. The absence of electrostatic repulsion also suggests that charged lipid impurities are the dominant source of electrostatic repulsion, which was previously observed in some experiments using overall neutral membranes.[66-67, 127] At pH 7.4, regardless of the deposition being at pH 5.8 or 7.4, a long-range electrostatic repulsion was observed. The electrostatic repulsion is clearly due to partially dissociated (negatively charged) oleic acid molecules in the membrane. The level of charge was lower in the case of the mixed monolayer being deposited from a water subphase (pH 5.8) than in a buffered subphase (pH 7.4). Under the former conditions, a constant surface charge density of 1.3 mC/m^2 was obtained, which corresponds to 0.9% of the oleic acid molecules dissociating. The degree of oleic acid dissociation was calculated using average the area per molecule of 34.2 $Å^2$ at 35 mN/m. The apparent pKa value of oleic acid in the 7:3 DPPC-oleic acid membrane was estimated to be 9.4±0.2 using the Henderson-Hasselbalch equation. In comparison, when the 7:3 DPPC-oleic acid outer layer was deposited on a pH 7.4 subphase, a higher surface charge density of 2.1 mC/m^2 was measured. The deprotonation degree of oleic acid under this experimental condition corresponds to 1.5% deprotonation, and an apparent pKa value of 9.2±0.1. These apparent pKa values should be an upper bound as the pH of the environment precisely at the membrane surface and oleic acid molecules is slightly reduced by

the stationary buffer layer above the membrane. Based on previous work by Kramer *et al*., the pH at the membrane surface was estimated to be 7.0 [199] and thus the lower bound of the apparent pKa of oleic acid would be 0.4 pH units lower than the upper bound values provided above.

The pKa of isolated carboxylic groups in water is much lower at 4.8.[186] Clearly, the fatty acid chain length and structure of the self-assembled system are key factors in shifting the apparent pKa to higher (more alkaline) values.[200] In particular, our work demonstrates that the apparent pKa of oleic acid in 7:3 DPPC-oleic acid ranges between 8.8-9.4±0.2. By their very definition, self-assembled structures of amphiphilic molecules require close proximity of the low dielectric environment of the acyl region and hydrophilic, potentially charged headgroup region. Low dielectric media greatly reduce charge dissociation and this is the main reason for the low deprotonation of oleic acid in mixed DPPC membranes. In addition, the measured negative excess Gibbs free energy of mixing, ΔG_{mix}, for mixed DPPC and oleic acid monolayers demonstrates favorable interactions between DPPC and oleic acid on a pure water subphase.[182] Favorable lateral association between and with lipid molecules and surfactants is also consistent with inhibition of oleic acid deprotonation.

The results further demonstrate that deprotonation of oleic acid in mixed monolayers decreases the quality of monolayer transfer during LB deposition. The 7:3 DPPC-oleic acid membrane prepared in pH 7.4 was thinner due to more defects and had a higher surface charge density than the membrane prepared in pH 5.8. The thinner membrane and presence of defects lower the lateral packing density and thus increased the spacing between headgroups. The lower lateral packing density enables greater deprotonation, primarily due to increasing the

effective dielectric in the headgroup region. The change in packing would also result in a larger spacing between molecules, further aiding deprotonation, as well as changes in the lateral interactions between headgroups such as hydrogen bond formation.

The alteration in the membrane surface charge density in conjunction with the increase in membrane fluidity should reduce the barrier function of the membrane towards external molecules, which would enhance insertion of external molecules into the membrane and increase cellular uptake efficiency of drugs. As membrane properties can be a key factor in membrane-associated interactions,[201] these changes in membrane properties could also affect the localization of membrane associated enzymes or proteins and thereby impact metabolic pathways. For example, oleic acid has been shown to modify G-protein-mediated signaling cascades that regulate adenylyl cyclase and phospholipase C.[202] Lastly, the properties of oleic acid are also modified by membrane composition and structure leading to changes in the apparent pKa. These findings enhance our understanding of the potential biological significance of free fatty acids.

CONCLUSION

Membrane interactions and the deprotonation behavior of oleic acid in a DPPC membrane at physiological pH were determined in this work. The interaction between 7:3 DPPC-oleic acid membranes was repulsive at pH 7.4, due to electrostatic interactions consistent with pH induced dissociation of oleic acid in the membrane. The apparent pKa of oleic acid in a DPPC membrane was 8.8-9.4±0.2, wherein oleic acid does not deprotonate at pH 5.8. More broadly, the deprotonation of oleic acid as a function of the pH is also relevant to non-biological

applications such as stabilization of nanoparticles by oleic acids[203] and emulsion stabilization in lipid droplets,[204] drug delivery systems, as well as food applications. The fluidization of saturated DPPC lipid membranes by oleic acid was apparent from the magnitude of adhesion between 7:3 DPPC-oleic acid membranes. The magnitude of adhesion was lower compared to the adhesion of gel phase DPPC membranes and was consistent with previously established value for adhesion between fluid phase PC membranes. The ability of oleic acid to interact with lipids and alter the interaction between membranes is important especially in the latest field of molecular therapy for the pharmaceutical industry. Oleic acid is able to regulate the localization and activity of membrane proteins in lipid rafts, which is important due to membrane proteins ability to control cell signaling and gene expression. In summary, the findings clearly demonstrate that oleic acid interacts favorably with saturated DPPC and that oleic acid's degree of deprotonation can be tailored by the solution pH enabling the interaction between oleic acid containing membranes, which have not previously studied, to be controlled. Additional studies, such as high resolution X-ray and neutron scattering measurements and other techniques, would help further characterize how oleic acid alters membrane structure and properties.

ACKNOWLEDGEMENT

This work was primarily supported by the NSF chemistry division through grant CHE-1413745. We thank Joao Ventrici for the assistance with atomic force microscopy. Keishi Suga expresses his gratitude for Engineering Science Young Researcher Dispatch Program and Multidisciplinary Research Laboratory System of Osaka University.

References

1. Darnell, J. E.; Lodish, H. F.; Baltimore, D., *Molecular cell biology*. 2nd ed.; Scientific American Books : Distributed by W.H. Freeman: New York, N.Y., 1990; p xl, 1105 p.
2. Kasahara, K.; Sanai, Y., Involvement of lipid raft signaling in ganglioside-mediated neural function. *Trends Glycosci Glyc* **2001,** *13* (74), 587-594.
3. Stoddart, A.; Dykstra, M. L.; Brown, B. K.; Song, W. X.; Pierce, S. K.; Brodsky, F. M., Lipid rafts unite signaling cascades with clathrin to regulate BCR internalization. *Immunity* **2002,** *17* (4), 451-462.
4. Lingwood, D.; Simons, K., Lipid Rafts As a Membrane-Organizing Principle. *Science* **2010,** *327* (5961), 46-50.
5. Gorter, E.; Grendel, F., On bimolecular layers of lipoids on the chromocytes of the blood. *J Exp Med* **1925,** *41* (4), 439-443.
6. Edidin, M., Timeline - Lipids on the frontier: a century of cell-membrane bilayers. *Nat Rev Mol Cell Bio* **2003,** *4* (5), 414-418.
7. Castellana, E. T.; Cremer, P. S., Solid supported lipid bilayers: From biophysical studies to sensor design. *Surf Sci Rep* **2006,** *61* (10), 429-444.
8. Bayerl, T. M.; Bloom, M., Physical-Properties of Single Phospholipid-Bilayers Adsorbed to Micro Glass-Beads - a New Vesicular Model System Studied by H-2-Nuclear Magnetic-Resonance. *Biophys J* **1990,** *58* (2), 357-362.
9. Johnson, S. J.; Bayerl, T. M.; Mcdermott, D. C.; Adam, G. W.; Rennie, A. R.; Thomas, R. K.; Sackmann, E., Structure of an Adsorbed Dimyristoylphosphatidylcholine Bilayer Measured with Specular Reflection of Neutrons. *Biophys J* **1991,** *59* (2), 289-294.
10. Lambacher, A.; Fromherz, P., Fluorescence interference-contrast microscopy on oxidized silicon using a monomolecular dye layer. *Appl Phys a-Mater* **1996,** *63* (3), 207-216.
11. Tanaka, M.; Sackmann, E., Supported membranes as biofunctional interfaces and smart biosensor platforms. *Phys Status Solidi A* **2006,** *203* (14), 3452-3462.
12. Sinner, E. K.; Knoll, W., Functional tethered membranes. *Curr Opin Chem Biol* **2001,** *5* (6), 705-711.
13. Budvytyte, R.; Valincius, G.; Niaura, G.; Voiciuk, V.; Mickevicius, M.; Chapman, H.; Goh, H. Z.; Shekhar, P.; Heinrich, F.; Shenoy, S.; Losche, M.; Vanderah, D. J., Structure and Properties of Tethered Bilayer Lipid Membranes with Unsaturated Anchor Molecules. *Langmuir* **2013,** *29* (27), 8645-8656.
14. Shenoy, S.; Moldovan, R.; Fitzpatrick, J.; Vanderah, D. J.; Deserno, M.; Losche, M., In-plane homogeneity and lipid dynamics in tethered bilayer lipid membranes (tBLMs). *Soft Matter* **2010,** *6* (6), 1263-1274.
15. Heinrich, F.; Ng, T.; Vanderah, D. J.; Shekhar, P.; Mihailescu, M.; Nanda, H.; Losche, M., A New Lipid Anchor for Sparsely Tethered Bilayer Lipid Membranes. *Langmuir* **2009,** *25* (7), 4219-4229.
16. McGillivray, D. J.; Valincius, G.; Heinrich, F.; Robertson, J. W. F.; Vanderah, D. J.; Febo-Ayala, W.; Ignatjev, I.; Losche, M.; Kasianowicz, J. J., Structure of Functional Staphylococcus aureus alpha-Hemolysin Channels in Tethered Bilayer Lipid Membranes. *Biophys J* **2009,** *96* (4), 1547-1553.
17. Langmuir, I., The constitution and fundamental properties of solids and liquids. II. Liquids. *J Am Chem Soc* **1917,** *39*, 1848-1906.
18. Blodgett, K. B., Films built by depositing successive monomolecular layers on a solid surface. *J Am Chem Soc* **1935,** *57* (1), 1007-1022.
19. Kienle, D. F.; de Souza, J. V.; Watkins, E. B.; Kuhl, T. L., Thickness and refractive index of DPPC and DPPE monolayers by multiple-beam interferometry. *Anal Bioanal Chem* **2014,** *406* (19), 4725-4733.
20. Marra, J.; Israelachvili, J., Direct Measurements of Forces between Phosphatidylcholine and Phosphatidylethanolamine Bilayers in Aqueous-Electrolyte Solutions. *Biochemistry-Us* **1985,** *24* (17),

4608-4618.
21. Tamm, L. K.; Mcconnell, H. M., Supported Phospholipid-Bilayers. *Biophys J* **1985,** *47* (1), 105-113.
22. Watkins, E. B.; Miller, C. E.; Mulder, D. J.; Kuhl, T. L.; Majewski, J., Structure and Orientational Texture of Self-Organizing Lipid Bilayers. *Phys Rev Lett* **2009,** *102* (23).
23. Cremer, P. S.; Boxer, S. G., Formation and spreading of lipid bilayers on planar glass supports. *J Phys Chem B* **1999,** *103* (13), 2554-2559.
24. Bunjes, N.; Schmidt, E. K.; Jonczyk, A.; Rippmann, F.; Beyer, D.; Ringsdorf, H.; Graber, P.; Knoll, W.; Naumann, R., Thiopeptide-supported lipid layers on solid substrates. *Langmuir* **1997,** *13* (23), 6188-6194.
25. Salamon, Z.; Wang, Y.; Tollin, G.; Macleod, H. A., Assembly and Molecular-Organization of Self-Assembled Lipid Bilayers on Solid Substrates Monitored by Surface-Plasmon Resonance Spectroscopy. *Bba-Biomembranes* **1994,** *1195* (2), 267-275.
26. Orozco-Alcaraz, R.; Kuhl, T. L., Interaction Forces between DPPC Bilayers on Glass. *Langmuir* **2013,** *29* (1), 337-343.
27. Watkins, E. B.; Miller, C. E.; Liao, W. P.; Kuhl, T. L., Equilibrium or Quenched: Fundamental Differences between Lipid Monolayers, Supported Bilayers, and Membranes. *Acs Nano* **2014,** *8* (4), 3181-3191.
28. Lee, K. Y. C.; Lipp, M. M.; Takamoto, D. Y.; Ter-Ovanesyan, E.; Zasadzinski, J. A.; Waring, A. J., Apparatus for the continuous monitoring of surface morphology via fluorescence microscopy during monolayer transfer to substrates. *Langmuir* **1998,** *14* (9), 2567-2572.
29. Girard-Egrot, A. P.; Blum, L. J., Langmuir-Blodgett Technique for Synthesis of Biomimetic Lipid Membranes. In *Nanobiotechnology of Biomimetic Membranes*, Martin, D. K., Ed. Springer US: Boston, MA, 2007; pp 23-74.
30. Langmuir, I.; Schaefer, V. J., Activities of urease and pepsin monolayers. *J Am Chem Soc* **1938,** *60*, 1351-1360.
31. Hughes, A. V.; Goldar, A.; Gerstenberg, M. C.; Roser, S. J.; Bradshaw, J., A hybrid SAM phospholipid approach to fabricating a free supported lipid bilayer. *Phys Chem Chem Phys* **2002,** *4* (11), 2371-2378.
32. Liu, J.; Conboy, J. C., 1,2-diacyl-phosphatidylcholine flip-flop measured directly by sum-frequency vibrational spectroscopy. *Biophys J* **2005,** *89* (4), 2522-2532.
33. Anglin, T. C.; Conboy, J. C., Lateral pressure dependence of the phospholipid transmembrane diffusion rate in planar-supported lipid bilayers. *Biophys J* **2008,** *95* (1), 186-193.
34. Anglin, T. C.; Cooper, M. P.; Li, H.; Chandler, K.; Conboy, J. C., Free Energy and Entropy of Activation for Phospholipid Flip-Flop in Planar Supported Lipid Bilayers. *J Phys Chem B* **2010,** *114* (5), 1903-1914.
35. Gerelli, Y.; Porcar, L.; Fragneto, G., Lipid Rearrangement in DSPC/DMPC Bilayers: A Neutron Reflectometry Study. *Langmuir* **2012,** *28* (45), 15922-15928.
36. Wacklin, H. P.; Thomas, R. K., Spontaneous formation of asymmetric lipid bilayers by adsorption of vesicles. *Langmuir* **2007,** *23* (14), 7644-7651.
37. Reviakine, I.; Brisson, A., Formation of supported phospholipid bilayers from unilamellar vesicles investigated by atomic force microscopy. *Langmuir* **2000,** *16* (4), 1806-1815.
38. Goksu, E. I.; Vanegas, J. M.; Blanchette, C. D.; Lin, W. C.; Longo, M. L., AFM for structure and dynamics of biomembranes. *Bba-Biomembranes* **2009,** *1788* (1), 254-266.
39. Reimhult, E.; Hook, F.; Kasemo, B., Intact vesicle adsorption and supported biomembrane formation from vesicles in solution: Influence of surface chemistry, vesicle size, temperature, and osmotic pressure. *Langmuir* **2003,** *19* (5), 1681-1691.
40. Morigaki, K.; Tawa, K., Vesicle fusion studied by surface plasmon resonance and surface plasmon fluorescence spectroscopy. *Biophys J* **2006,** *91* (4), 1380-1387.
41. Kalb, E.; Frey, S.; Tamm, L. K., Formation of Supported Planar Bilayers by Fusion of Vesicles to

Supported Phospholipid Monolayers. *Biochim Biophys Acta* **1992,** *1103* (2), 307-316.
42. Crane, J. M.; Kiessling, V.; Tamm, L. K., Measuring lipid asymmetry in planar supported bilayers by fluorescence interference contrast microscopy. *Langmuir* **2005,** *21* (4), 1377-1388.
43. Sugihara, K.; Jang, B.; Schneider, M.; Voros, J.; Zambelli, T., A universal method for planar lipid bilayer formation by freeze and thaw. *Soft Matter* **2012,** *8* (20), 5525-5531.
44. Seul, M.; Sammon, M. J., Preparation of Surfactant Multilayer Films on Solid Substrates by Deposition from Organic Solution. *Thin Solid Films* **1990,** *185* (2), 287-305.
45. Mennicke, U.; Salditt, T., Preparation of solid-supported lipid bilayers by spin-coating. *Langmuir* **2002,** *18* (21), 8172-8177.
46. Simonsen, A. C.; Bagatolli, L. A., Structure of spin-coated lipid films and domain formation in supported membranes formed by hydration. *Langmuir* **2004,** *20* (22), 9720-9728.
47. Loren, N.; Hagman, J.; Jonasson, J. K.; Deschout, H.; Bernin, D.; Cella-Zanacchi, F.; Diaspro, A.; McNally, J. G.; Ameloot, M.; Smisdom, N.; Nyden, M.; Hermansson, A. M.; Rudemo, M.; Braeckmans, K., Fluorescence recovery after photobleaching in material and life sciences: putting theory into practice. *Q Rev Biophys* **2015,** *48* (3), 323-387.
48. Rayan, G.; Guet, J. E.; Taulier, N.; Pincet, F.; Urbach, W., Recent Applications of Fluorescence Recovery after Photobleaching (FRAP) to Membrane Bio-Macromolecules. *Sensors-Basel* **2010,** *10* (6), 5927-5948.
49. Silvius, J. R.; Nabi, I. R., Fluorescence-quenching and resonance energy transfer studies of lipid microdomains in model and biological membranes (Review). *Mol Membr Biol* **2006,** *23* (1), 5-16.
50. Pollok, B. A.; Heim, R., Using GFP in FRET-based applications. *Trends Cell Biol* **1999,** *9* (2), 57-60.
51. Lippincott-Schwartz, J.; Snapp, E.; Kenworthy, A., Studying protein dynamics in living cells. *Nat Rev Mol Cell Bio* **2001,** *2* (6), 444-456.
52. Thompson, N. L.; Pearce, K. H.; Hsieh, H. V., Total Internal-Reflection Fluorescence Microscopy - Application to Substrate-Supported Planar Membranes. *Eur Biophys J Biophy* **1993,** *22* (5), 367-378.
53. Bernchou, U.; Brewer, J.; Midtiby, H. S.; Ipsen, J. H.; Bagatolli, L. A.; Simonsen, A. C., Texture of Lipid Bilayer Domains. *J Am Chem Soc* **2009,** *131* (40), 14130-+.
54. Benda, A.; Benes, M.; Marecek, V.; Lhotsky, A.; Hermens, W. T.; Hof, M., How to determine diffusion coefficients in planar phospholipid systems by confocal fluorescence correlation spectroscopy. *Langmuir* **2003,** *19* (10), 4120-4126.
55. Berezin, M. Y.; Achilefu, S., Fluorescence Lifetime Measurements and Biological Imaging. *Chem Rev* **2010,** *110* (5), 2641-2684.
56. https://www.thermofisher.com/us/en/home/life-science/cell-analysis/labeling-chemistry/fluorescence-spectraviewer.html.
57. Frederix, P. L. T. M.; Bosshart, P. D.; Engel, A., Atomic Force Microscopy of Biological Membranes. *Biophys J* **2009,** *96* (2), 329-338.
58. Hansma, H. G.; Hoh, J. H., Biomolecular Imaging with the Atomic-Force Microscope. *Annu Rev Bioph Biom* **1994,** *23*, 115-139.
59. Mingeot-Leclercq, M. P.; Deleu, M.; Brasseur, R.; Dufrene, Y. F., Atomic force microscopy of supported lipid bilayers. *Nat Protoc* **2008,** *3* (10), 1654-1659.
60. El Kirat, K.; Morandat, S.; Dufrene, Y. F., Nanoscale analysis of supported lipid bilayers using atomic force microscopy. *Bba-Biomembranes* **2010,** *1798* (4), 750-765.
61. Merkel, R.; Nassoy, P.; Leung, A.; Ritchie, K.; Evans, E., Energy landscapes of receptor-ligand bonds explored with dynamic force spectroscopy. *Nature* **1999,** *397* (6714), 50-53.
62. Lee, G. U.; Kidwell, D. A.; Colton, R. J., Sensing Discrete Streptavidin Biotin Interactions with Atomic-Force Microscopy. *Langmuir* **1994,** *10* (2), 354-357.
63. Moy, V. T.; Florin, E. L.; Gaub, H. E., Intermolecular Forces and Energies between Ligands and Receptors. *Science* **1994,** *266* (5183), 257-259.

64. Unsay, J. D.; Cosentino, K.; Garcia-Saez, A. J., Atomic Force Microscopy Imaging and Force Spectroscopy of Supported Lipid Bilayers. *Jove-J Vis Exp* **2015,** (101).
65. Parsegian, V. A.; Rand, R. P.; Fuller, N. L.; Rau, D. C., Osmotic-Stress for the Direct Measurement of Intermolecular Forces. *Method Enzymol* **1986,** *127*, 400-416.
66. Kurniawan, J.; Yin, N. N.; Liu, G. Y.; Kuhl, T. L., Interaction Forces between Ternary Lipid Bilayers Containing Cholesterol. *Langmuir* **2014,** *30* (17), 4997-5004.
67. Kurniawan, J.; Kuhl, T. L., Characterization of Solid-Supported Dipalmitoylphosphatidylcholine Membranes Containing Cholesterol. *Langmuir* **2015,** *31* (8), 2527-2532.
68. Anderson, T. H.; Min, Y. J.; Weirich, K. L.; Zeng, H. B.; Fygenson, D.; Israelachvili, J. N., Formation of Supported Bilayers on Silica Substrates. *Langmuir* **2009,** *25* (12), 6997-7005.
69. Leckband, D. E.; Helm, C. A.; Israelachvili, J., Role of Calcium in the Adhesion and Fusion of Bilayers. *Biochemistry-Us* **1993,** *32* (4), 1127-1140.
70. Benz, M.; Gutsmann, T.; Chen, N. H.; Tadmor, R.; Israelachvili, J., Correlation of AFM and SFA measurements concerning the stability of supported lipid bilayers. *Biophys J* **2004,** *86* (2), 870-879.
71. Leckband, D. E.; Schmitt, F. J.; Israelachvili, J. N.; Knoll, W., Direct Force Measurements of Specific and Nonspecific Protein Interactions. *Biochemistry-Us* **1994,** *33* (15), 4611-4624.
72. Moore, N. W.; Mulder, D. J.; Kuhl, T. L., Adhesion from tethered ligand-receptor bonds with microsecond lifetimes. *Langmuir* **2008,** *24* (4), 1212-1218.
73. Fragneto, G., Neutrons and model membranes. *Eur Phys J-Spec Top* **2012,** *213* (1), 327-342.
74. Wacklin, H. P., Neutron reflection from supported lipid membranes. *Curr Opin Colloid In* **2010,** *15* (6), 445-454.
75. Kucerka, N.; Nieh, M. P.; Pencer, J.; Harroun, T.; Katsaras, J., The study of liposomes, lamellae and membranes using neutrons and X-rays. *Curr Opin Colloid In* **2007,** *12* (1), 17-22.
76. Novakova, E.; Giewekemeyer, K.; Salditt, T., Structure of two-component lipid membranes on solid support: An x-ray reflectivity study. *Phys Rev E* **2006,** *74* (5).
77. Miller, C. E.; Majewski, J.; Gog, T.; Kuhl, T. L., Characterization of biological thin films at the solid-liquid interface by X-ray reflectivity. *Phys Rev Lett* **2005,** *94* (23).
78. Salditt, T.; Brotons, G., Biomolecular and amphiphilic films probed by surface sensitive X-ray and neutron scattering. *Anal Bioanal Chem* **2004,** *379* (7-8), 960-973.
79. Krueger, S., Neutron reflection from interfaces with biological and biomimetic materials. *Curr Opin Colloid In* **2001,** *6* (2), 111-117.
80. Junghans, A.; Watkins, E. B.; Barker, R. D.; Singh, S.; Waltman, M. J.; Smith, H. L.; Pocivavsek, L.; Majewski, J., Analysis of biosurfaces by neutron reflectometry: From simple to complex interfaces. *Biointerphases* **2015,** *10* (1).
81. Vacklin, H. P.; Tiberg, F.; Fragneto, G.; Thomas, R. K., Composition of supported model membranes determined by neutron reflection. *Langmuir* **2005,** *21* (7), 2827-2837.
82. Cooper, M. A.; Singleton, V. T., A survey of the 2001 to 2005 quartz crystal microbalance biosensor literature: applications of acoustic physics to the analysis of biomolecular interactions. *J Mol Recognit* **2007,** *20* (3), 154-184.
83. Reimhult, E.; Hook, F.; Kasemo, B., Vesicle adsorption on SiO2 and TiO2: Dependence on vesicle size. *J Chem Phys* **2002,** *117* (16), 7401-7404.
84. Keller, C. A.; Kasemo, B., Surface specific kinetics of lipid vesicle adsorption measured with a quartz crystal microbalance. *Biophys J* **1998,** *75* (3), 1397-1402.
85. Seantier, B.; Breffa, C.; Felix, O.; Decher, G., Dissipation-enhanced quartz crystal microbalance studies on the experimental parameters controlling the formation of supported lipid bilayers. *J Phys Chem B* **2005,** *109* (46), 21755-21765.
86. Richter, R.; Mukhopadhyay, A.; Brisson, A., Pathways of lipid vesicle deposition on solid surfaces: A combined QCM-D and AFM study. *Biophys J* **2003,** *85* (5), 3035-3047.

87. Richter, R. P.; Brisson, A. R., Following the formation of supported lipid bilayers on mica: A study combining AFM, QCM-D, and ellipsometry. *Biophys J* **2005,** *88* (5), 3422-3433.
88. Cho, N. J.; Frank, C. W.; Kasemo, B.; Hook, F., Quartz crystal microbalance with dissipation monitoring of supported lipid bilayers on various substrates. *Nat Protoc* **2010,** *5* (6), 1096-1106.
89. Glasmastar, K.; Larsson, C.; Hook, F.; Kasemo, B., Protein adsorption on supported phospholipid bilayers. *J Colloid Interf Sci* **2002,** *246* (1), 40-47.
90. Bailey, C. M.; Kamaloo, E.; Waterman, K. L.; Wang, K. F.; Nagarajan, R.; Camesano, T. A., Size dependence of gold nanoparticle interactions with a supported lipid bilayer: A QCM-D study. *Biophys Chem* **2015,** *203*, 51-61.
91. Becker, B.; Cooper, M. A., A survey of the 2006-2009 quartz crystal microbalance biosensor literature. *J Mol Recognit* **2011,** *24* (5), 754-787.
92. Dufrene, Y. F.; Barger, W. R.; Green, J. B. D.; Lee, G. U., Nanometer-scale surface properties of mixed phospholipid monolayers and bilayers. *Langmuir* **1997,** *13* (18), 4779-4784.
93. Bassereau, P.; Pincet, F., Quantitative analysis of holes in supported bilayers providing the adsorption energy of surfactants on solid substrate. *Langmuir* **1997,** *13* (26), 7003-7007.
94. Rinia, H. A.; Demel, R. A.; van der Eerden, J. P. J. M.; de Kruijff, B., Blistering of Langmuir-Blodgett bilayers containing anionic phospholipids as observed by atomic force microscopy. *Biophys J* **1999,** *77* (3), 1683-1693.
95. Jung, S. Y.; Holden, M. A.; Cremer, P. S.; Collier, C. P., Two-component membrane lithography via lipid backfilling. *Chemphyschem* **2005,** *6* (3), 423-426.
96. Yee, C. K.; Amweg, M. L.; Parikh, A. N., Membrane photolithography: Direct micropatterning and manipulation of fluid phospholipid membranes in the aqueous phase using deep-UV light. *Adv Mater* **2004,** *16* (14), 1184-+.
97. Yee, C. K.; Amweg, M. L.; Parikh, A. N., Direct photochemical patterning and refunctionalization of supported phospholipid bilayers. *J Am Chem Soc* **2004,** *126* (43), 13962-13972.
98. Leonenko, Z. V.; Carnini, A.; Cramb, D. T., Supported planar bilayer formation by vesicle fusion: the interaction of phospholipid vesicles with surfaces and the effect of gramicidin on bilayer properties using atomic force microscopy. *Bba-Biomembranes* **2000,** *1509* (1-2), 131-147.
99. Marsh, D., Liquid-ordered phases induced by cholesterol: A compendium of binary phase diagrams. *Bba-Biomembranes* **2010,** *1798* (3), 688-699.
100. Drolle, E.; Kucerka, N.; Hoopes, M. I.; Choi, Y.; Katsaras, J.; Karttunen, M.; Leonenko, Z., Effect of melatonin and cholesterol on the structure of DOPC and DPPC membranes. *Bba-Biomembranes* **2013,** *1828* (9), 2247-2254.
101. Rawicz, W.; Smith, B. A.; McIntosh, T. J.; Simon, S. A.; Evans, E., Elasticity, strength, and water permeability of bilayers that contain raft microdomain-forming lipids. *Biophys J* **2008,** *94* (12), 4725-4736.
102. Jurak, M., Thermodynamic Aspects of Cholesterol Effect on Properties of Phospholipid Monolayers: Langmuir and Langmuir-Blodgett Monolayer Study. *J Phys Chem B* **2013,** *117* (13), 3496-3502.
103. Almeida, P. F. F., Thermodynamics of lipid interactions in complex bilayers. *Bba-Biomembranes* **2009,** *1788* (1), 72-85.
104. Needham, D.; Nunn, R. S., Elastic-Deformation and Failure of Lipid Bilayer-Membranes Containing Cholesterol. *Biophys J* **1990,** *58* (4), 997-1009.
105. Dietrich, C.; Bagatolli, L. A.; Volovyk, Z. N.; Thompson, N. L.; Levi, M.; Jacobson, K.; Gratton, E., Lipid rafts reconstituted in model membranes. *Biophys J* **2001,** *80* (3), 1417-1428.
106. Silvius, J. R., Role of cholesterol in lipid raft formation: lessons from lipid model systems. *Bba-Biomembranes* **2003,** *1610* (2), 174-183.
107. Crane, J. M.; Tamm, L. K., Role of cholesterol in the formation and nature of lipid rafts in planar

and spherical model membranes. *Biophys J* **2004,** *86* (5), 2965-2979.
108. Cinek, T.; Horejsi, V., The Nature of Large Noncovalent Complexes Containing Glycosyl-Phosphatidylinositol-Anchored Membrane-Glycoproteins and Protein Tyrosine Kinases. *J Immunol* **1992,** *149* (7), 2262-2270.
109. Ahmed, S. N.; Brown, D. A.; London, E., On the origin of sphingolipid/cholesterol-rich detergent-insoluble cell membranes: Physiological concentrations of cholesterol and sphingolipid induce formation of a detergent-insoluble, liquid-ordered lipid phase in model membranes. *Biochemistry-Us* **1997,** *36* (36), 10944-10953.
110. Smaby, J. M.; Brockman, H. L.; Brown, R. E., Cholesterols Interfacial Interactions with Sphingomyelins and Phosphatidylcholines - Hydrocarbon Chain Structure Determines the Magnitude of Condensation. *Biochemistry-Us* **1994,** *33* (31), 9135-9142.
111. Wydro, P.; Knapczyk, S.; Lapczynska, M., Variations in the Condensing Effect of Cholesterol on Saturated versus Unsaturated Phosphatidylcholines at Low and High Sterol Concentration. *Langmuir* **2011,** *27* (9), 5433-5444.
112. Fliesler, S. J.; Schroepfer, G. J., Sterol Composition of Bovine Retinal Rod Outer Segment Membranes and Whole Retinas. *Biochim Biophys Acta* **1982,** *711* (1), 138-148.
113. Bloch, K., Cholesterol: evolution of structure and function. In *Biochemistry of lipids, lipoproteins, and membranes*, Vance, D. E.; Vance, J. E., Eds. Elsevier: Amsterdam ; New York, 1991; pp 363-381.
114. Anderson, T. G.; McConnell, H. M., Condensed complexes and the calorimetry of cholesterol-phospholipid bilayers. *Biophys J* **2001,** *81* (5), 2774-2785.
115. Brown, D. A.; London, E., Structure and function of sphingolipid- and cholesterol-rich membrane rafts. *J Biol Chem* **2000,** *275* (23), 17221-17224.
116. Yuan, C.; Johnston, L. J., Phase evolution in cholesterol/DPPC monolayers: atomic force microscopy and near field scanning optical microscopy studies. *J Microsc-Oxford* **2002,** *205*, 136-146.
117. Marsh, D., Cholesterol-induced fluid membrane domains: A compendium of lipid-raft ternary phase diagrams. *Bba-Biomembranes* **2009,** *1788* (10), 2114-2123.
118. Stottrup, B. L.; Keller, S. L., Phase behavior of lipid monolayers containing DPPC and cholesterol analogs. *Biophys J* **2006,** *90* (9), 3176-3183.
119. Mills, T. T.; Huang, J. Y.; Feigenson, G. W.; Nagle, J. F., Effects of cholesterol and unsaturated DOPC lipid on chain packing of saturated gel-phase DPPC bilayers. *Gen Physiol Biophys* **2009,** *28* (2), 126-139.
120. Israelachvili, J. N.; Adams, G. E., Measurement of Forces between 2 Mica Surfaces in Aqueous-Electrolyte Solutions in Range 0-100 Nm. *J Chem Soc Farad T 1* **1978,** *74*, 975-&.
121. Israelachvili, J. N., Thin-Film Studies Using Multiple-Beam Interferometry. *J Colloid Interf Sci* **1973,** *44* (2), 259-272.
122. Kuhl, T. L.; Leckband, D. E.; Lasic, D. D.; Israelachvili, J. N., Modulation of Interaction Forces between Bilayers Exposing Short-Chained Ethylene-Oxide Headgroups. *Biophys J* **1994,** *66* (5), 1479-1488.
123. Kjaer, K., Some Simple Ideas on X-Ray Reflection and Grazing-Incidence Diffraction from Thin Surfactant Films. *Physica B* **1994,** *198* (1-3), 100-109.
124. Grabbe, A.; Horn, R. G., Double-Layer and Hydration Forces Measured between Silica Sheets Subjected to Various Surface Treatments. *J Colloid Interf Sci* **1993,** *157* (2), 375-383.
125. Tsui, F. C.; Ojcius, D. M.; Hubbell, W. L., The Intrinsic Pka Values for Phosphatidylserine and Phosphatidylethanolamine in Phosphatidylcholine Host Bilayers. *Biophys J* **1986,** *49* (2), 459-468.
126. Moncelli, M. R.; Becucci, L.; Guidelli, R., The Intrinsic Pk(a), Values for Phosphatidylcholine, Phosphatidylethanolamine, and Phosphatidylserine in Monolayers Deposited on Mercury-Electrodes. *Biophys J* **1994,** *66* (6), 1969-1980.
127. Pincet, F.; Cribier, S.; Perez, E., Bilayers of neutral lipids bear a small but significant charge. *Eur Phys J B* **1999,** *11* (1), 127-130.

128. Fragneto, G.; Graner, F.; Charitat, T.; Dubos, P.; Bellet-Amalric, E., Interaction of the third helix of Antennapedia homeodomain with a deposited phospholipid bilayer: A neutron reflectivity structural study. *Langmuir* **2000,** *16* (10), 4581-4588.
129. Greenwood, A. I.; Tristram-Nagle, S.; Nagle, J. F., Partial molecular volumes of lipids and cholesterol. *Chem Phys Lipids* **2006,** *143* (1-2), 1-10.
130. Risselada, H. J.; Marrink, S. J., The molecular face of lipid rafts in model membranes. *P Natl Acad Sci USA* **2008,** *105* (45), 17367-17372.
131. Stottrup, B. L.; Veatch, S. L.; Keller, S. L., Nonequilibrium behavior in supported lipid membranes containing cholesterol. *Biophys J* **2004,** *86* (5), 2942-2950.
132. Stottrup, B. L.; Stevens, D. S.; Keller, S. L., Miscibility of ternary mixtures of phospholipids and cholesterol in monolayers, and application to bilayer systems. *Biophys J* **2005,** *88* (1), 269-276.
133. Veatch, S. L.; Keller, S. L., Seeing spots: Complex phase behavior in simple membranes. *Bba-Mol Cell Res* **2005,** *1746* (3), 172-185.
134. Pitman, M. C.; Suits, F.; MacKerell, A. D.; Feller, S. E., Molecular-level organization of saturated and polyunsaturated fatty acids in a phosphatidylcholine bilayer containing cholesteral. *Biochemistry-Us* **2004,** *43* (49), 15318-15328.
135. de Joannis, J.; Coppock, P. S.; Yin, F. C.; Mori, M.; Zamorano, A.; Kindt, J. T., Atomistic Simulation of Cholesterol Effects on Miscibility of Saturated and Unsaturated Phospholipids: Implications for Liquid-Ordered/Liquid-Disordered Phase Coexistence. *J Am Chem Soc* **2011,** *133* (10), 3625-3634.
136. Kienle, D. F.; De Souza, J. V.; Watkins, E. B.; Kuhl, T. L., Thickness and Refractive Index of DPPC and DPPE Monolayers by Multiple-Beam Interferometry. *Anal Bioanal Chem* **submitted**.
137. Hemmerle, A.; Malaquin, L.; Charitat, T.; Lecuyer, S.; Fragneto, G.; Daillant, J., Controlling interactions in supported bilayers from weak electrostatic repulsion to high osmotic pressure. *P Natl Acad Sci USA* **2012,** *109* (49), 19938-19942.
138. Helm, C. A.; Israelachvili, J. N.; Mcguiggan, P. M., Molecular Mechanisms and Forces Involved in the Adhesion and Fusion of Amphiphilic Bilayers. *Science* **1989,** *246* (4932), 919-922.
139. Safran, S. A.; Kuhl, T. L.; Israelachvili, J. N., Polymer-induced membrane contraction, phase separation, and fusion via Marangoni flow. *Biophys J* **2001,** *81* (2), 659-666.
140. Kuhl, T.; Guo, Y. Q.; Alderfer, J. L.; Berman, A. D.; Leckband, D.; Israelachvili, J.; Hui, S. W., Direct measurement of polyethylene glycol induced depletion attraction between lipid bilayers. *Langmuir* **1996,** *12* (12), 3003-3014.
141. Marsh, D., *CRC handbook of lipid bilayers*. CRC Press: Boca Raton, Fla., 1990; p 387 p.
142. Guven, N., Crystal-Structures of 2m1 Phengite and 2m1 Muscovite. *Z Kristallogr Krist* **1971,** *134* (3-4), 196-&.
143. Huang, J. Y.; Feigenson, G. W., A microscopic interaction model of maximum solubility of cholesterol in lipid bilayers. *Biophys J* **1999,** *76* (4), 2142-2157.
144. Mahanty, J.; Ninham, B. W., *Dispersion forces*. Academic Press: London ; New York, 1976; p ix, 236 p.
145. Rawicz, W.; Olbrich, K. C.; McIntosh, T.; Needham, D.; Evans, E., Effect of chain length and unsaturation on elasticity of lipid bilayers. *Biophys J* **2000,** *79* (1), 328-339.
146. Petruzielo, R. S.; Heberle, F. A.; Drazba, P.; Katsaras, J.; Feigenson, G. W., Phase behavior and domain size in sphingomyelin-containing lipid bilayers. *Bba-Biomembranes* **2013,** *1828* (4), 1302-1313.
147. Simons, K.; Ikonen, E., Functional rafts in cell membranes. *Nature* **1997,** *387* (6633), 569-572.
148. Pokorny, A.; Yandek, L. E.; Elegbede, A. I.; Hinderliter, A.; Almeida, P. F. F., Temperature and composition dependence of the interaction of delta-lysin with ternary mixtures of sphingomyelin/cholesterol/POPC. *Biophys J* **2006,** *91* (6), 2184-2197.
149. Frazier, M. L.; Wright, J. R.; Pokorny, A.; Almeida, P. F. F., Investigation of domain formation in sphingomyelin/cholesterol/POPC mixtures by fluorescence resonance energy transfer and Monte Carlo

simulations. *Biophys J* **2007,** *92* (7), 2422-2433.
150. Heberle, F. A.; Feigenson, G. W., Phase Separation in Lipid Membranes. *Csh Perspect Biol* **2011,** *3* (4).
151. Schroeder, R.; London, E.; Brown, D., Interactions between Saturated Acyl Chains Confer Detergent Resistance on Lipids and Glycosylphosphatidylinositol (Gpi)-Anchored Proteins - Gpi-Anchored Proteins in Liposomes and Cells Show Similar Behavior. *P Natl Acad Sci USA* **1994,** *91* (25), 12130-12134.
152. de Almeida, R. F. M.; Fedorov, A.; Prieto, M., Sphingomyelin/phosphatidylcholine/cholesterol phase diagram: Boundaries and composition of lipid rafts. *Biophys J* **2003,** *85* (4), 2406-2416.
153. Barenholz, Y.; Thompson, T. E., Sphingomyelin: biophysical aspects. *Chem Phys Lipids* **1999,** *102* (1-2), 29-34.
154. Zachowski, A., Phospholipids in Animal Eukaryotic Membranes - Transverse Asymmetry and Movement. *Biochem J* **1993,** *294*, 1-14.
155. Niemela, P. S.; Hyvonen, M. T.; Vattulainen, I., Influence of chain length and unsaturation on sphingomyelin bilayers. *Biophys J* **2006,** *90* (3), 851-863.
156. Niemela, P. S.; Hyvonen, M. T.; Vattulainen, I., Atom-scale molecular interactions in lipid raft mixtures. *Bba-Biomembranes* **2009,** *1788* (1), 122-135.
157. Schmidt, C. F.; Barenholz, Y.; Huang, C.; Thompson, T. E., Monolayer Coupling in Sphingomyelin Bilayer Systems. *Nature* **1978,** *271* (5647), 775-777.
158. Jensen, M. O.; Mouritsen, O. G., Lipids do influence protein function - the hydrophobic matching hypothesis revisited. *Bba-Biomembranes* **2004,** *1666* (1-2), 205-226.
159. Davey, J., Biomembranes - Molecular-Structure and Function - Gennis,Rb. *Nature* **1989,** *339* (6226), 591-591.
160. Kiessling, V.; Wan, C.; Tamm, L. K., Domain coupling in asymmetric lipid bilayers. *Bba-Biomembranes* **2009,** *1788* (1), 64-71.
161. Huang, C. H.; Mason, J. T., Structure and Properties of Mixed-Chain Phospholipid Assemblies. *Biochim Biophys Acta* **1986,** *864* (3-4), 423-470.
162. Maulik, P. R.; Atkinson, D.; Shipley, G. G., X-Ray-Scattering of Vesicles of N-Acyl Sphingomyelins - Determination of Bilayer Thickness. *Biophys J* **1986,** *50* (6), 1071-1077.
163. Kiessling, V.; Crane, J. M.; Tamm, L. K., Transbilayer effects of raft-like lipid domains in asymmetric planar bilayers measured by single molecule tracking. *Biophys J* **2006,** *91* (9), 3313-3326.
164. Hardman, W. E., (n-3) Fatty acids and cancer therapy. *J Nutr* **2004,** *134* (12), 3427s-3430s.
165. Pagnan, A.; Corrocher, R.; Ambrosio, G. B.; Ferrari, S.; Guarini, P.; Piccolo, D.; Opportuno, A.; Bassi, A.; Olivieri, O.; Baggio, G., Effects of an Olive-Oil-Rich Diet on Erythrocyte-Membrane Lipid-Composition and Cation-Transport Systems. *Clin Sci* **1989,** *76* (1), 87-93.
166. Kagan, A.; Harris, B. R.; Winkelst.W; Johnson, K. G.; Kato, H.; Syme, S. L.; Rhoads, G. G.; Gay, M. L.; Nichaman, M. Z.; Hamilton, H. B.; Tillotso.J, Epidemiologic Studies of Coronary Heart-Disease and Stroke in Japanese Men Living in Japan, Hawaii and California - Demographic, Physical, Dietary and Biochemical Characteristics. *J Chron Dis* **1974,** *27* (7-8), 345-364.
167. Kushi, L. H.; Lew, R. A.; Stare, F. J.; Ellison, C. R.; Ellozy, M.; Bourke, G.; Daly, L.; Graham, I.; Hickey, N.; Mulcahy, R.; Kevaney, J., Diet and 20-Year Mortality from Coronary Heart-Disease - the Ireland-Boston Diet Heart Study. *New Engl J Med* **1985,** *312* (13), 811-818.
168. Hu, F. B.; Stampfer, M. J.; Manson, J. E.; Rimm, E.; Colditz, G. A.; Rosner, B. A.; Hennekens, C. H.; Willett, W. C., Dietary fat intake and the risk of coronary heart disease in women. *New Engl J Med* **1997,** *337* (21), 1491-1499.
169. Delorgeril, M.; Renaud, S.; Mamelle, N.; Salen, P.; Martin, J. L.; Monjaud, I.; Guidollet, J.; Touboul, P.; Delaye, J., Mediterranean Alpha-Linolenic Acid-Rich Diet in Secondary Prevention of Coronary Heart-Disease. *Lancet* **1994,** *343* (8911), 1454-1459.
170. Hartweg, J.; Perera, R.; Montori, V.; Dinneen, S.; Neil, H. A. W.; Farmer, A., Omega-3

polyunsaturated fatty acids (PUFA) for type 2 diabetes mellitus. *Cochrane Db Syst Rev* **2008,** (1).
171. Lim, W. S.; Gammack, J. K.; Van Niekerk, J.; Dangour, A. D., Omega 3 fatty acid for the prevention of dementia. *Cochrane Db Syst Rev* **2006,** (1).
172. McKarney, C.; Everard, M.; N'Diaye, T., Omega-3 fatty acids (from fish oils) for cystic fibrosis. *Cochrane Db Syst Rev* **2007,** (4).
173. Dayton, S.; Pearce, M. L.; Hashimot.S; Dixon, W. J.; Tomiyasu, U., A Controlled Clinical Trial of a Diet High in Unsaturated Fat in Preventing Complications of Atherosclerosis. *Circulation* **1969,** *40* (1s2), Ii1-&.
174. Miettinen, M.; Turpeinen, O.; Karvonen, M. J.; Pekkarinen, M.; Paavilainen, E.; Elosuo, R., Dietary Prevention of Coronary Heart-Disease in Women - the Finnish Mental-Hospital Study. *Int J Epidemiol* **1983,** *12* (1), 17-25.
175. Dontas, A. S.; Zerefos, N. S.; Panagiotakos, D. B.; Valis, D. A., Mediterranean diet and prevention of coronary heart disease in the elderly. *Clin Interv Aging* **2007,** *2* (1), 109-115.
176. Nestel, P.; Clifton, P.; Colquhoun, D.; Noakes, M.; Mori, T. A.; Sullivan, D.; Thomas, B., Indications for Omega-3 Long Chain Polyunsaturated Fatty Acid in the Prevention and Treatment of Cardiovascular Disease. *Heart Lung Circ* **2015,** *24* (8), 769-779.
177. Usher, J. R.; Epand, R. M.; Papahadjopoulos, D., Effect of Free Fatty-Acids on Thermotropic Phase-Transition of Dimyristoyl Glycerophosphocholine. *Chem Phys Lipids* **1978,** *22* (3), 245-253.
178. Klausner, R. D.; Kleinfeld, A. M.; Hoover, R. L.; Karnovsky, M. J., Lipid Domains in Membranes - Evidence Derived from Structural Perturbations Induced by Free Fatty-Acids and Lifetime Heterogeneity Analysis. *J Biol Chem* **1980,** *255* (4), 1286-1295.
179. Muranushi, N.; Takagi, N.; Muranishi, S.; Sezaki, H., Effect of Fatty-Acids and Monoglycerides on Permeability of Lipid Bilayer. *Chem Phys Lipids* **1981,** *28* (3), 269-279.
180. Ibarguren, M.; Lopez, D. J.; Escriba, P. V., The effect of natural and synthetic fatty acids on membrane structure, microdomain organization, cellular functions and human health. *Bba-Biomembranes* **2014,** *1838* (6), 1518-1528.
181. Funari, S. S.; Barcelo, F.; Escriba, P. V., Effects of oleic acid and its congeners, elaidic and stearic acids, on the structural properties of phosphatidylethanolamine membranes. *J Lipid Res* **2003,** *44* (3), 567-575.
182. da Silva, A. M. G.; Romao, R. I. S., Mixed monolayers involving DPPC, DODAB and oleic acid and their interaction with nicotinic acid at the air-water interface. *Chem Phys Lipids* **2005,** *137* (1-2), 62-76.
183. Inoue, T.; Yanagihara, S.; Misono, Y.; Suzuki, M., Effect of fatty acids on phase behavior of hydrated dipalmitoylphosphatidylcholine bilayer: saturated versus unsaturated fatty acids. *Chem Phys Lipids* **2001,** *109* (2), 117-133.
184. Onuki, Y.; Morishita, M.; Chiba, Y.; Tokiwa, S.; Takayama, K., Docosapentaenoic acid and eicosapentaenoic acid induce changes in the physical properties of a lipid bilayer model membrane. *Chem Pharm Bull* **2006,** *54* (1), 68-71.
185. Cerezo, J.; Zuniga, J.; Bastida, A.; Requena, A.; Ceron-Carrasco, J. P., Atomistic Molecular Dynamics Simulations of the Interactions of Oleic and 2-Hydroxyoleic Acids with Phosphatidylcholine Bilayers. *J Phys Chem B* **2011,** *115* (40), 11727-11738.
186. Cistola, D. P.; Hamilton, J. A.; Jackson, D.; Small, D. M., Ionization and Phase-Behavior of Fatty-Acids in Water - Application of the Gibbs Phase Rule. *Biochemistry-Us* **1988,** *27* (6), 1881-1888.
187. Salentinig, S.; Sagalowicz, L.; Glatter, O., Self-Assembled Structures and pK(a) Value of Oleic Acid in Systems of Biological Relevance. *Langmuir* **2010,** *26* (14), 11670-11679.
188. Trier, S.; Henriksen, J. R.; Andresen, T. L., Membrane fusion of pH-sensitive liposomes - a quantitative study using giant unilamellar vesicles. *Soft Matter* **2011,** *7* (19), 9027-9034.
189. Kanicky, J. R.; Shah, D. O., Effect of degree, type, and position of unsaturation on the pK(a) of long-chain fatty acids. *J Colloid Interf Sci* **2002,** *256* (1), 201-207.

190. Suga, K.; Yokoi, T.; Kondo, D.; Hayashi, K.; Morita, S.; Okamoto, Y.; Shimanouchi, T.; Umakoshi, H., Systematical Characterization of Phase Behaviors and Membrane Properties of Fatty Acid/Didecyldimethylammonium Bromide Vesicles. *Langmuir* **2014,** *30* (43), 12721-12728.
191. Duzgunes, N.; Straubinger, R. M.; Baldwin, P. A.; Friend, D. S.; Papahadjopoulos, D., Proton-Induced Fusion of Oleic Acid Phosphatidylethanolamine Liposomes. *Biochemistry-Us* **1985,** *24* (13), 3091-3098.
192. Duzgunes, N.; Nir, S., Mechanisms and kinetics of liposome-cell interactions. *Adv Drug Deliver Rev* **1999,** *40* (1-2), 3-18.
193. Gaines, G. L., *Insoluble monolayers at liquid-gas interfaces*. Interscience Publishers: New York,, 1966; p xiv, 386 p.
194. Goodrich, F. C. In *Molecular Interaction in Mixed Monolayers*, Proceedings of the Second International Congress of Surface Activity, Butterworth, London, Butterworth, London, 1957; p 85.
195. Dejanovic, B.; Noethig-Laslo, V.; Sentjurc, M.; Walde, P., On the surface properties of oleate micelles and oleic acid/oleate vesicles studied by spin labeling. *Chem Phys Lipids* **2011,** *164* (1), 83-88.
196. Onuki, Y.; Hagiwara, C.; Sugibayashi, K.; Takayama, K., Specific effect of polyunsaturated fatty acids on the cholesterol-poor membrane domain in a model membrane. *Chem Pharm Bull* **2008,** *56* (8), 1103-1109.
197. Fukuda, H.; Goto, A.; Yoshioka, H.; Goto, R.; Morigaki, K.; Walde, P., Electron spin resonance study of the pH-induced transformation of micelles to vesicles in an aqueous oleic acid/oleate system. *Langmuir* **2001,** *17* (14), 4223-4231.
198. Janke, J. J.; Bennett, W. F. D.; Tieleman, D. P., Oleic Acid Phase Behavior from Molecular Dynamics Simulations. *Langmuir* **2014,** *30* (35), 10661-10667.
199. Kramer, S. D.; JakitsDeiser, C.; WunderliAllenspach, H., Free fatty acids cause pH-dependent changes in drug-lipid membrane interactions around physiological pH. *Pharmaceut Res* **1997,** *14* (6), 827-832.
200. Kanicky, J. R.; Shah, D. O., Effect of premicellar aggregation on the pK(a) of fatty acid soap solutions. *Langmuir* **2003,** *19* (6), 2034-2038.
201. Onuki, Y.; Obata, Y.; Kawano, K.; Sano, H.; Matsumoto, R.; Hayashi, Y.; Takayama, K., Membrane Microdomain Structures of Liposomes and Their Contribution to the Cellular Uptake Efficiency into HeLa Cells. *Mol Pharmaceut* **2016,** *13* (2), 369-378.
202. Teres, S.; Barcelo-Coblijn, G.; Benet, M.; Alvarez, R.; Bressani, R.; Halver, J. E.; Escriba, P. V., Oleic acid content is responsible for the reduction in blood pressure induced by olive oil. *P Natl Acad Sci USA* **2008,** *105* (37), 13811-13816.
203. Nistor, C. L.; Ianchis, R.; Ghiurea, M.; Nicolae, C. A.; Spataru, C. I.; Culita, D. C.; Cusu, J. P.; Fruth, V.; Oancea, F.; Donescu, D., Aqueous Dispersions of Silica Stabilized with Oleic Acid Obtained by Green Chemistry. *Nanomaterials-Basel* **2016,** *6* (1).
204. Thiam, A. R.; Farese, R. V.; Walther, T. C., The biophysics and cell biology of lipid droplets. *Nat Rev Mol Cell Bio* **2013,** *14* (12), 775-786.